

BIOMECHANICAL RESPONSE OF THE ANKLE TO
EXCESSIVE EXTERNAL ROTATION

By

Keith D. Button

A DISSERTATION

Submitted to
Michigan State University
in partial fulfillment of the requirements
for the degree of

Engineering Mechanics-Doctor of Philosophy

2015

ABSTRACT

BIOMECHANICAL RESPONSE OF THE ANKLE TO EXCESSIVE EXTERNAL ROTATION

By

Keith D. Button

Acute ankle damage is one of the most commonly observed athletic injuries, accounting for 10-30% of sports-related injuries in young athletes. Most frequently, damage occurs to the lateral ligamentous complex, involving the anterior talofibular ligament and calcaneofibular ligament. Medial ankle injuries involve damage to the anterior deltoid ligament, while syndesmotic (or high) ankle injuries are defined as damage to the anterior tibiofibular ligament. While less common than lateral ankle injuries, both medial and high ankle injuries are of particular interest to researchers due to their longer recovery time and potential for long-term ankle dysfunction. While combinations of eversion, dorsiflexion, and external rotation are often implicated in medial and high ankle sprains, the exact mechanisms are still unclear. Additionally, although studies have investigated the effect of shoe-surface interface on injury risk, few researchers have examined the effect of shoe rotational stiffness on motion of the ankle, torque generated, and subsequent injury location and severity during external rotation. One hypothesis of this dissertation was that the motion of the ankle joint and the location of injury during external rotation are functions of both the position of the ankle prior to rotation and the amount of constraint on the ankle. A second hypothesis was that specimen-specific, rigid body modeling could be utilized to simulate injury-level ankle rotation in addition to modeling the effect of different footwear on motion of the ankle. Computational modeling, in addition to cadaveric and *in vivo* human subject testing was utilized to test these hypotheses.

Specimen-specific computational models simulating injuries observed experimentally revealed that external foot rotation primarily strains the medial ankle ligaments, but pre-everting the ankles prior to rotation puts the primary strain on the syndesmotic ankle ligaments. Additionally, there was a significant difference in the amount of strain in simulations modelling complete ruptures versus partial tears. A follow-up study involving the measurement of cadaver joint kinematics during external foot rotation concluded there was significantly more talocrural joint rotation, but significantly less subtalar joint rotation in a neutral versus pre-everted ankle, potentially explaining the location of injury during external rotation. In a separate cadaver study investigating the effect of foot constraint, ankles constrained by a 'stiff' football shoe experienced more ankle joint rotation, but less eversion than ankles constrained by a more 'flexible' shoe. As a result, ankles in stiff shoes experienced combination syndesmotic and medial ankle injuries in addition to high strains in these ligaments. Ankles in flexible shoes saw less combination injuries, but higher strains in the subtalar ligaments. This effect of ankle constraint on joint motion was then quantified by measuring joint kinematics in human subjects, and computational modelling provided an estimation of injury risk as a function of foot rotation and constraint. A final human subject study involved calculating the stiffness of the unconstrained ankle joint during voluntary external foot rotation in order to more accurately model the ankle in the future. The information from these studies may aid in the implementation of preventative measures in order to mitigate the risk of future ankle injury resulting from excessive levels of external rotation.

Thank you Mom, Dad, Rachael, and Erin. You are my heroes and your support means everything.

ACKNOWLEDGEMENTS

I would like to thank my mentor, Dr. Roger C. Haut, for his support, expertise, and leadership throughout my research at the Orthopaedic Biomechanics Laboratories (OBL). I would like to acknowledge Dr. Dashin Liu, Dr. Eric Meyer, Dr. John Powell, Dr. Feng Wei, and Dr. Neil Wright for their insight when serving on my committee. I would also like to thank Mr. Jerrod Braman for his expertise in gait analysis, Mr. Cliff Beckett for his technical assistance, Mrs. Jean Atkinson for help with specimen preparation, and Dr. Maureen Schaefer for clinical advice. I would like to thank my co-investigators at Colorado State University: Garrett Coatney, Dr. Tammy Haut Donahue, Kristine Fischenich, Hannah Pauly, and Benjamin Wheatley. I would lastly like to thank all my coworkers in the OBL for their help and friendship: Benjamin Carruthers, Mark Davison, Trevor Deland, Kathleen Fitzsimons, Mike Klein, Katie Landwehr, Kevin Leikert, Patrick Vaughn, and Brian Weaver.

TABLE OF CONTENTS

LIST OF TABLES	ix
LIST OF FIGURES	x
CHAPTER 1: INTRODUCTION AND BACKGROUND	1
Ankle Anatomy and Kinematics	1
Ankle Injury in Sports	3
Inversion Injuries	4
External Rotation Injuries	4
Risk Factors for External Rotation Injuries	6
Shoe Surface Interface	6
Shoe Stiffness	7
Computational Modelling	8
Summary and Objectives	9
CHAPTER 2: SPECIMEN-SPECIFIC COMPUTATIONAL MODELS OF ANKLE SPRAINS PRODUCED IN A LABORATORY SETTING	11
ABSTRACT	11
INTRODUCTION	13
METHODS	15
Cadaver Experiment	15
Model Development	17
Simulation	19
RESULTS	20
DISCUSSION	26
CHAPTER 3: EFFECT OF PRE-EVERSION ON TALOCRURAL AND SUBTALAR JOINT MOTION DURING ANKLE EXTERNAL ROTATION	31
ABSTRACT	31
INTRODUCTION	32
METHODS	33
RESULTS	36
DISCUSSION	37

CHAPTER 4: ROTATIONAL STIFFNESS OF AMERICAN FOOTBALL SHOES AFFECTS ANKLE BIOMECHANICS AND INJURY SEVERITY	42
ABSTRACT	42
INTRODUCTION	43
METHODS	46
Shoe Selection.....	46
Cadaver Tests.....	47
Motion Analysis.....	51
Computational Modelling	52
Statistical Analysis.....	52
RESULTS	53
Experimental	53
Computational Modelling	56
DISCUSSION	59
CHAPTER 5: THE EFFECT OF ROTATIONAL STIFFNESS ON ANKLE JOINT MOTION AND LIGAMENT STRAIN DURING EXTERNAL ROTATION	65
ABSTRACT	65
INTRODUCTION	66
METHODS	69
Tape Stiffness Tests	69
Human Subject Tests	71
Computational Modelling	74
Statistical Analysis.....	76
RESULTS	76
DISCUSSION	82
CHAPTER 6: A METHOD OF DETERMINING IN VIVO DYNAMIC HUMAN ANKLE STIFFNESS DURING EXTERNAL ROTATION.....	87
ABSTRACT.....	87
INTRODUCTION	87
METHODS	89
RESULTS	93
DISCUSSION	93

CHAPTER 7: CONCLUSIONS	97
Overview	97
Chapter 2	98
Chapter 3	99
Chapter 4	100
Chapter 5	102
Chapter 6	104
Contributions to the Literature	106
Influence of shoe design on ankle movement and injury	106
Determination of failure-level ligament strains	106
Use of specimen-specific computational models	107
APPENDICES	108
RESEARCH PUBLICATIONS	109
SOP (Standard Operating Procedure) for Building Specimen-Specific Computational Ankle Models	112
SOP (Standard Operating Procedure) For Calculating Ankle Joint Motion Given Vicon Data	118
REFERENCES	132

LIST OF TABLES

Table 2-1 <i>Results of the cadaver experiment for the neutral and everted ankle</i>	25
Table 2-2 <i>Comparison of the talus external rotations with respect to the tibia (deg) from the cadaver study with the computational talus rotations</i>	25
Table 3-1 <i>Motions of the subtalar and talocrural joint for 20 degrees of external rotation</i>	37
Table 4-1 <i>Lateral (a), posterior (b), and medial (c) views of one of the specimen-specific models in SolidWorks with linear springs representing ligaments.</i>	54
Table 4-2 <i>Strains at failure rotation for the anterior tibiofibular ligament (ATiFL), anterior tibiotalar ligament (ATiTL), posterior tibiotalar ligament (PTiTL), interosseous talocalcaneal ligament (ITaCL), lateral talocalcaneal ligament (LTaCL), medial talocalcaneal ligament (MTaCL), and posterior talocalcaneal ligament (PTaCL). (Underlining represents ligaments that ruptured or avulsed)</i>	55
Table 6-1 <i>Ankle stiffnesses in three directions obtained from subjects performing a single legged external rotation of the foot with standard deviations in parenthesis. Note: the absolute value of the inversion-eversion slope was taken so that the reported number was positive.</i>	92
Table 6-2 <i>Stiffness values from previous studies</i>	94
Table 7-1 <i>Motions of the subtalar and talocrural joint for 20 degrees of external rotation</i>	100
Table 7-2 <i>Summary of injury mechanisms and failure metrics from cadaver experiment</i>	101
Table 7-3 <i>Ankle stiffness in three directions obtained from subjects performing a single legged external rotation of the foot.</i>	105
Table A-1 <i>Raw Data from Cadaver Failure Tests (Chapter 4)</i>	124
Table A-2 <i>Raw Data from Tape Stiffness Tests (Chapter 5)</i>	127
Table A-3 <i>Input Motions for Computational Model (Chapter 5)</i>	128

LIST OF FIGURES

Figure 1-1 <i>Medial view of the bony anatomy of the ankle</i>	1
Figure 1-2 <i>Lateral (left) and medial (right) view of the osteoligamentous ankle anatomy</i>	2
Figure 1-3 <i>The three motions of the ankle illustrated about a Cartesian coordinate system</i>	3
Figure 2-1 <i>Setup for the cadaver experiment by Wei et al.</i>	16
Figure 2-2 <i>The cadaver taping pattern (a) and the model taping pattern represented by springs (b). Note: for clarity all ligament springs and the plate springs on the medial side of the ankle were set invisible.</i>	18
Figure 2-3 <i>Injury mechanisms reported from the cadaver study by Wei et al. (Wei et al., 2012b). Partial tear of the ATiFL (a); Rupture of the ATiFL (b); Partial tear of the ATiTL (c); Rupture of the ATiTL (d); Tibial avulsion of the ATiTL (e); Partial tear of the TiNL(f). Note: the location of injury is shown with a hemostat.</i>	21
Figure 2-4 <i>Ligaments with average model predicted strains greater than 2% for the neutral case in 3 of 4 cases in which ligament injury occurred</i>	22
Figure 2-5 <i>Strains in the ATiFL and the two deltoid ligaments (ATiTL and TiNL) for the neutral case for each specimen modeled</i>	23
Figure 2-6 <i>Ligaments with average model predicted strains greater than 2% for the everted simulations</i>	24
Figure 2-7 <i>Strains in the ATiFL and the two deltoid ligaments (ATiTL and TiNL) for the everted simulations</i>	24
Figure 3-1 <i>Cadaver foot taped to a polycarbonate plate (a). Ankle with reflective marker array in the tibia, talus, and calcaneus in the testing fixture (b).</i>	34
Figure 3-2 <i>Orthogonal coordinate axes on the tibia, talus, and calcaneus.</i>	36
Figure 3-3 <i>The sustentaculum tali of the calcaneus locks with the articulating surface of the talus in a neutral position shown from the posterior (a) and medial (b) view. When everted, these surfaces unlock, shown in the posterior (c) and medial (d) view.</i>	40
Figure 4-1 <i>Posterior view of a neutral (left) and everted foot (right).</i>	44
Figure 4-2 <i>Football shoes used for the current study: Nike Flyposite (a) and Nike Zoom Air (b).</i>	47
Figure 4-3 <i>Football cleat mold made of epoxy resin used to fix the shoe to the testing fixture</i>	48

Figure 4-4 <i>The experiments were performed on a biaxial testing machine with the motions of the talus and tibia tracked by a 5-camera motion capture system.</i>	50
Figure 4-5 <i>An example of the torque data from a sub-failure (a) and a failure (b) test. The failure occurs when there is a steep drop in torque, as indicated by the arrow.</i>	50
Figure 4-6 <i>Lateral (a), posterior (b), and medial (c) views of one of the specimen-specific models in SolidWorks with linear springs representing ligaments.</i>	51
Figure 4-7 <i>Fibular fracture (a), medial malleolus fracture (b), ATiFL avulsion (c), ATiTL avulsion (d), ATiFL tear (e), and ATiTL tear (f).</i>	57
Figure 4-8 <i>Representative plot of the ATiFL and ATiTL strains versus tibia rotation in a simulation of the combination ATiFL and ATiTL injury scenario (specimen 2, stiff shoe).</i>	58
Figure 5-1 <i>The surrogate ankle taped to the polycarbonate plate using Elastikon (a), PowerFlex (b), and Sher-Light (c).</i>	69
Figure 5-2 <i>The surrogate limb was attached to the testing machine</i>	70
Figure 5-3 <i>Marker arrays were placed on the subject's anterior tibia, about 10 cm distal to the patella, and the calcaneal tuberosity.</i>	72
Figure 5-4 <i>Three orthogonal axes of the ankle. Rotations about these axes are described as plantarflexion/dorsiflexion, eversion/inversion, and internal/external rotation.</i>	74
Figure 5-5 <i>Torque-rotation curves for the three tape designs and two shoe designs from rotational stiffness tests (a), and rotational stiffness values determined from the slopes of the torque-rotation curves (b). Curves with different symbols (* # † ¥) indicate statistically different stiffness between designs.</i>	77
Figure 5-6 <i>Mean ankle joint dorsiflexion-tibia rotation curves for the three tape (and no-tape) designs from an in vivo external foot rotation (n=6). There were no significant differences between tape designs.</i>	78
Figure 5-7 <i>Mean ankle joint dorsiflexion-tibia rotation curves for the three tape (and no-tape) designs from an in vivo external foot rotation (n=6). There were no significant differences between tape designs.</i>	78
Figure 5-8 <i>Mean ankle joint eversion-tibia rotation curves for the three tape (and no-tape) designs from an in vivo external foot rotation (n=6). Different symbols (* #) indicate statistically different curves.</i>	79

Figure 5-9 Predicted anterior tibiofibular ligament (ATiFL) (a) and anterior tibiotalar ligament (ATiTL) (b) strain versus tibia rotation for an ankle constrained with tape stiffness ranging from 0 to 30 Nm/deg. Inputs for ankle joint motion were based on predictive equations 3a-3c.	81
Figure 6-1 Marker set of the Oxford Foot Model (Carson et al., 2001). The subjects stood on one foot and performed an internal rotation of the body (external rotation of the foot).....	89
Figure 6-2 Sample of a moment versus time plot (left) and rotation versus time plot (right) for all three movements: internal-external rotation, inversion-eversion, and plantarflexion-dorsiflexion. Data from the loading phase (shaded in the figure) for moment vs. time were extracted and plotted against the extracted rotation vs. time data, as shown in Figure 6-3.....	90
Figure 6-3 Samples of moment versus rotation plots in the loading phase for internal-external rotation (left), inversion-eversion (right), and plantarflexion-dorsiflexion (bottom).....	91
Figure 7-1 Strains in the ATiFL and two deltoid ligaments (ATiTL and TiNL) for neutral and everted simulations.	98
Figure 7-2 Representative plot of the ATiFL and ATiTL strains versus tibia rotation.....	101
Figure 7-3 Mean ankle joint dorsiflexion, external rotation, and eversion vs. tibia rotation for three tapes and a tapeless condition.	103
Figure 7-4 Predicted anterior tibiofibular ligament (ATiFL) (a) and anterior tibiotalar ligament (ATiTL) (b) strain versus tibia rotation for an ankle constrained with tape stiffness ranging from 0 to 30 Nm/deg. Inputs for ankle joint motion were based on predictive equations 3a-3c.	104
Figure A-1 Typical MIMICS interface	112
Figure A-2 Orthogonal coordinate axes on the tibia, talus, and calcaneus.....	118
Figure A-3 Marker arrays in a cadaver ankle (a) and human subject (b)	119

CHAPTER 1:

INTRODUCTION AND BACKGROUND

Ankle Anatomy and Kinematics

The ankle plays an important role in both athletic performance and everyday movement. The ankle bones include the tibia, fibula, talus, and calcaneus and contacts between these bones define the distal syndesmotic joint, the talocrural joint, and the subtalar joint (Figure 1-1). The ligaments that connect the ankle bones can be divided into three groups (Figure 1-2). The lateral collateral ligaments consist of the anterior talofibular ligament (ATaFL), interosseous talocalcaneal ligament (ITaCL), calcaneofibular ligament (CaFL), and posterior talofibular ligament (PTaFL). The medial ligaments consist of the anterior deltoid—the anterior tibiotalar ligament (ATiTL) and tibionavicular ligament (TiNL)—and the posterior deltoid—the posterior tibiotalar ligament (PTiTL) and tibiocalcaneal ligament (TiCL). The distal syndesmotic ligaments include the anterior tibiofibular ligament (ATiFL), interosseous ligament (IOL), and posterior tibiofibular ligament PTiFL) (Golano et al., 2010).



Figure 1-1 *Medial view of the bony anatomy of the ankle*

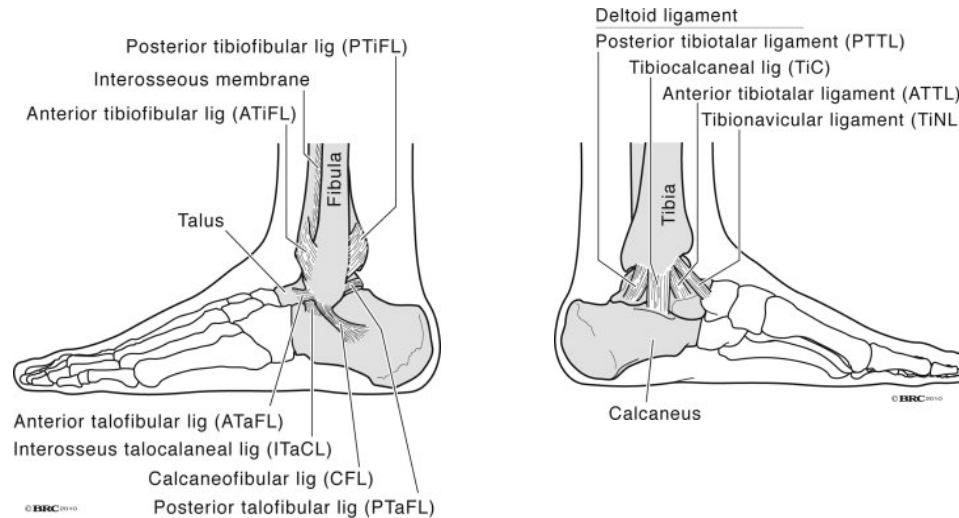


Figure 1-2 Lateral (left) and medial (right) view of the osteoligamentous ankle anatomy

Motion of the ankle is complex and involves coupled motion across three axes (Figure 1-3).

Rotation about the y-axis (medial-lateral) is called plantarflexion when the toes rotate away from the body and dorsiflexion when the toes rotate towards the body. Rotation about the x-axis (long axis) is called eversion when the bottom of the foot faces away from the body center and inversion when the bottom of the foot points towards the body center. Rotation about the z-axis (inferior-superior) is called internal rotation when the long axis points towards body center and external rotation when the long axis points away from the body center. Motion of the talocrural joint is primarily responsible for plantarflexion/dorsiflexion and internal/external rotation while motion of the subtalar joint is primarily responsible for inversion/eversion.

Motion of the ankle rarely isolates one of these three rotations, resulting in coupled motions due to the bony and ligamentous constraints of the ankle. Eversion and external rotation are strongly coupled and both weakly coupled with dorsiflexion. Inversion and internal rotation are also

strongly coupled and weakly coupled with plantarflexion. Forced rotation about one axis usually results in a ‘transferral of rotation’ in which rotations occur about the other axes in order to dissipate torsion (Hicks, 1953, Lundberg et al., 1989b). When this natural response of the ankle is compromised by restricting movement about one or more axes, increased strain is generated in ligaments or bones resulting in injury.

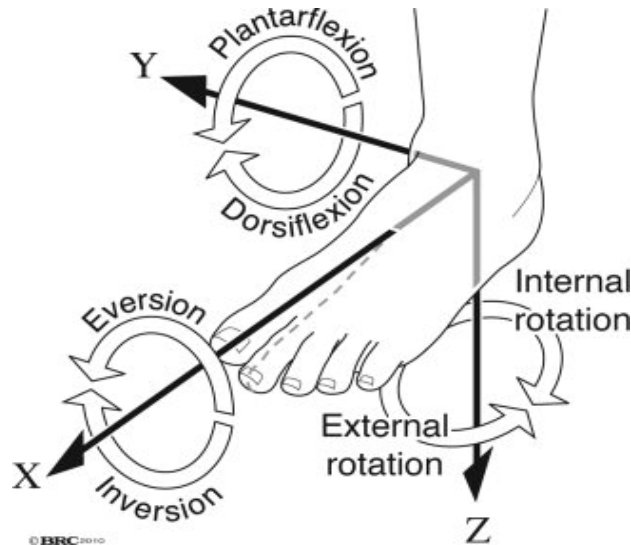


Figure 1-3 *The three motions of the ankle illustrated about a Cartesian coordinate system*

Ankle Injury in Sports

Damage to the ankle is the most frequently observed injury in the emergency room (Boruta et al., 1990) and accounts for 10-30% of all sports injuries (Waterman et al., 2010). In some sports, these percentages can be even higher: Garrick and Requa report that the rate could be as high as 74% in softball, 76% in racquet sports and football, 77% in weight lifting and dancing, 79% in basketball, and 82% in volleyball (Garrick and Requa, 1989). These injuries can also be debilitating with up to 40% of individuals with a history of ankle injury having complaints interfering with daily life (Golano et al., 2010, Gerber et al., 1998). These interferences with

daily life include pain, instability, crepitus, weakness, stiffness, and swelling (Yeung et al., 1994). In professional sports, absence of key players due to ankle injury may result in defeats in major games, as well as tremendous economic losses (Fong et al., 2007). Because of these detrimental effects, researchers are continuously working on ankle injury prevention.

Inversion Injuries

Most commonly, damage occurs to the lateral ligamentous complex and the primary mechanism of these injuries is inversion (Renstrom and Konradsen, 1997, Beynnon et al., 2002). If the ankle is in plantarflexion, the first ligament injured during inversion is the ATaFL (Dias, 1979). When the ankle is in neutral flexion, some studies report that the first ligament injured is the CaFL (Parenteau et al., 1998), while others report a roughly even distribution between CaFL and ATaFL injury (Funk et al., 2002, Rasmussen and Kromannandersen, 1983). Continued inversion has also been shown to injure the PTaFL (Dias, 1979). Many cases of lateral ankle sprain involve additional injury to other soft tissue structures (Fallat et al., 1998) and, in severe cases, avulsion fractures to the lateral malleolus common in children and adults over 40 years old.

External Rotation Injuries

Excessive external rotation has been shown to result in both medial and high ankle injuries (Waterman et al., 2010, Gerber et al., 1998). Medial ankle injuries involve damage to the TiNL and the ATiTL, while high (or syndesmotic) ankle injuries are defined as damage to the ATiFL (Figures 1,2). High ankle sprains are mostly prevalent in football, team handball, basketball, and soccer while medial ankle sprains occur most commonly in rugby, gymnastics, and soccer (Waterman et al., 2011). While less common than inversion injuries, medial and high ankle injuries are of particular interest to researchers due to their longer recovery time (Boytim et al.,

1991), and potential for long-term ankle dysfunction (Gerber et al., 1998, Waterman et al., 2010), especially in high-intensity sports.

Often the above ankle injuries occur in conjunction with one another (Williams et al., 2007, Miller et al., 1995, Edwards and Delee, 1984). The various mechanisms of these injuries have been described in previous studies (Hughes et al., 1979, Laugehansen, 1950), but all occur as a result of external rotation. According to the Weber-C classification, external rotation to an everted ankle puts maximum tension on the medial side of the ankle, first causing rupture of the ATiTL, or fracture of the medial malleolus. The injury may stop here, referred to as the pronation-external rotation stage [25]. Once the ATiTL ruptures, the talus may continue to externally rotate and move laterally causing rupture of the ATiFL. However, another mechanism of failure has been proposed in which the ATiFL fails first: axial loading of a pre-everted ankle causes lateral translation of the talus and pre-strain in the ATiFL, followed by external rotation which fails the ATiFL (Wei et al., 2012b).

Previous laboratory studies have produced medial and syndesmotic injuries in cadavers, but the majority of these injuries were fractures. A recent study by Haraguchi and Armiger show that external rotation to an everted foot with 700 N of axial load results in the classic Lauge-Hansens *supination*-external rotation injury pattern: a short oblique fibular fracture starting at the level of the tibial plafond and running in a postero-superior direction, disruption of the ATiFL and PTiFL complexes, and either a medial malleolar fracture or ATiTL tear (Haraguchi and Armiger, 2009). These findings have been confirmed by an analysis of injury videos posted on YouTube.com which show that five out of seven ankles subjected to pronation-external rotation

loading show a fracture pattern that is consistent with the pattern described by Haraguchi (Kwon et al., 2010). Other studies which have rotated ankles to failure in a neutral position result in a nearly even distribution of medial and lateral injuries with a low incidence of syndesmotric injuries and a high incidence of fractures (Rasmussen and Kromannandersen, 1983, Hirsch and Lewis, 1965). A recent study by Wei, however, produced both medial and syndesmotric ligamentous injuries in cadaver ankles (Wei et al., 2012b). All ankles were pre-dorsiflexed prior to rotation, but left ankles were pre-everted as well. Wei observed high ankle sprain in the pre-everted left ankles and medial ankle sprain in the neutral right ankles.

Risk Factors for External Rotation Injuries

Shoe-Surface Interface

Traction, the resistance to relative motion between a shoe outsole and sports surface (Villwock et al., 2009b), can be quantified in either the linear or rotational motions (Kent et al., 2012). While linear traction is necessary for performance, it is generally accepted that excessive rotational traction may increase the risk of ankle injury (Nigg and Yeadon, 1987, Lambson et al., 1996). Torg and Quedenfeld (Torg and Quedenfeld, 1973) were among the first researchers to document the interaction between shoes and surfaces as an injury risk factor. They noted that the size and number of cleats are correlated with the frequency of ankle injury, with less aggressive cleats generating fewer injuries. Livesay et al. (Livesay et al., 2006) later noted that shoe-surface rotational stiffness, defined as the rate at which moment is developed under shoe rotation on the surface, may act as another risk factor for external rotation ankle injuries. The Livesay study involved measuring the rotational traction and shoe-surface rotational stiffness between 5 playing surfaces and 2 types of shoes. The results show that differences in shoe-surface rotational stiffness were greater than differences in traction, suggesting that rotational stiffness

may be a more sensitive indicator of interaction between shoes and surfaces than rotational traction. A more recent study by Villwock et al. (Villwock et al., 2009c) involved measuring both the traction and shoe-surface rotational stiffness between 10 football shoe models and 4 playing surfaces. The study concludes that artificial surfaces yield significantly higher peak moments and shoe-surface rotational stiffness than natural grass, indicating that natural grass may be a better surface for mitigating rotational injury risk.

Shoe Stiffness

While shoe-surface interface has been studied as an ankle injury risk factor for decades, it has only recently been proposed that the constraint on the ankle has an effect on the type of injury generated under external rotation (Wei et al., 2011d). A cadaver study by Wei et al. has compared the effect of two different foot constraints on motion of a cadaver ankle during external rotation: a potted constraint in which the calcaneus was fixed and a taped constraint in which the calcaneus was free to collapse (Wei et al., 2010). When the potted foot was externally rotated, the talus experienced dorsiflexion and inversion, stretching the posterior-lateral aspect of the ankle and generating PTaFL injury. However, external rotation of the taped foot resulted in talus eversion and plantarflexion, stretching the anterior-medial aspect of the ankle and generating ATiTL failure.

Another study compared the motion of the talus when externally rotated in football shoes (Wei et al., 2012a). The study first measured the rotational stiffness (the rate at which moment was developed under external foot rotation in the shoe) of four different shoes. The rotational stiffness in each of the four designs was significantly different from one another, indicating that the material constructing the upper of the shoe may be a unique property. The stiffest and most

flexible shoe designs were selected for the cadaver study. Twelve (six pairs) cadaver ankles were externally rotated 30 degrees in either the stiff or flexible shoe while motion capture tracked the rotations of the talocrural joint using reflective marker arrays screwed into the talus and tibia. Results of the motion capture analysis have shown that ankles in the stiff shoe yielded more talocrural rotation, but less talocrural eversion than the ankles in a flexible shoe. This suggests that ankles in stiff shoes experience higher ATiFL injury risk, but lower ATiTL injury risk than those in flexible shoes, but this had not yet been tested at failure levels.

Computational Modelling

Validated computational models can be used to understand joint function and, clinically, to understand and prevent sports injuries. Researchers generally develop models that are either finite element analysis-based (FEA) or multibody kinematic- or dynamic- based (Chao, 2003, Cheung et al., 2006, Konradsen and Voigt, 2002, Kwak et al., 2000, Iaquinto and Wayne, 2010). Since both approaches have their advantages, the method chosen depends on the information sought. While FEA models have the advantage of solving for small deformations, rigid body models are able to solve the mechanics of large structures using highly efficient algorithms, which execute much faster than FEA models (Kwak et al., 2000). These models are driven by experimental measurements of bone movements, assumptions about joint degrees of freedom, and assumptions regarding muscle forces that drive the motion of bones (Holzbaur et al., 2005, Kitaoka et al., 1997, Konradsen and Voigt, 2002, Kwak et al., 2000). Liacouras and Wayne have developed a 3D computational approach to model the lower leg in order to simulate cadaver ligament sectioning studies of syndesmotoc injury and ankle inversion stability (Liacouras and Waynel, 2007). A more recent model by Wei et al. (Wei et al., 2011c) has been developed and validated against two cadaver studies of ankle ligament strains (Colville et al., 1990a) and ankle

joint torques (Wei et al., 2010). This model has proven its ability to simulate footwear behavior in the ankle (Wei et al., 2012a), predict ligament strains during an *in vivo* inversion ankle sprain (Fong et al., 2011), and estimate ligament strains in human subjects during external rotation (Wei et al., 2011c). However, fewer models incorporate ‘subject-specific’ parameters such as articulation geometry, ligaments, and other anatomical features. Specifically in the ankle, the curvature of the talar dome (top surface of the talus) determines the stability of the ankle in the anterior-posterior direction (Kleipool and Blankevoort, 2010) and the talar facets (contacting surfaces) have a significant impact on the position of the axis for movements between the talus and calcaneus (Barbaix et al., 2000). Variations in these parameters could have a significant impact on the results of a rigid-body simulation.

Summary and Objectives

Two key phases in preventing injury include understanding the mechanism responsible for the injury and decreasing the probability of this mechanism occurring. This can be accomplished through investigations of clinical injuries, cadaveric testing, understanding *in vivo* kinematics, and computational modelling. Cadaveric testing offers advantages in the control that can be taken with experimental design, precision when measuring the forces and motions during injury, and in-depth pathology afforded by post-test dissection. However, these tests often neglect muscle action, which occurs during *in vivo* injuries. Yet, researchers can supplement information drawn from cadaver studies with that measured from *in vivo* human subjects performing similar motions in order to gain a fuller understanding of human ankle joint movement. Additionally, specimen-specific rigid body modelling provides a way to cost-effectively assess injury risk using boundary conditions from both cadaveric and *in vivo* tests.

One of the hypotheses of the current research is that the movement of the talocrural joint and location of injury during ankle external rotation depends on the position of the ankle prior to rotation and the amount of constraint on the ankle. Reporting the specific injury generated as a result of foot constraint during external ankle rotation could aid in designing athletic shoes that mitigate injury risk without compromising performance and comfort. Another hypothesis of the research is that specimen-specific, rigid body modelling can be utilized to simulate injury-level ankle rotation in addition to modelling the effect of various shoe rotational stiffnesses on talocrural and subtalar joint movement. The information from these models could help quantify failure properties of various structures of the ankle and may help mitigate the risk of rotational ankle injury through footwear design.

CHAPTER 2:

SPECIMEN-SPECIFIC COMPUTATIONAL MODELS OF ANKLE SPRAINS PRODUCED IN A LABORATORY SETTING

ABSTRACT

The use of computational modeling to predict injury mechanisms and severity has recently been investigated, but few models report failure level ligament strains. The hypothesis of the study was that models built off neutral ankle experimental studies would generate the highest ligament strain at failure in the anterior deltoid ligament, comprised of the anterior tibiotalar ligament (ATiTL) and tibionavicular ligament (TiNL). For models built off everted ankle experimental studies the highest strain at failure would be developed in the anterior tibiofibular ligament (ATiFL). An additional objective of the study was to show that in these computational models ligament strain would be lower when modeling a partial versus complete ligament rupture experiment. To simulate a prior cadaver study in which six pairs of cadaver ankles underwent external rotation until gross failure, six specimen-specific models were built based on computed tomography (CT) scans from each specimen. The models were initially positioned with 20° dorsiflexion and either everted 20° or maintained at neutral to simulate the cadaver experiments. Then each model underwent dynamic external rotation up to the maximum angle at failure in the experiments, at which point the peak strains in the ligaments were calculated. Neutral ankle models predicted the average of highest strain in the ATiTL ($29.1 \pm 5.3\%$), correlating with the medial ankle sprains in the neutral cadaver experiments. Everted ankle models predicted the average of highest strain in the ATiFL ($31.2 \pm 4.3\%$) correlating with the high ankle sprains documented in everted experiments. Strains predicted for ligaments that suffered gross injuries were significantly higher than the strains in ligaments suffering only a partial tear. The

correlation between strain and ligament damage demonstrates the potential for modeling to provide important information for the study of injury mechanisms and for aiding in treatment procedure.

INTRODUCTION

Ankle injury is the most common injury in sports and accounts for 10-30% of sports injuries (Waterman et al., 2010). Injury to the lateral ligamentous complex occurs under excessive foot inversion and is known as a “lateral ankle sprain” (Colville et al., 1990b). Injury to the anterior deltoid ligament (ADL), which consists of the tibionavicular ligament (TiNL) and the anterior tibiotalar ligament (ATiTL), is known as a “medial ankle sprain” (Wolfe et al., 2001). High ankle sprains occur in the distal tibiofibular syndesmosis, which is comprised of the anterior and posterior tibiofibular ligaments (ATiFL and PTiFL) and the interosseous ligament (IOL) (Dattani et al., 2008). While most ankle sprains are lateral ankle injuries, high and medial ankle injuries are typically more severe and result in more recovery time (Wolfe et al., 2001). High ankle sprains, in particular, occur in 11-20% of ankle injuries, depending on the level of competition (Hopkinson et al., 1990, Guise, 1976). Historically these injuries have been underdiagnosed and assessment in terms of severity and optimal treatment has not been determined. More recently, a heightened awareness in sports medicine has resulted in more frequent diagnoses of high ankle sprains (Williams et al., 2007).

The clinical literature has mostly attributed both high and medial ankle sprains to external foot rotation (Waterman et al., 2010, Boytim et al., 1991). Other studies, however, have indicated that the mechanism of high ankle sprain involves a combination of dorsiflexion, eversion, and external rotation (Wolfe et al., 2001, Boytim et al., 1991, Waterman et al., 2011). A computational model of the ankle was developed in our laboratory in order to further investigate ankle injuries occurring in cadaver studies or a clinical setting. The model was first built to study the effect of constraints of the foot on ankle injury using human cadaver studies (Wei et

al., 2010, Wei et al., 2011d). The model generated ankle torques, rotational stiffnesses, and ligament strains that were consistent with the cadaver data. The model was later used to parametrically investigate the roles of dorsiflexion, eversion, and external rotation on high ankle sprains. Since the damage experienced in ankle sprains is primarily due to mechanical disruption from excessive deformation of ligaments (Villwock et al., 2009c), ligament strain was used in the model to indicate ankle sprain risk. In a Wei et al. study (Wei et al., 2012b), the simulations suggest that an everted, externally rotated foot generates the highest strains in the ATiFL, while a neutral (non-everted), externally rotated foot generates the highest strains in the ADL. Despite this useful information provided by the previous model, the input motions used in those simulations correlate with subfailure level of sprains, and therefore injurious ligament strains are unknown.

Recently our laboratory conducted external rotation, failure level experiments on pairs of dorsiflexed, human cadaver ankles that were either everted 20 degrees or kept neutral prior to failure (Wei et al., 2012b). Neutral ankles failed by injury to the ADL. The injuries involved partial and complete ruptures, tibial avulsion in one case, and, in another case, a combination of partial tears in the ADL and ATiFL. In all everted ankles taken to failure under external rotation, cases of complete and partial ruptures of the ATiFL were reported. This was the first study to produce isolated ATiFL injury, representative of a high ankle sprain, in a laboratory setting.

In the current study, specimen-specific computational models were developed to investigate ankle ligament strains generated in the eversion study of Wei et al. (Wei et al., 2012b). Knowing the relative motion of the tibia and talus during that study, commercial software was used to

determine the ligament strains at failure in the current study. Our hypothesis was that in the neutral ankle externally rotated to failure, the highest ligament strain would be generated in the ADL. For everted ankles the highest strain would be developed in the ATiFL. An additional objective of the study was to show that in these computational models ligament strain would be lower in specimens with a partial ligament rupture.

METHODS

No new experimental work was performed for this study. However, details of the previous study from which the specimen-specific computational models were based will be presented, in brief, in order to adequately describe the current study.

Cadaver Experiment

Six male cadaver lower limbs(aged 56 ± 12 years) were thawed for 24 hours and were transected approximately 15 cm distal to the center of the knee (Wei et al., 2012b). The foot was taped to a polycarbonate plate and inserted into a rectangular tray (Figure 2-1). Both the right and the left limbs were dorsiflexed 20 degrees. The left limbs were positioned at 20 degrees of eversion, while the right limbs were initially positioned in neutral with regard to the inversion/eversion rotation prior to dynamic external foot rotation.

A compressive preload of 1500 N was applied axially and internal tibia rotation (external foot rotation) was input in position control at a frequency of 1 Hz (0.5 seconds to peak rotation for each test). The tests started with 20 degrees of rotation and then repeated in 10 degree increments successively until an observed injury to the ankle. A steep drop in the magnitude of

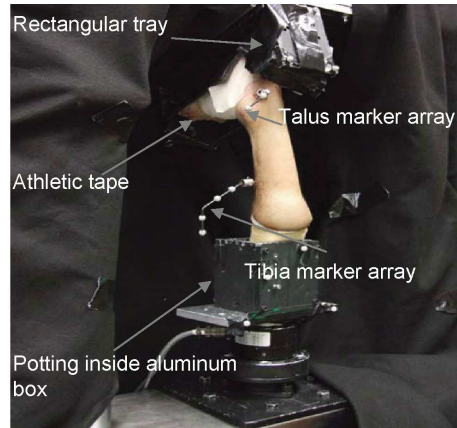


Figure 2-1 *Setup for the cadaver experiment by Wei et al..*

the torque signal indicated failure, at which point the foot rotation was documented and the ankle was examined for injury after each experiment (Table 2-2-1). Prior to the test, reflective marker arrays were screwed into the talus and tibia, allowing an analysis of the motion of the talus with respect to the tibia using a Vicon motion capture system (Oxford Metrics Ltd., Oxford, United Kingdom) (Figure 2-1 and Table 2-2). While these arrays were randomly oriented on the tibia and talus, coordinate transformations were set-up to determine the orientation of the tibia marker set with respect to the long axis of the tibia and the talus marker set with respect to the medial-lateral axis of the talus, based on the initial orientation of a line between the medial and lateral malleoli. This provided an anatomical axis for each bone. The third joint coordinate axis (floating axis) was determined by the cross product of these anatomical-based vectors. Clinical angles were determined as previously described by Soutas-Little et al. (Soutas-Little et al., 1987) (Table 2-2).

Model Development

Computed tomography (CT) scans were performed on the right limb from each specimen pair to obtain three-dimensional joint anatomy with 0.6 mm spacing between images and in-plane spatial resolution of 0.508 mm. Scans were performed with the foot taped to a polycarbonate plate and placed in a fixture to maintain neutral flexion during scanning. The CT scans were transferred from Digital Imaging and Communications in Medicine (DICOM) files into Materialise's Interactive Imaging Control System (MIMICS, Leuven, Belgium) software. The individual bones were separated and meshed as solid bodies. A "mask" was created for each bone, accurately reflecting the surface geometry of the bone. In order to reduce the size of the files, the bones were remeshed using the auto remesh feature. Each bone was then exported as a stereolithography (STL) file and imported into Solidworks 2009 (Trimech Solutions, LLC, Columbia, MD) as mesh files where they were simplified using the ScanTo3D package.

SolidWorks Motion was used to add ligaments (modeled as tension-only linear springs) and assemble the bones in their anatomically correct orientation based on the CT scans. Insertion locations of the ligaments were determined from both dissection and an anatomical atlas (Netter and JT, 2003). A pre-load was induced on each ligament by reducing its length by 2% from the scanned lengths, as in Wei et al. (Wei et al., 2011d). Three-dimensional contacts were implemented, similar to the procedure outlined by Iaquinto and Wayne (Iaquinto and Wayne, 2010), between adjacent bones in order to prevent overlap during the simulation. This was done by calculating the interference at each time step and applying an outward force if any overlap was detected. The force was a function of the material stiffness k (10,000 N/mm), the penetration depth g (0.001 mm), the exponent e (1.75), the damping coefficient c_{max} (50 N/mm-

s), penetration depth at maximum damping d_{max} , and penetration velocity $\frac{dg}{dt}$. Friction and the effects of gravity were considered negligible.

$$F_n = kg^e + \left(\frac{dg}{dt} \right) f(c_{max}, d_{max})$$

Since toe involvement was likely minimal in the cadaver study, the phalanges were excluded from the model.

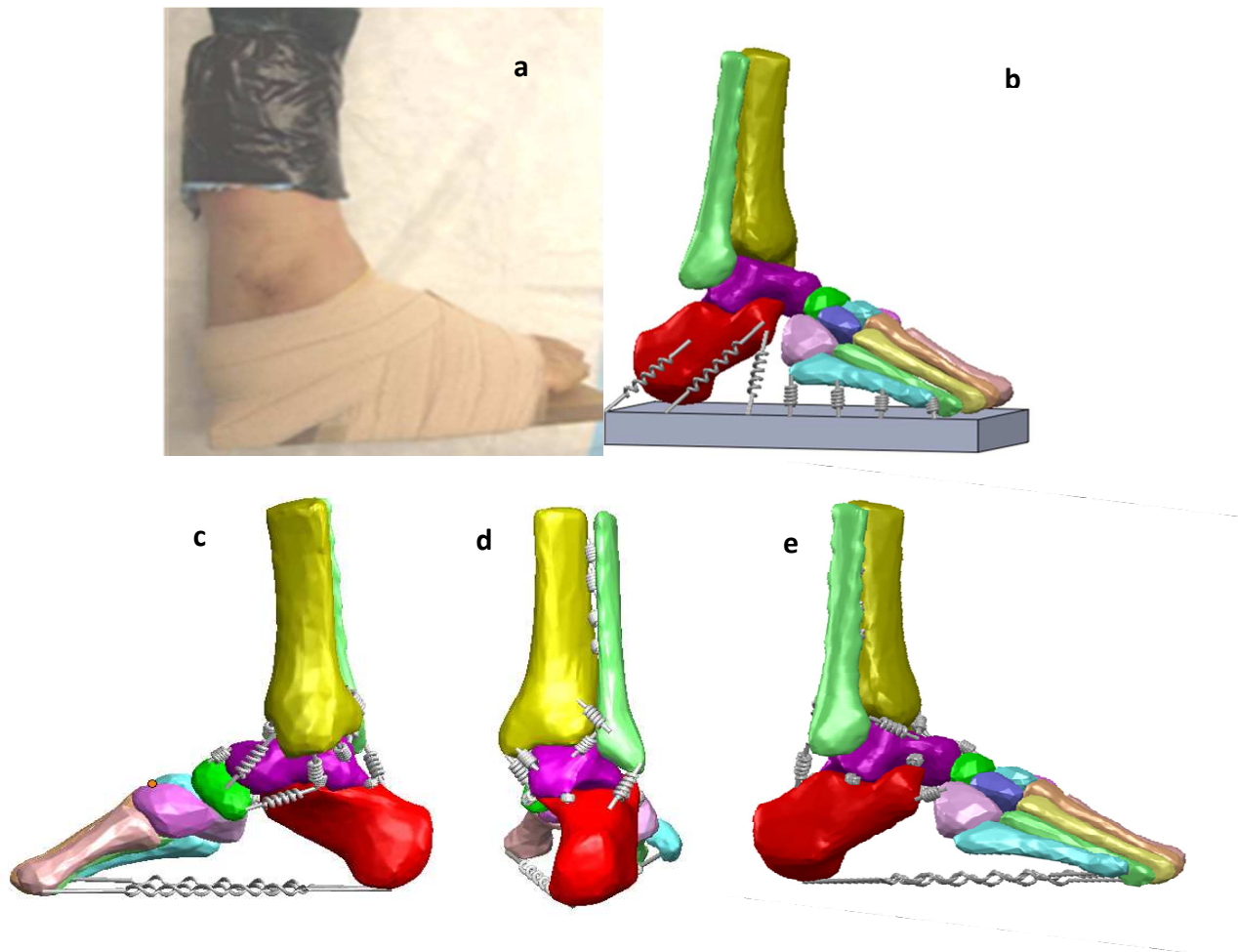


Figure 2-2 *The cadaver taping pattern (a) and the model taping pattern represented by springs (b). Note: for clarity all ligament springs and the plate springs on the medial side of the ankle were set invisible.*

The neutral position of the ankle from the CT scan was maintained. The tibia was fixed in space while the fibula, calcaneus, and talus were free to move. Due to minimal relative motion among the forefoot bones and in order to reduce run-time, the rest of the bones were fused together and moved as a rigid body. The model included 22 linear spring elements (Figure 2-2) to represent ligaments with stiffness values taken from the literature, as referenced by Wei et al. (Wei et al., 2011d).

Simulation

To simulate the cadaver ankle rotation, a plate was created in SolidWorks with dimensions from the experiment. The plate was attached to the foot with 14 springs representing the athletic taping pattern used on the cadaver feet (Figure 2-2b).

Motors were used to drive the motion of the plate, with reference to the fixed tibia (as per the cadaver experiment), with one motor for plate dorsiflexion, one for plate eversion, and one for plate external rotation. For each ankle model in SolidWorks Motion, the plate was dorsiflexed 20 degrees, everted 20 degrees (for models based on everted foot tests), and an axial pre-load of 1500 N was applied to the proximal end of the model (distributing the load between tibia and fibula with one-sixth of the loading on the fibula). The plate was then externally rotated to the angle at which injury was documented in the cadaver experiments. All motions were relative to the fixed tibia. Since the stiffness and preload of the athletic tape were not quantified in the experiment, stiffness of all spring elements representing the athletic taping pattern (Figure 2-2b) was iteratively and simultaneously adjusted in 10 N/mm increments to help match the model external talus rotation to the experimental talus rotation. Thus one stiffness was applied to all

those springs that represented the effect of tape. Ligament strains, defined in percentage as the relative elongations of ligaments, were determined at the plate rotation needed to generate gross ankle injury in the cadaver experiments (Table 2-1).

Two-sample t-tests were performed to compare failure strains for partial tears and total ruptures, for comparing the model generated talus rotations with experimental talus rotations, for comparing ATiFL failure strains with ADL failure strains, and for comparing experimental plate rotations with experimental talus rotations. P values less than 0.05 were considered significant in all tests.

RESULTS

Injuries reported in the cadaver experiments of Wei et al. (Wei et al., 2012b) were used in this study (Table 2-1). The injuries consisted of partial tears and complete ruptures of the ATiFL (Figure 2-3a and 2-3b, respectively), partial tears and ruptures of the ATiTL (Figures 3c and 3d, respectively), tibial avulsion of the ATiTL (Figure 2-3e), partial tear of the TiNL (Figure 2-3f), and a spiral fracture of the fibula. At failure, comparisons between the rotations of the plate and talus showed that in the neutral case, talus rotations were significantly less than plate rotations ($p < 0.001$), but not so in the everted case ($p = 0.11$) (Tables 2-1 and 2-2) [13].

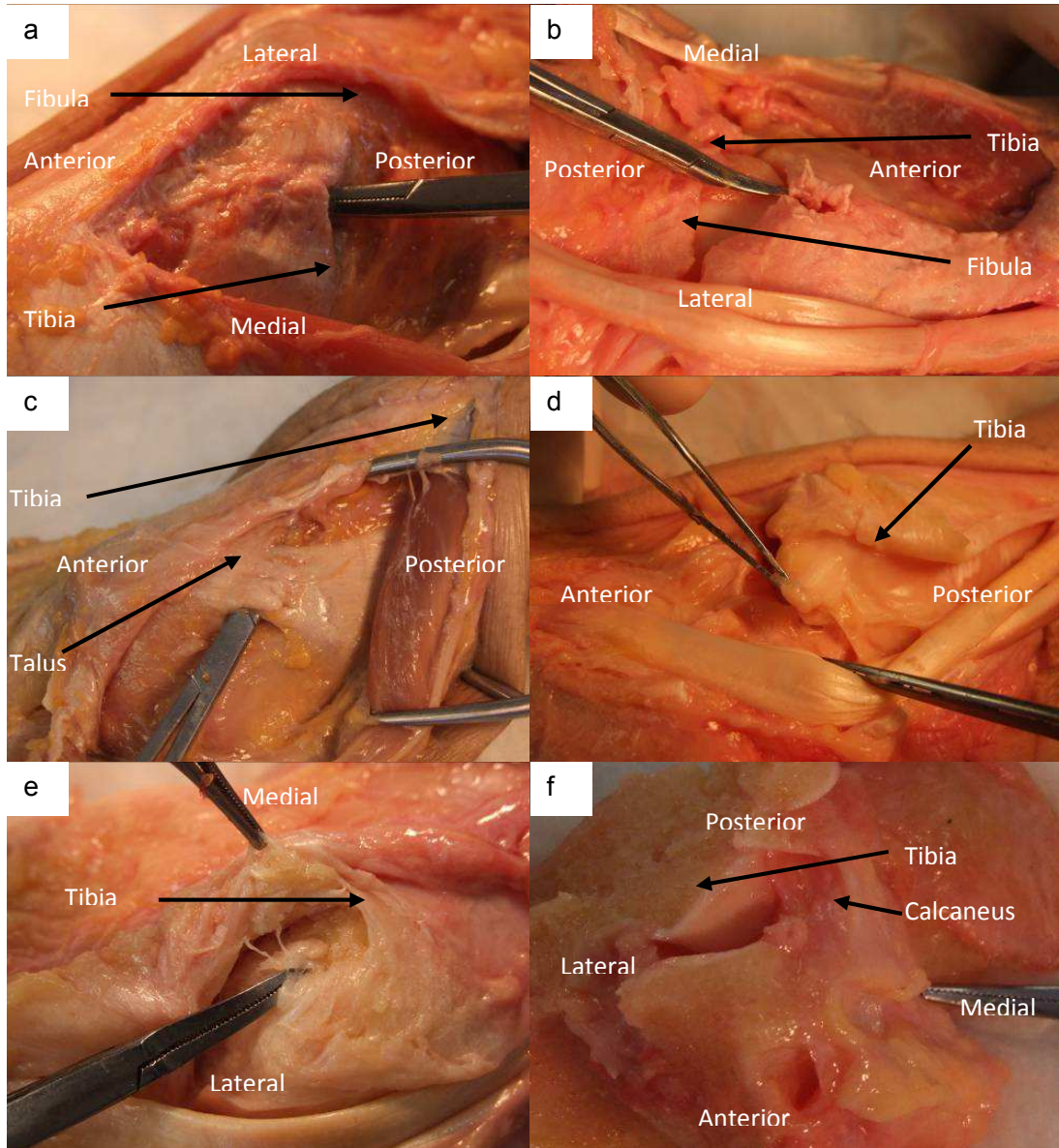


Figure 2-3 Injury mechanisms reported from the cadaver study by Wei et al. (Wei et al., 2012b). Partial tear of the ATiFL (a); Rupture of the ATiFL (b); Partial tear of the ATiTL (c); Rupture of the ATiTL (d); Tibial avulsion of the ATiTL (e); Partial tear of the TiNL(f). Note: the location of injury is shown with a hemostat.

The stiffness of the simulated athletic tape was variable between specimens and between 300 N/mm to 400 N/mm. Comparisons of the talus rotations showed that the model generated talus rotations were not statistically different than the experimental rotations ($p>0.88$) (Table 2-2).

Models developed for the neutral experiments showed the highest strain generated in the ATiTL ($29.1 \pm 5.3\%$) followed by the ATiFL ($22.3 \pm 0.8\%$) and the TiNL ($16.1 \pm 4.2\%$) in the three of four cases in which ligament failure occurred (Figure 2-4). These results are in agreement with observations of ATiTL failure from the cadaveric experiment that occurred in all but one of the neutral cadaver experiments in which ligament failure occurred (Table 2-1). In specimen 3, failures were reported in the TiNL and ATiFL (Table 2-1). In this model the ATiFL strain was comparable with that of the TiNL, and it was the highest among all ATiFL strains for the neutral simulations (Figure 2-5).

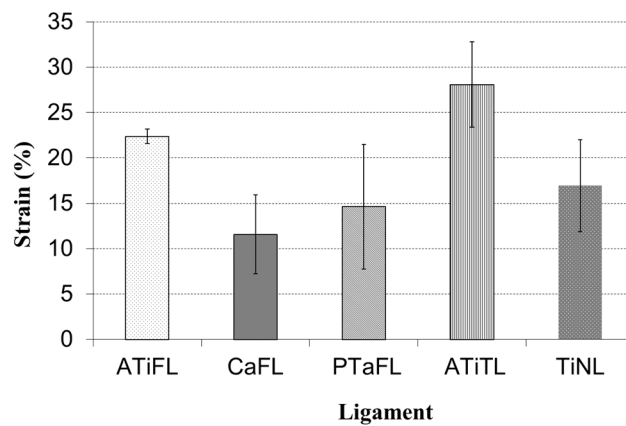


Figure 2-4 Ligaments with average model predicted strains greater than 2% for the neutral case in 3 of 4 cases in which ligament injury occurred

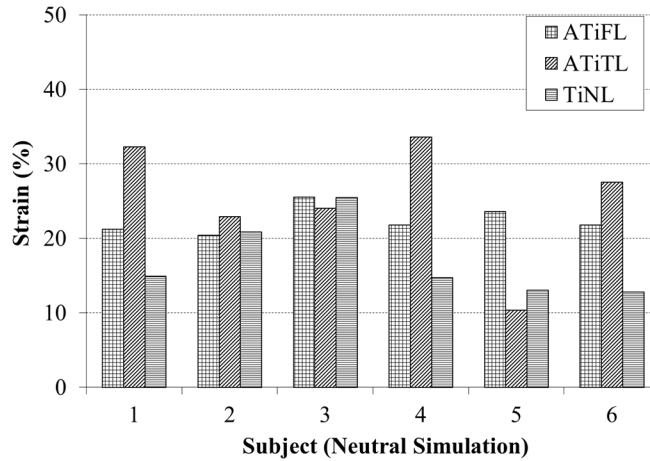


Figure 2-5 Strains in the ATiFL and the two deltoid ligaments (ATiTL and TiNL) for the neutral case for each specimen modeled

Computational models of the everted ankle experiments showed the highest strains in the ATiFL ($31.2 \pm 4.3\%$) followed by the TiNL ($18.5 \pm 5.6\%$) and the ATiTL ($18.1 \pm 5.0\%$) (Figure 2-6). These data coincided with the observation of ATiFL injury in all of these cadaver experiments (Table 2-1). All but two of the specimens from the cadaver study suffered complete ruptures (specimens 2 and 5 suffered partial tears) and the corresponding strains can be seen in Figure 2-7. For ruptured ligament cases there was no significant difference between ATiFL failure strain and ATiTL failure strain ($p > 0.7$). For partial tears, there was no significant difference between ATiFL failure strain and ADL failure strain (combining cases of ATiTL failure and TiNL failure) ($p > 0.45$).

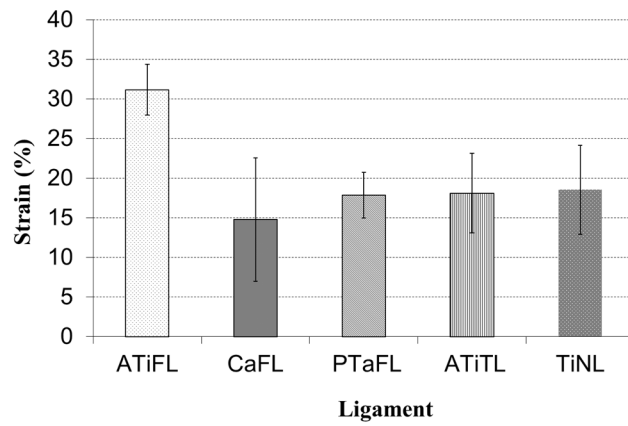


Figure 2-6 Ligaments with average model predicted strains greater than 2% for the everted simulations

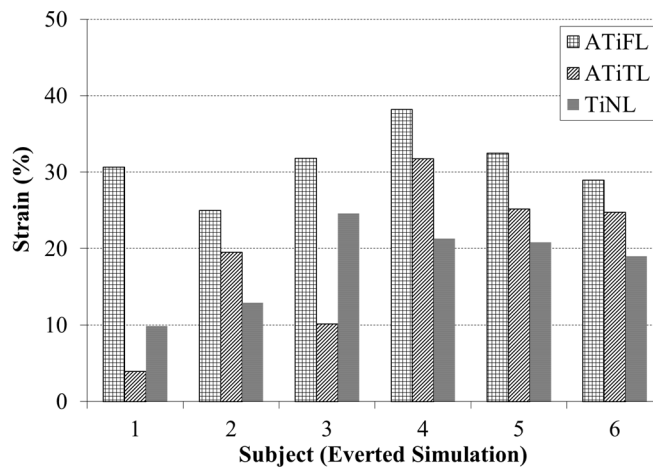


Figure 2-7 Strains in the ATiFL and the two deltoid ligaments (ATiTL and TiNL) for the everted simulations

Table 2-1 *Results of the cadaver experiment for the neutral and everted ankle*

Specimen	Plate failure rotation (deg)		Failure mode	
	Neutral	Everted	Neutral (R)	Everted (L)
1	36.0	43.4	Tibial avulsion of the ATiTL	Rupture of the ATiFL
2	47.1	55.3	Partial tear of the ATiTL	Partial tear of the ATiFL
3	35.1	50.1	Partial tear of the TiNL and partial tear of the ATiFL	Rupture of the ATiFL
4	39.8	50.0	Rupture of the ATiTL	Rupture of the ATiFL
5	31.1	43.4	Spiral fracture of the fibula	Partial tear of the ATiFL
6	37.0	38.6	Rupture of the ATiTL	Rupture of the ATiFL

Table 2-2 *Comparison of the talus external rotations with respect to the tibia (deg) from the cadaver study with the computational talus rotations*

Specimen	Experimental talus failure rotation (deg)		Computational talus failure rotation (deg)	
	Neutral	Everted	Neutral	Everted
1	20.9	37.7	18.7	38.2
2	29.7	46.4	31.3	44.8
3	23.4	45.7	21.0	47.0
4	25.2	44.7	24.2	43.1
5	17.9	39.7	18.1	37.6
6	22.5	36.5	20.9	37.9

Combining both neutral and everted simulations, strains of $31.8 \pm 3.8\%$ (n=6) computed from the models of experiments that showed grossly ruptured ligaments were statistically greater than $25.5 \pm 4.2\%$ (n=4) for the partial tear simulations ($p=0.046$). Most of the strains for partial tear simulations were less than those for complete ruptures except for the ATiFL strain for specimen 5 in the everted case and for the ATiTL strain for specimen 6 in the neutral case. Additionally the ATiTL strain for specimen 4 in the everted case suggests failure, but this did not occur experimentally. This suggests a slightly mixed correlation between strains and injury modes.

Furthermore, in the neutral model that suffered a spiral fracture experimentally (specimen 5), the ATiFL, ATiTL and TiNL strains (23.6%, 10.4%, and 13.0%, respectively) were below failure levels documented in other experiments. In the ATiTL avulsion case (specimen 1), the ATiFL and TiNL strains (21.2% and 14.9%, respectively) were also below the average failure levels of other simulations. The ATiTL strain, on the other hand, from the model was 32.2%, well above the failure levels given in other simulations.

DISCUSSION

The study supported the hypothesis that the models would generate the highest strains in the ATiFL for the everted foot and in the deltoid ligaments for the neutral foot. As suggested by Wei et al. (Wei et al., 2012b), the lateral talar translation resulting from an everted foot puts strain on the ATiFL by pushing the fibula away from the tibia, since the ligament is oriented along the coronal plane. In the neutral foot, lateral talar translation was minimal during axial load and external rotation, and thus external rotation resulted in straining the deltoid, as this ligament is oriented along the sagittal plane. The study also confirmed that there was a significant difference in strains for cases of complete versus partially ruptured ligaments. In the neutral case, specimen 3 revealed the correct prediction of injury, despite yielding a different result than the other simulations. In all other cases of a neutral foot ligament failure the ATiTL experienced the highest strain, yet the highest strain in specimen 3 was found in the TiNL followed by the ATiFL. This was consistent with the injuries generated in the TiNL and ATiFL in the cadaver study (Table 2-1 and Figure 2-5). Furthermore, the rotations to failure for the neutral foot in specimens 1, 3, and 6 were similar, yet corresponded to different computational ligament strains (Figure 2-5) and this was supported by the observation of different injuries (Table 2-1). This information indicates that specimen-specific modeling may, in some cases,

predict injuries that may not be predictable with a generic model, such as used previously by this laboratory. While differences in the geometry of the trochlea tali and talar facets have both been identified as potential explanations for differences between specimens, a detailed presentation of these differences was beyond the scope of the current experiment.

While little data exists on the failure strains of the ankle ligaments of interest in this study, these failure data are consistent with experimental failure calculations from other ligaments. A study by Beumer et al. (Beumer et al., 2003), for example, reported the force required to rupture the ATiFL, PTiFL, and posterior tibiotalar ligament (PTiTL) to be 500 ± 105 N, 708 ± 91 N, and 446 ± 51 N, respectively. Using the stiffnesses from the literature (Wei et al., 2011d) and ligament lengths from the simulations, the failure forces of the ATiFL, TiNL, respectively, were 610 ± 98 N and 750 ± 190 N, comparable to Beumer's values, while the ATiTL prediction, 170 ± 0 N, was considerably lower. Attarian et al. (Attarian et al., 1985) measured failure strains of bone-ligament-bone preparations in tensile experiments. They documented values of, on average, 53% and 38% for the anterior talofibular ligament (ATaFL) and calcaneofibular ligament (CaFL), respectively, which are higher than the failure strains reported in the current study.

Given that ligament collagen fibers start to tear at approximately half of the failure strain (a so-called grade I ligament sprain) (Yahia et al., 1990), the partial tears might be more representative of grade II sprain injuries, as they occurred at approximately 70% of the total rupture strain. Interestingly, the strains for non-injured ligaments fell below this partial-tear failure strain average for all ligaments in the neutral simulation and all but one ligament (ATiTL for specimen

4) in the everted simulations. This may indicate a low risk of falsely predicting ligament failure for non-injured ligaments in future injury simulation studies.

One limitation of the current study was that we were not able to accurately quantify the ankle-tape structural stiffness of the cadaver study, and thus had to estimate it in our simulations. We attempted to compensate for this aspect by adjusting the spring stiffness that represented the taping of the foot to the plate for each specimen so that the motion of the model talus was similar to that of the cadaver talus for a given level of plate rotation at failure. These values varied between specimens, as the structural stiffness due to the amount of tape stretch in the cadaver study may have actually varied between specimens. Despite potential errors in matching tape stiffness, we believe that as long as the talar motions in the simulations closely matched those of the experiments, the model's ligament strains would provide reasonable estimates of strain. Another limitation of the study was that it assumed simple, linear elastic behavior of the ankle ligaments. While ligaments may behave linearly for small deformations, they do behave non-linearly for failure strains. Because of this, non-linear computational models should be used for failure-level studies in the future. The model also did not account for the viscoelastic properties of ligaments. Funk et al. (Funk et al., 2000) produced non-linear models for eight major ligaments of the foot-ankle complex, which accounted for both their elastic and viscoelastic properties. They concluded that a viscoelastic assumption could also be neglected for very slow ($<0.0001/s$) or very fast ($>1/s$) strain rates, but substantial effects seem to exist on ligament behavior for intermediate strain rates. In the cadaver experiment by Wei et al. (Wei et al., 2012b), the tibia rotation was input at 1 Hz, so the ligaments reached their maximum strain at 0.5s. This means that the failure strain rates were, on average, 1.000/s for partial tears and 0.933

/s for ruptures, indicating that there could be some viscoelastic effect. However, while the model may not currently predict the exact mechanical behavior of ligaments, quantifying failure ligament strains, rather than forces, may be a better indicator of injury tolerance due to the viscoelastic nature of ankle ligaments (Edwards and Delee, 1984, Boytim et al., 1991). This may be supported by earlier studies that show that the ultimate tensile strength of ligaments and tendons increases significantly with strain rate, while ultimate strain does not (France et al., 1987), (Ng et al., 2004). Yet, in order to improve upon the model in future predictions of ankle ligament failure strains from *in vitro* and *in vivo* studies, more accurate constitutive modeling would still seem to be warranted.

The use of specimen-specific ankle modeling could be expanded to investigate *in vivo* injury cases simulating situations where the geometry and motion of the foot/ankle complex from a specimen are known. For example, in the 2008 Beijing Olympic Games two ankle inversion injuries were captured on film and analyzed using a model-based image matching (MBIM) motion analysis technique from calibrated video sequences. The results of the study indicated a disparity in injury mechanics from previous studies. Previous studies of lateral ankle injuries suggest that the injurious motion involves inversion plus an internal rotation of the foot (Safran et al., 1999) with plantarflexion (Vitale and Fallat, 1988). However, the MBIM study revealed that plantarflexion was not involved in these ankle sprains, indicating that the talocrural joint was less involved in these inversion ankle sprains (Mok et al., 2011). By combining the MBIM with computational foot and ankle models developed from CT or magnetic resonance images (MRI), ankle injury mechanisms may be better understood. Such studies could aid in the design of intervention strategies and new equipment designs that might help limit the severity and

frequency of athletic ankle injuries. Based on the results of the current study, specimen-specific modeling may help provide even better data for the study of ankle injury mechanics on the athletic field.

CHAPTER 3:

EFFECT OF PRE-EVERSION ON TALOCRURAL AND SUBTALAR JOINT MOTION DURING ANKLE EXTERNAL ROTATION

ABSTRACT

Eversion prior to excessive external foot rotation has been shown to predispose the anterior tibiofibular ligament (ATiFL) to failure, yet protect the anterior deltoid ligament (ADL) from failure despite high levels of foot rotation. The purpose of the current study was to measure the rotations of both the subtalar and talocrural joints during foot external rotation in either a neutral or a pre-everted position in order to better understand injury generated during rotation. Fourteen (seven pairs) cadaver lower extremities were externally rotated 20 degrees in either a pre-everted or neutral configuration. Marker arrays were screwed into the tibia, talus, and calcaneus and motion capture was performed to track the motion of these bones. A joint coordinate system was used to analyze motions of the two joints. While talocrural joint rotation was greater in the neutral ankle (13.33 ± 2.09 deg versus 10.51 ± 2.75 deg, $p=0.006$), subtalar joint rotation was greater in the pre-everted ankle (2.38 ± 1.89 deg versus 1.12 ± 1.04 deg, $p=0.014$). Overall, the talocrural joint rotated more than the subtalar joint (11.92 ± 2.77 deg versus 1.75 ± 1.61 degrees, $p<0.001$). It was proposed that the calcaneus and talus ‘lock’ in a neutral position, but ‘unlock’ when the ankle is everted prior to rotation. This locking/unlocking mechanism could be responsible for an increased subtalar rotation, but decreased talocrural rotation when the ankle is pre-everted, protecting the ADL from failure. This study may provide information valuable to the study of external rotation kinematics and injury risk.

INTRODUCTION

Positioning of the ankle prior to external rotation affects the behavior of the talus and therefore location of injury (Wei et al., 2012b, Button et al., 2013, Haraguchi and Armiger, 2009). A previous study in this laboratory has shown that the combination of ankle eversion and dorsiflexion followed by axial load and external rotation produces isolated anterior tibiofibular ligament (ATiFL) injury, also known as high (or syndesmotic) ankle sprain. In a similar set of experiments, removing the eversion component mostly results in anterior deltoid ligament (ADL) injury, or a medial ankle sprain. Since the ATiFL restricts both fibular movement and external talus rotation (Sarsam and Hughes, 1988), the mechanism of high ankle sprain is attributed to a pre-tensioning of the ATiFL, as a result of the eversion and axial load, following by external rotation of the talus (Wei et al., 2012b). Oriented approximately in the antero-posterior direction in the sagittal plane (Wei et al., 2012b), the ADL is ruptured due to external rotation of the foot, supported by a clinical review which states that external rotation of the foot will “first rupture the deltoid ligament, with subsequent injury to the ATiFL” (Dattani et al., 2008, Wei et al., 2011d). Yet, despite no observation of ADL injury in the pre-everted ankles, the amount of foot rotation at failure was significantly *higher* than the failure rotation in neutral ankles (Wei et al., 2012b), seemingly contradicting the notion that external foot rotation primarily strains the ADL. However, while there is more overall foot rotation in the pre-everted ankles, ligament strain is dependent on relative bone motion which was not documented at the point of failure in this previous study.

While strain in the ADL is strongly correlated with talocrural joint rotation, it has been suggested that the subtalar joint equally contributes to overall foot rotation (Siegler et al., 1988). Excessive

subtalar joint rotation could also be problematic due to increased risk of subtalar ligament injury, which has been implicated in subtalar joint instability and calcaneal tilt (Kato, 1995, Heilman et al., 1990). Previous studies have measured subtalar and talocrural joint rotation during plantarflexion/dorsiflexion, inversion/eversion (Wong et al., 2005, Fassbind et al., 2011), and passive rotation (Siegler et al., 1988). While these studies noted that the contribution of both the subtalar and talocrural joints to foot rotation was dependent on the positioning of the ankle, they did not document the effect of pre-eversion and axial load on joint motion during rotation. The objectives of the current study were 1) to measure the contributions from the talocrural and subtalar joints to the overall rotation of the foot-shank in an axially loaded foot and 2) to identify the effect of pre-eversion on these contributions.

METHODS

Fourteen (seven pairs) fresh-frozen human cadaver (age 58.5 ± 9.2 years) lower-extremities were used in this study. The limbs were stored at -20°C and thawed to room temperature for 24 hours prior to testing. The tibia and fibula were transected 15 cm distal to the center of the knee, and the proximal 10 cm of the bones was removed of tissue and cleaned with 70% alcohol. The cleaned portion of the bone was potted in an aluminum box with room-temperature curing epoxy (Fiber Strand, Martin Senior Corp., Cleveland, OH). Two screws were placed in the anterior and medial tibia before potting to help restrain the tibia in the potting material. Reflective marker arrays were screwed in the anterior medial aspect of the talus, posterior calcaneus, and on the tibia approximately 20 cm proximal to the articular surface. CT scans verified the placement of the marker arrays.

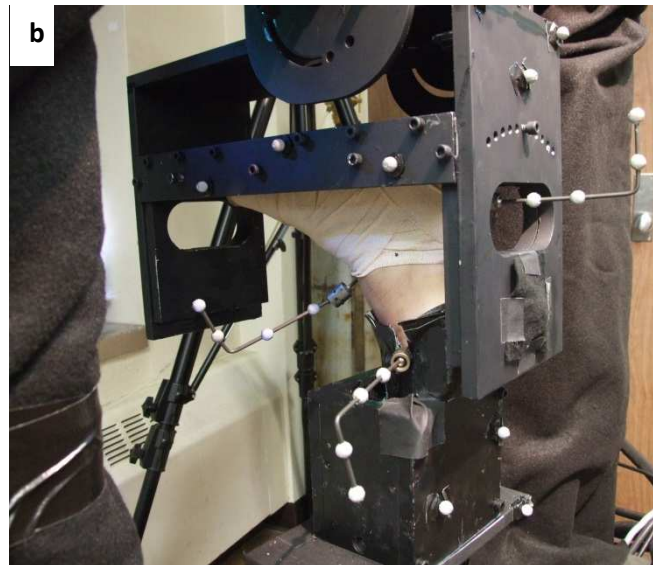


Figure 3-1 *Cadaver foot taped to a polycarbonate plate (a). Ankle with reflective marker array in the tibia, talus, and calcaneus in the testing fixture (b).*

Elastic athletic tape (Elastikon, J&J, New Brunswick, NJ) was used to constrain the foot onto a polycarbonate plate (32 cm x 8 cm) (Figure 3-1a). Experiments were performed with a customized hydraulic biaxial testing machine with a 244 Nm rotary actuator (Model SS-001-1C,

Micromatic, Berne, IN) and a vertically oriented linear actuator (Model 204.52, MTS Corp., Eden Prairie, MN). The proximal (potted) end of the foot was attached to the rotary actuator through a biaxial load cell (Model 1216CEW-2K, Interface, Scottsdale, AZ) with a capacity of 8896 N of axial force and 113 Nm of torsion (Figure 3-1b). Right ankles were pre-everted 20 degrees prior to rotation and left ankles were neutral in the coronal plane. A 1500 N compressive preload was applied to simulate dynamic weight bearing prior to rotation and 20 degrees of internal tibia rotation (external foot rotation) was input in position control at 1Hz.

A Vicon motion capture system (Oxford Metrics Ltd, Oxford, UK) was used to document the position of the marker arrays during motion. Coordinate transformations were performed on the tibia, talus, and calcaneus marker arrays in order to establish orthogonal coordinate systems in line with the three axes of the ankle (Figure 3-2). Joint coordinate systems (JCS) were established between the tibia and talus (talocrural joint) and between the talus and calcaneus (subtalar joint), similar to previously defined systems (Soutas-Little et al., 1987, Wu et al., 2002). Calculations for flexion, rotation, and inversion/eversion of the talocrural joint are shown below (Equations 1-2) (note: the same procedure is used for the subtalar joint).

$$e_1 = Ti_y \quad [1a]$$

$$e_2 = Ta_z \quad [1b]$$

$$e_3 = \frac{e_2 \times e_1}{|e_2 \times e_1|} \quad [1c]$$

$$\alpha = \sin^{-1}(e_3 \cdot Ti_z) \text{ (flexion)} \quad [2a]$$

$$\gamma = \sin^{-1}(e_3 \cdot Ta_y) \text{ (rotation)} \quad [2b]$$

$$\beta = \sin^{-1}(e_1 \cdot e_2) \text{ (inversion/eversion)} \quad [2c]$$

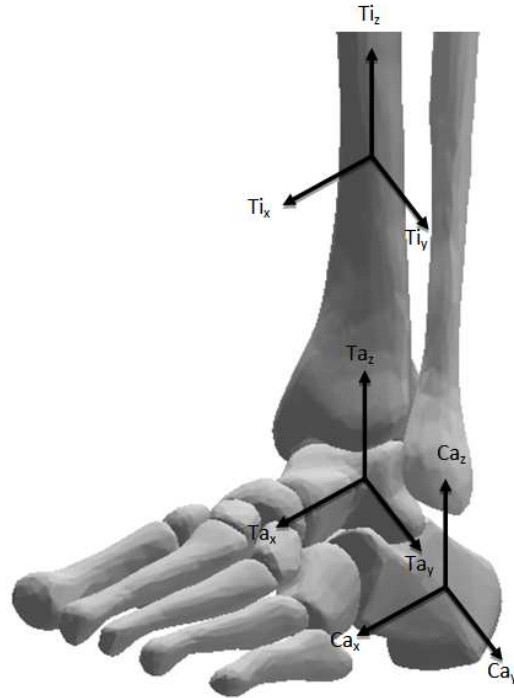


Figure 3-2 *Orthogonal coordinate axes on the tibia, talus, and calcaneus.*

Paired t-tests were used to compare the amount of joint flexion, rotation, and inversion/eversion between neutral and everted ankles. Two-way repeated measures ANOVA (pre-positioning, joint) was used to compare the amount of flexion, rotation, and inversion/eversion between the two joints. P-values less than 0.05 were considered significant in all tests.

RESULTS

Motions of the subtalar and talocrural joints during 20 degrees of internal tibia rotation were shown in Table 3-1 (Note: talocrural motion refers to talus motion with respect to the tibia, while subtalar motion refers to calcaneus motion with respect to the talus). There was significantly more external rotation in the talocrural joint compared with the subtalar joint ($p < 0.001$).

Additionally there was significantly more talocrural external rotation ($p = 0.006$), but significantly

less subtalar external rotation ($p=0.014$) in the neutral foot when compared with the pre-everted foot.

Table 3-1 *Motions of the subtalar and talocrural joint for 20 degrees of external rotation*

Specimen	Subtalar Eversion (deg)		Talocrural Eversion (deg)		Subtalar Dorsiflexion (deg)		Talocrural Dorsiflexion (deg)		Subtalar Rotation (deg)		Talocrural Rotation (deg)	
	Neutral	Everted	Neutral	Everted	Neutral	Everted	Neutral	Everted	Neutral	Everted	Neutral	Everted
1	0.59	0.29	0.39	0.19	1.46	0.16	0.03	0.34	0.04	0.69	15.81	11.08
2	1.66	2.43	2.68	3.80	2.24	1.43	0.98	4.09	1.11	1.70	12.30	10.97
3	0.50	0.21	1.53	1.03	1.29	0.75	3.11	3.50	2.53	5.78	11.84	6.41
4	0.25	0.32	1.35	0.30	0.97	0.53	0.55	0.52	0.23	0.88	15.67	12.87
5	0.97	0.41	1.30	1.34	0.84	0.16	0.79	0.02	0.02	0.94	14.93	14.20
6	1.04	1.99	1.50	1.31	1.23	1.02	2.91	0.78	1.98	2.88	12.09	10.53
7	1.71	0.84	0.58	0.85	0.04	0.52	0.72	0.48	1.90	3.81	10.65	7.52
AVG	0.96	0.93	1.33	1.26	1.15	0.65	1.30	1.39	1.12	2.38	13.33	10.51
STDEV	0.56	0.91	0.74	1.21	0.67	0.46	1.21	1.67	1.04	1.89	2.09	2.75
p-value	0.39		0.79		0.054		0.882		0.014		0.006	
	0.787				0.197				<0.001			

DISCUSSION

While previous studies have investigated the effects of ankle pre-eversion on location of injury and strain generated in key ankle ligaments during external rotation of an axially-loaded foot (Button et al., 2013, Wei et al., 2012b), the current study examined the effects that pre-eversion had on talocrural and subtalar joint movement. Specifically, a key aim of the current study was to investigate why pre-everted ankles saw no ADL injury despite high levels of foot rotation at failure. The study involved using a JCS to calculate joint motion during 20 degrees of external ankle rotation in either a pre-everted or a neutral foot. Results of the study indicated that when the foot was axially loaded and externally rotated most of the foot-shank rotation comes from the talocrural joint. However, pre-eversion lowered the amount of talocrural rotation, potentially lowering ADL injury risk.

The geometry of the subtalar joint may explain the differences in rotation between the subtalar and talocrural joints. The talus contacts the calcaneus on two articular surfaces: the subtalar posterior joint and anterior subtalar joint (Viladot et al., 1984). The calcaneal surface on the medial section of the anterior subtalar joint is called the “sustenaculum tali”, which the articulating surface of the talus fits into (Figure 3-3) (Viladot et al., 1984), and the movement of this complex is fundamental to the transmission of rotations from the foot to leg (Leardini et al., 2001). In a neutral ankle, the sustentaculum tali may ‘lock’ with the articulating surface of the talus, restricting its rotation (Figure 3a,b). As a result, when the tibia rotates, this ‘locking’ restricts the talus from rotating with the tibia, resulting in a high talocrural rotation between the tibia and talus. In contrast, when the ankle is everted, (Figure 3-3c,3-d) the contact between the sustentaculum tali and articulating surface of the talus ‘unlocks’. Consequently, this ‘unlocking’ enables the tibiotalar ligaments to pull the talus with the rotation of the tibia, resulting in lower relative motion.

This phenomenon can possibly explain the injuries observed in the Wei et al. study (Wei et al., 2012b). In that study, the neutral ankles experienced ADL injury in 5 of 6 cases while the pre-everted ankles experienced no instances of ADL injury, despite failing at significantly higher foot rotations. Since the ADL is the primary ligament resisting ankle rotation (Wei et al., 2011d), one would have expected the significantly higher foot rotation in the everted ankles to fail the ADL as well. However, results of the current study may imply that even though the pre-everted ankles experienced more foot rotation at failure in Wei et al. (2012), the ‘unlocking’ of the subtalar joint (due to pre-eversion) might have protected the ADL from failure by limiting talocrural joint rotation. As suggested by Wei et al. (2012), axial loading may have translated

the talus laterally, thereby pushing the fibula away from the tibia, producing pre-strain in the ATiFL, and potentially predisposing the foot to a high ankle sprain. Increased subtalar joint rotation in the pre-everted ankles of the current study potentially could increase the risk of subtalar ligament failure, resulting in chronic instability of the joint. On the other hand, the subtalar joint remained 'locked' in the neutral scenario, explaining ADL injury for these ankle (Wei et al., 2012b).

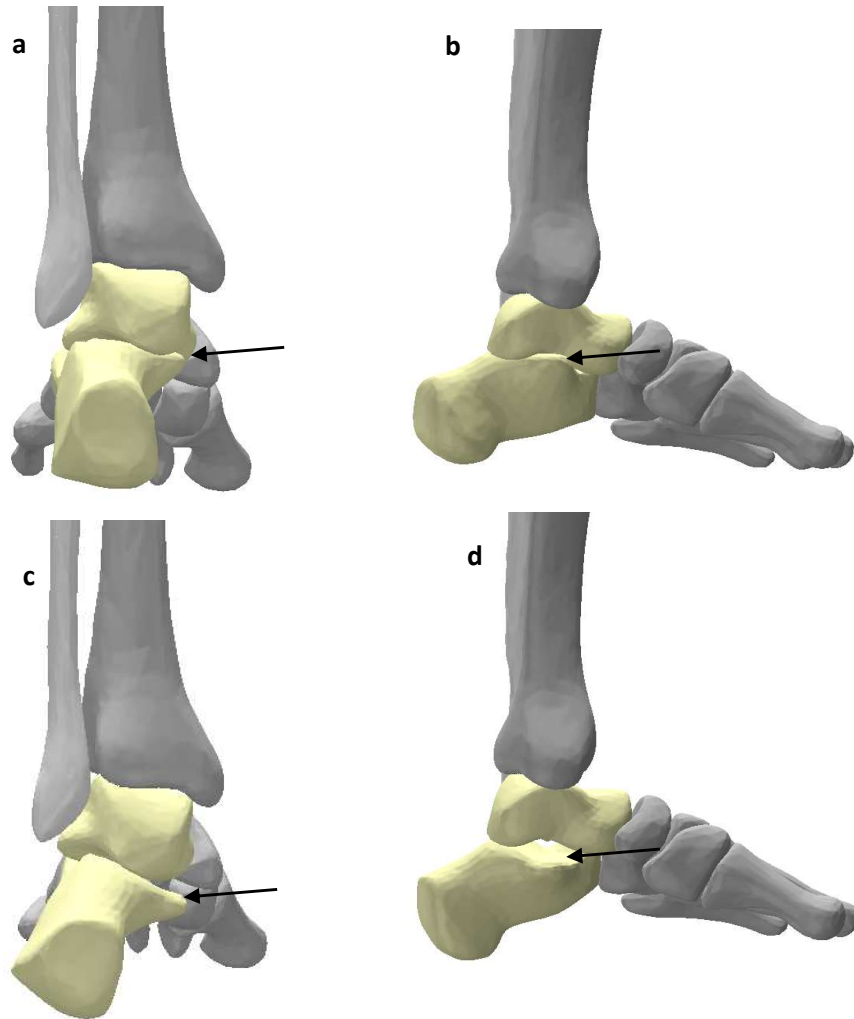


Figure 3-3 *The sustentaculum tali of the calcaneus locks with the articulating surface of the talus in a neutral position shown from the posterior (a) and medial (b) view. When everted, these surfaces unlock, shown in the posterior (c) and medial (d) view.*

Results of the current study appear to contradict conclusions from another study measuring subtalar and talocrural rotations using a JCS (Siegler et al., 1988). The Siegler study concluded that the talocrural and subtalar joints contributed nearly equally to overall foot rotation.

However, that study involved applying rotation to an unloaded ankle, while the current study involved preloading the joint with 1500 N. The difference in experimental results of the two studies may suggest that compressing the subtalar joint prior to rotation may be essential for the ‘locking’ mechanism to occur—suggesting that axial load may increase the risk of ADL injury.

A limitation of the current study was that the tests were run at sub-failure levels. While the motions of the joints at failure levels could be estimated based on extrapolations of the motions from this study, a future failure-level study is warranted. Additionally, the Wei 2012 failure-level study involved pre-dorsiflexion to both neutral and everted ankles (Wei et al., 2012b), while the current study did not. While pre-dorsiflexing the ankles in the current study may have better replicated the previous experiment, a previous parametric study concluded that pre-dorsiflexion has little effect on ADL strain during external rotation (Wei et al., 2011b) indicating that pre-dorsiflexion may have changed the results of this study very little.

In conclusion, everting the foot prior to external rotation affects the kinematics of the subtalar and talocrural joints. When the ankle is in neutral, the subtalar joint ‘locks’, restricting rotation of the joint and straining the ADL. Everting the ankle prior to rotation ‘unlocks’ the subtalar joint which allows the talus to rotate with the tibia, potentially limiting ADL strain and putting the primary strain on the ATiFL. This study may improve our understanding of the various mechanisms of ankle injury during external rotation of the foot.

CHAPTER 4:

ROTATIONAL STIFFNESS OF AMERICAN FOOTBALL SHOES AFFECTS ANKLE BIOMECHANICS AND INJURY SEVERITY

ABSTRACT

While previous studies have investigated the effect of shoe-surface interaction on injury risk, few studies have examined the effect of shoe rotational stiffness. The hypothesis of the current study was that ankles externally rotated to failure in shoes with low rotational stiffness would allow more talus eversion than those in shoes with a higher rotational stiffness, resulting in less severe injury. Twelve (six pairs) cadaver lower extremities were externally rotated to gross failure while positioned in 20 degrees of pre-eversion and 20 degrees of pre-dorsiflexion by fixing the distal end of the foot, axially loading the proximal tibia, and internally rotating the tibia. One ankle in each pair was constrained by an American football shoe with a stiff upper, while the other was constrained by an American football shoe with a flexible upper.

Experimental bone motions were input into specimen-specific computational models to measure ligament strains at failure. Ankles in flexible shoes failed at 97.4 ± 47.0 Nm which was greater than the failure torque for ankles in stiff shoes (89.2 ± 44.9 Nm, $p=0.049$) in addition to allowing 6.7 ± 2.4 degrees of talus eversion during rotation, significantly greater than the 1.7 ± 1.0 degrees for ankles in stiff shoes ($p=0.01$). The significantly greater eversion in flexible shoes was potentially due to a more natural response of the ankle during rotation, possibly affecting the injuries that were produced. All ankles failed by either medial ankle injury or syndesmotic injury, or a combination of both. Complex (more than one ligament or bone) injuries were noted in 4 of 6 ankles in stiff shoes and 1 of 6 ankles in flexible shoes. Models of ankles in flexible shoes showed significantly less strain in the deltoid at failure ($p=0.023$), but significantly more

strain in three of four subtalar ligaments ($p=0.025$, 0.03 , and 0.047). The current study suggests flexibility (or rotational stiffness) of the shoe may play an important role in both the risk and severity of ankle injuries for athletes.

INTRODUCTION

Ankle injury can result from a variety of loading situations and accounts for 10-30% of all sports injuries (Waterman et al., 2011). In American football, ankle injuries can occur in contact and noncontact situations, but frequently the mechanism of injury involves a foot planted on the playing surface with internal rotation of the upper body (Williams et al., 2007). This external rotation of the foot with respect to the body is known to result in both medial and syndesmotic ankle injuries (Waterman et al., 2011), as well as acute bone fractures (Haraguchi and Armiger, 2009, Laugehansen, 1950), and makes up 10-15% of all ankle injuries (Gerber et al., 1998, Fallat et al., 1998). While less common than other types of ankle injuries, syndesmotic and medial ankle injuries are of particular interest to researchers due to their long recovery time (Boytim et al., 1991), and the potential for chronic ankle dysfunction (Gerber et al., 1998, Waterman et al., 2011, Wolfe et al., 2001).

Syndesmotic ankles sprains (also known as high ankle sprains) involve injury to the anterior tibiofibular ligament (ATiFL). While most clinical literature attribute high ankle sprains to external rotation (Norkus and Floyd, 2001), a recent study with cadavers has produced high ankle sprain when the ankles are everted (rotated about the long axis of the foot (Figure 4-1)) prior to external rotation (Wei et al., 2012b). The same study indicates that when keeping the ankle neutral in the coronal plane (no eversion), external rotation results in medial ankle injury,

involving injury to the anterior deltoid, also known as the anterior tibiotalar ligament (ATiTL). Another study also indicates that a neutral foot undergoing external rotation will result in rupture of the deltoid ligament with subsequent injury to the ATiFL and fibula [11]. These studies suggest that pre-eversion of the talus is an important factor in the type of injury produced during external rotation of the ankle.



Figure 4-1 *Posterior view of a neutral (left) and everted foot (right).*

While previous studies have examined the effects of running shoe structure on joint kinematics (Peltz et al., 2014, Bonacci et al., 2013, Williams et al., 2012) as well as surface type (Meyers, 2010) and shoe-surface interface (Villwock et al., 2009a, Kuhlman et al., 2010) on injury potential, few studies have investigated the effect of a shoe's rotational stiffness on motion of the

talus and the subsequent type and risk of ankle injury. One recent study, however, investigated the role of an American football shoe's rotational stiffness on talus motion at sub-injurious levels (Wei et al., 2012a). The study involved rotating cadaver ankles in either stiff or flexible shoes, while tracking motion of the talus with respect to the tibia. The results show that ankles in flexible shoes experience more eversion of the talus with respect to the tibia, but less external rotation. In addition to this sub-failure study, another cadaver study (Haraguchi and Armiger, 2009), using a rigid foot constraint, shows that external rotation of the ankle results in deltoid injury prior to ATiFL injury with fibular fracture. Other studies (Wei et al., 2011d) suggest that more subtalar motion and arch collapse occur with a more flexible constraint of the ankle, thus allowing a more 'natural' response of the foot during external rotation of the ankle. As suggested by Lundberg et al., these 'natural' motions of the ankle bones may act as a torsion dissipating devices to increase the ankle's resistance to injury (Lundberg et al., 1989a).

Computational models of the ankle have previously been utilized to understand how different boundary conditions affect the biomechanics and ligament strains in the ankle under external rotation (Button et al., 2013, Wei et al., 2011d). Given the complicated manner in which the various ankle structures develop strain in the three planes of motion (Lin et al., 2006), these models have the advantage of quickly determining ligament strains and reaction forces during solid-body motion of the ankle. By inputting motions from experimental studies, the simulations can provide information about the foot's ability to respond to a given motion with various constraints. The current plan was to develop a model to help in the assessment of different footwear during injurious scenarios.

The purpose of the current study was to utilize a setup similar to a previous study (Wei et al., 2012a), but rotate the ankles to failure in order to investigate the effect of shoe stiffness on injury risk and type of injury. In order to produce conditions that result in high ankle sprain, the ankles were pre-dorsiflexed and pre-everted, per a previous study (Wei et al., 2012b). Additionally, the bone motions were input into specimen-specific computational models in order to study ankle ligament strains and compare these to experimental injuries. The hypothesis of the study was that ankles in flexible shoes would allow more talus eversion during external rotation of the foot than those in stiff shoes, thus allowing the subtalar ligaments to carry some of the applied torque and result in a less severe ankle injury.

METHODS

Shoe Selection

Shoes were selected based on a previous experimental study (Wei et al., 2012a). Briefly, four styles of American football shoes were tested in order to determine rotational stiffness using a surrogate (rigid) ankle. The four shoes were subjected to a compressive pre-load of 1500 N, a rotational pre-torque of 2 Nm, and a dynamic torque of 60 Nm input in load control at a frequency of 1 Hz. The rotational stiffness of the shoes was defined as the slope of the loading portion of the torque-rotation curve. The study found that the shoe with the highest rotational stiffness (50.0 ± 1.7 Nm/deg) was the Nike Flyposite and the lowest rotational stiffness (21.9 ± 2.8 Nm/deg) was the Nike Air (Wei et al., 2012a) (Figure 4-2). These two styles of shoe were selected for the current study.

Cadaver Tests

Twelve (six pairs) human cadaver (age 60 ± 6 years) lower-extremities were used in the current study. The limbs were stored at -20°C and thawed to room temperature for 24 hours prior to testing. The tibia and fibula were transected approximately 15 cm distal to the center of the knee, and the proximal ends of the bones were removed of tissue and cleaned with 70% alcohol. The proximal tibia and fibula were potted in an aluminum box with room-temperature curing epoxy (Fiber Strand, Martin Senour Corp., Cleveland, OH). Two screws were placed in the anterior and medial tibia before potting to help restrain the tibia in the potting material.



Figure 4-2 Football shoes used for the current study: Nike Flyposite (a) and Nike Zoom Air (b).

For each pair of lower extremities, one foot was randomly fit into the stiff shoe and the other foot was fit into a flexible shoe and equal numbers of right and left feet were assigned to the different shoe types. Shoes were selected to fit the size of each cadaver ankle. Regular-length cotton socks were used on each ankle. The base of the shoe was held by an epoxy cleat mold (Figure 4-3), which was attached to the testing fixture (Figure 4-4). Each shoe, with an attached mold in an aluminum tray, was dorsiflexed 20 degrees and everted 20 degrees to replicate conditions that previously produced high ankle sprains during external rotation of the foot (Wei et al., 2012b).



Figure 4-3 Football cleat mold made of epoxy resin used to fix the shoe to the testing fixture

Experiments were performed with a customized hydraulic biaxial testing machine with a 244 Nm rotary actuator (Model SS-001-1C, Micromatic, Berne, IN) and a vertically oriented linear actuator (Model 204.52, MTS Corp., Eden Prairie, MN). The proximal (potted) end of the foot

was attached to the rotary actuator through a biaxial load cell (Model 1216CEW-2K, Interface, Scottsdale, AZ) with a capacity of 8896 N of axial force and 113 Nm of torsion (Note: because of the high resistive torque for specimen 6, another load cell (Model 6467-107, serial #229, Lowell) with a capacity of 20kN of axial force and 1130 Nm of torsion was used). The distal end of the extremity was then attached to the aluminum tray via the cleat mold. The tray was attached to a plate that allowed for x-y adjustments to align the tibia with the linear and torsional actuators. A 1500 N compressive preload was applied to simulate dynamic weight bearing prior to rotation, as used in previous studies (Wei et al., 2012b). Internal tibia rotation (external foot rotation) was input in position control at 1 Hz (0.5s to peak rotation). The first experiment was to 20° rotation and subsequent experiments were repeated on the same ankle in increments of 10° until the torque signal indicated an injury (Figure 4-5). At failure, tibia rotation and torque were documented. Dissections of the ankle (by MCS) were performed after joint failure.



Figure 4-4 *The experiments were performed on a biaxial testing machine with the motions of the talus and tibia tracked by a 5-camera motion capture system.*

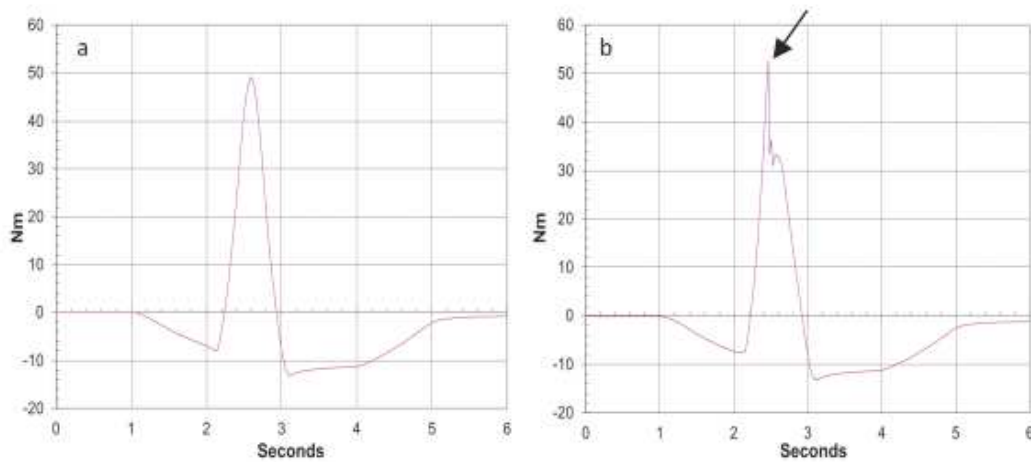


Figure 4-5 *An example of the torque data from a sub-failure (a) and a failure (b) test. The failure occurs when there is a steep drop in torque, as indicated by the arrow.*

Motion Analysis

Reflective marker arrays were screwed into the anteriomedial aspect of the talus and on the tibia approximately 20 cm proximal to the articular surface. Care was taken not to damage any ligaments during marker insertion. CT scans verified the placement of the marker arrays. A Vicon motion capture system (Oxford Metrics Ltd, Oxford, UK) was used to document the position of the markers during the experiments. A joint coordinate system (JCS), as defined by the International Society of Biomechanics (ISB) (Wu et al., 2002), was established between the talus and tibia to determine the talocrural motions (talus motion with respect to the tibia) up to ankle failure. This involved aligning the local coordinate systems (based on the reflective marker triad) on the talus and tibia (Figure 4-4) with their respective anatomical axes through coordinate transformations. The JCS took one coordinate axis from each of these local coordinate systems and a final floating coordinate axis perpendicular to the other two. By calculating the dot product between the coordinate axes, as described by the ISB, the amount of ankle flexion, eversion, and rotation was determined at joint failure.

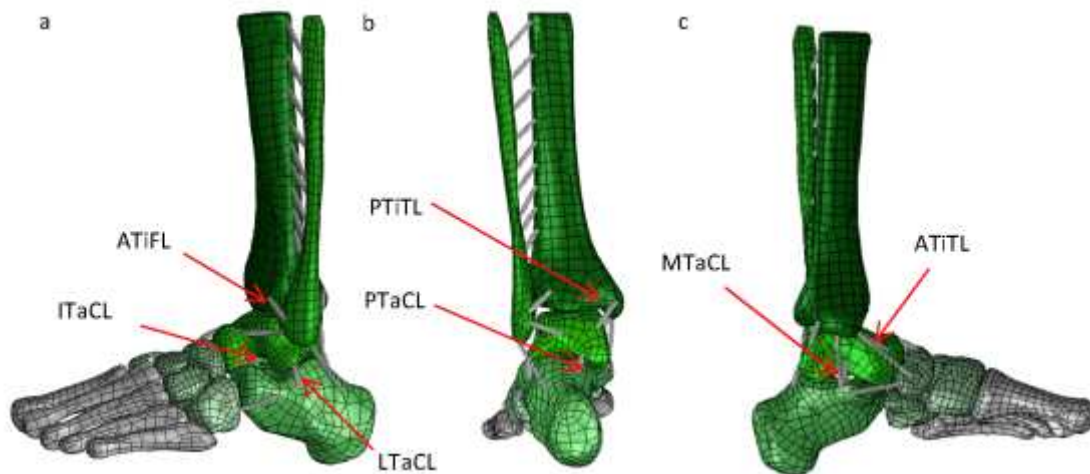


Figure 4-6 Lateral (a), posterior (b), and medial (c) views of one of the specimen-specific models in SolidWorks with linear springs representing ligaments.

Computational Modelling

Model development has been previously described in depth (Button et al., 2013). Briefly, specimen-specific computational models were created based on CT scans (0.6 mm per slice) of each ankle specimen. Digital Imaging and Communications in Medicine (DICOM) files of each specimen were imported into Materialise's Interactive Medical Imaging Control System (MIMICS)(Materialise, Ann Arbor, MI), yielding three-dimensional surface models of the bones as Stereolithography (STL) files. Motion data from the JCS analysis were used to drive each specimen-specific computational model. Nineteen linear springs were used to model ankle ligaments and nine linear springs were used to model the tibiofibular interosseous ligament (Figure 4-6); with the initial length reduced 2% prior to motion in order to induce a small pre-load in each ligament to represent *in situ* pre-tensions (Liacouras and Waynel, 2007). Ligament stiffness values were taken from the literature, as described by Wei et al. (Wei et al., 2011d). Three-dimensional contacts were implemented between adjacent bones in order to prevent overlap during simulation, with the parameters for the contact described previously by Button et al. (Button et al., 2013). The forefoot was fixed and motors simulating rotation of the tibia and talus, eversion of the talus, and the bone displacement as a result of axial pre-load were used to drive each model. The calcaneus was fixed in the inferior-superior direction simulating contact between the hind foot and the shoe. Strains were documented at the experimental point of gross ankle failure.

Statistical Analysis

Paired t-tests were used to compare the differences between shoe constraints in failure torque, talocrural eversion at failure, talocrural eversion per degree tibia rotation, talocrural rotation at

failure, talocrural rotation per degree of tibia rotation, and ligament strain. A one-way chi-square test was used to test for a difference in complex injury rates in the two different shoe types. A multiple regression analysis with categorical factors (subject, shoe) was used to analyze the correlation between torque and eversion. P-values less than 0.05 were considered significant.

RESULTS

Experimental

Table 4-1 summarizes the injury mechanisms and failure metrics. The ankles in flexible shoes failed at an average torque of 97.4 ± 47.0 Nm, significantly higher than the failure torque in stiff shoes, 89.2 ± 44.9 Nm ($p=0.049$). While there was no difference in tibia failure rotation ($p=0.53$) or talocrural failure rotation ($p=0.51$) between flexible and stiff shoes, there was significantly more talocrural eversion at failure for ankles in flexible shoes (6.7 ± 2.4 versus 1.7 ± 1.0 , $p=0.01$).

Table 4-1 Summary of the injury mechanisms and failure metrics (* indicates significant difference between stiff and flexible shoes)

Specimen	Failure Torque (Nm)		Tibia Failure Rotation (deg)		Talocrural Failure Rotation (deg)		Talocrural Failure Eversion (deg)		Injury Mechanism	
	<i>Stiff</i>	<i>Flexible</i>	<i>Stiff</i>	<i>Flexible</i>	<i>Stiff</i>	<i>Flexible</i>	<i>Stiff</i>	<i>Flexible</i>	<i>Stiff</i>	<i>Flexible</i>
1	85.6	83.4	44.7	46.5	19.3	17.5	3.5	3.9	1) Medial malleolus fracture 2) Spiral fracture of the fibula	ATiFL avulsion
2	75.8	93.4	37.0	39.4	27.9	21.5	0.9	7.4	1) ATiFL rupture 2) ATiTL rupture	ATiFL rupture
3	44.9	51.0	44.6	31.1	28.4	18.5	0.8	5.2	Medial malleolus fracture	1) ATiFL avulsion 2) ATiTL avulsion
4	55.8	59.0	29.4	33.2	19.3	13.9	1.7	5.1	1) ATiFL rupture 2) ATiTL rupture	ATiTL rupture
5	102.4	117.9	37.4	43.0	13.9	15.1	2.0	8.2	ATiFL avulsion	Fibular head fracture
6	170.7	179.7	48.1	63.2	20.3	27.2	1.1	10.4	1) ATiFL rupture 2) ATiTL rupture	ATiTL rupture
Average	89.2	97.4	40.2	42.7	21.5	19.0	1.7	6.7*		
<i>Standard Deviation</i>	44.9	47.0	6.9	11.6	5.6	4.9	1.0	2.4		

Table 4-2 Strains at failure rotation for the anterior tibiofibular ligament (ATiFL), anterior tibiotalar ligament (ATiTL), posterior tibiotalar ligament (PTiTL), interosseous talocalcaneal ligament (ITaCL), lateral talocalcaneal ligament (LTaCL), medial talocalcaneal ligament (MTaCL), and posterior talocalcaneal ligament (PTaCL). (Underlining represents ligaments that ruptured or avulsed)

Specimen	Percent Elongation at Failure Rotation (%)													
	ATiFL		ATiTL		PTiTL		ITaCL		LTaCL		MTaCL		PTaCL	
	Stiff	Flexible	Stiff	Flexible	Stiff	Flexible	Stiff	Flexible	Stiff	Flexible	Stiff	Flexible	Stiff	Flexible
1	19.9	<u>21.2</u>	18.9	14.6	14.9	17.2	11.4	14.3	16.0	16.7	0.1	2.9	9.1	12.0
2	<u>35.5</u>	<u>34.4</u>	<u>37.2</u>	28.3	1.8	10.6	3.0	18.8	1.8	18.1	1.9	2.0	1.9	17.4
3	19.1	<u>21.1</u>	34.6	<u>20.7</u>	10.3	12.3	3.8	1.3	1.9	11.1	11.9	1.7	1.9	1.8
4	<u>18.3</u>	7.3	<u>26.8</u>	<u>20.0</u>	5.5	8.0	1.9	11.7	1.9	1.4	2.0	17.3	7.2	18.1
5	<u>33.4</u>	32.8	4.2	2.0	17.4	19.8	3.7	10.8	20.0	31.1	2.7	1.8	18.3	22.8
6	<u>29.8</u>	15.9	<u>32.9</u>	<u>31.6</u>	7.7	23.3	1.9	7.5	2.0	15.3	20.9	30.7	9.0	12.5
Average	26.0	22.1	25.7	19.5	9.6	15.2	3.3	10.7	7.3	15.6	6.6	9.4	7.9	14.1
<i>Standard Deviation</i>	8.5	10.9	13.3	9.8	6.4	4.8	4.4	6.4	8.9	10.8	4.7	16.2	6.8	8.0

Additionally, the amount of talocrural eversion per degree tibia rotation in the flexible shoe (0.16 ± 0.04 degree/degree) was significantly greater than that for the stiff shoe (0.04 ± 0.02 degree/degree ($p=0.023$)). There was slightly more talocrural rotation per degree of tibia rotation in the stiff shoe versus the flexible shoe (0.55 ± 0.16 degree/degree and 0.45 ± 0.10 degree/degree, respectively), although this was not quite significant ($p=0.082$). There was no correlation between torque and eversion at failure ($p=0.189$).

The injury mechanisms also differed between the two types of shoes (Figure 4-7 and Table 4-1). Medial injuries were observed in 5 of 6 stiff-shoe ankles and 3 of 6 flexible-shoe ankles. Syndesmotoc injuries were observed in 5 of 6 stiff-shoe ankles and 4 of 6 flexible-shoe ankles. When the specimens were compared with a chi-square analysis, the effect of shoe type on the frequency of complex injuries was not quite significant ($p=0.079$): there were combination (complex) medial and syndesmotoc injuries in 4 of 6 stiff-shoe ankles while only 1 of 6 ankles in the flexible shoes suffered combination injuries. Bone injuries were also more prevalent in stiff-shoe ankles, occurring three times compared with only one occurrence in flexible-shoe ankles.

Computational Modelling

Results of the SolidWorks simulations are shown in Table 4-2 for the seven ligaments that developed the highest levels of strain during external rotation of the ankle: the ATiFL, ATiTL, posterior tibiotalar ligament (PTiTL), interosseous talocalcaneal ligament (ITaCL), lateral talocalcaneal ligament (LTaCL), medial talocalcaneal ligament (MTaCL), and posterior talocalcaneal ligament (PTaCL). Models of the stiff and flexible shoe cases showed no difference in ligament strains for the ATiFL ($p=0.221$) and MTaCL ($p=0.264$) at ankle failure.

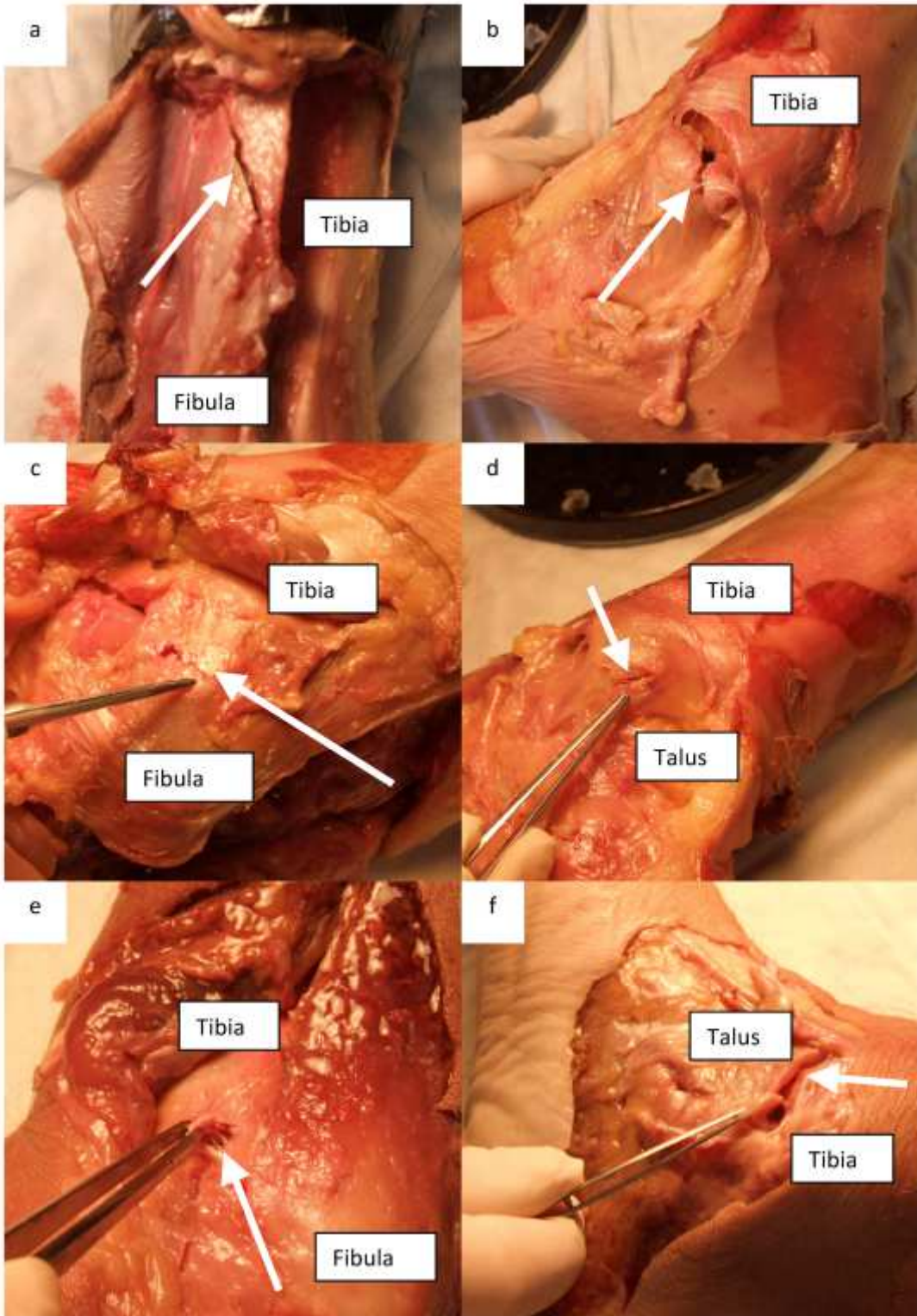


Figure 4-7 Fibular fracture (a), medial malleolus fracture (b), ATiFL avulsion (c), ATiTL avulsion (d), ATiFL tear (e), and ATiTL tear (f).

However, the stiff shoe models showed significantly higher levels of strain in the ATiTL ($25.7 \pm 13.3\%$ versus $19.5 \pm 9.8\%$ in the flexible models, $p=0.023$). Stiff shoe models also showed significantly lower levels of strain in the ITaCL ($3.3 \pm 4.4\%$ versus $10.7 \pm 6.4\%$), LTaCL ($7.3 \pm 8.9\%$ versus $15.6 \pm 10.8\%$), and PTaCL ($7.9 \pm 6.8\%$ versus $14.1 \pm 8.0\%$) at ankle failure, ($p=0.035$, 0.03 , and 0.047 , respectively). Additionally, there was a decrease in PTiFL strain in the stiff versus flexible shoe models ($9.6 \pm 6.4\%$ versus $15.2 \pm 4.8\%$), but not significantly ($p=0.056$).

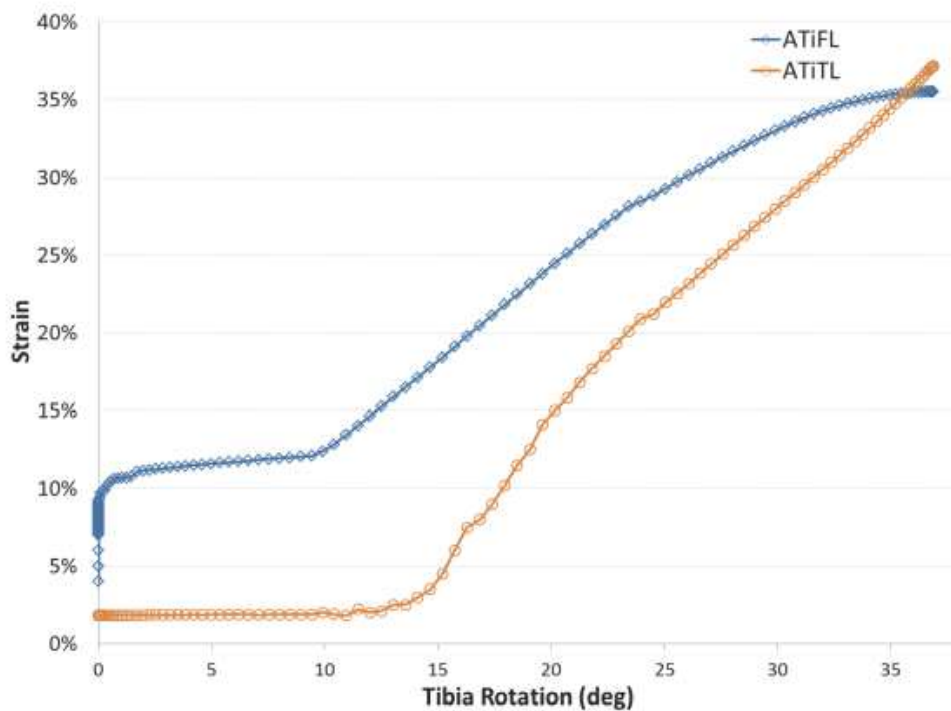


Figure 4-8 Representative plot of the ATiFL and ATiTL strains versus tibia rotation in a simulation of the combination ATiFL and ATiTL injury scenario (specimen 2, stiff shoe).

In all four cases of complex ligamentous injury, the combination of pre-dorsiflexion, pre-eversion, and axial load pre-strained the ATiFL more than the ATiTL. This resulted in higher ATiFL strains for low levels of rotation, but an increasing ATiTL strain at near-failure levels of rotation, while the ATiFL strain leveled off. In models 2, 4, and 6, the ATiTL strain level surpassed the ATiFL strain in the last 3-5° of rotation before failure. In the other case (specimen 3 flexible) the ATiTL strain nearly equaled the ATiFL strain, but did not surpass it. A representative plot of simulations that showed combined ATiFL/ATiTL failure is shown in Figure 4-8 (specimen 2, stiff shoe).

DISCUSSION

The rotational stiffness of American football shoes may affect high and medial ankle injury risks. The current study investigated this premise by rotating pairs of cadaver ankles to failure in either a stiff or flexible shoe. All ankles showed high or medial ankle injury, or a combination of each. The ankles in flexible shoes failed at statistically higher torques and at significantly higher levels of talocrural eversion than the ankles in stiff shoes. Computational models simulating flexible shoe experiments exhibited statistically higher strains in subtalar ligaments during experimental rotations, but lower strains in the ATiTL. Additionally, there was a higher frequency of complex (combination) injuries in the stiff shoes, but not quite at a significant level. These results indicate that shoes with a flexible upper may result in less severe ankle injuries than those with a stiff upper.

The increased ankle eversion in the flexible shoe may be due to less restriction of the subtalar joint to allow more motion between the talus and calcaneus, which may more closely simulate the ankle's natural, unrestrained response to external rotation. Previous investigations on anatomical specimens have concluded that external rotation of the unrestrained ankle results in pronation (the combination of eversion, abduction, and dorsiflexion) of the ankle (Lundberg et al., 1989b). Rotations about the anteroposterior and vertical axes of the talonavicular joint have been shown larger than the external rotation input about the tibia (Vanlangelaan, 1983). This is described as the natural 'transferal of rotation' (Lundberg et al., 1989b). In the current study, a lower talus constraint may have allowed the ankles in flexible shoes to undergo this 'transferal of rotation' resulting in significantly more eversion than in a more stiff constraining type of shoe. This natural sequence of rotations may help the ankle absorb applied rotational torques, offering a possible explanation as to why ankles in flexible shoes failed at slightly higher torques, but similar levels of shoe rotation.

The modelling aspect of this paper provided insight into what occurs at a ligamentous level in the stiff versus flexibly constrained ankle. In the stiff shoe simulations, the subtalar joint remained relatively closed during external rotation and as a result the applied torque primarily stretched the ATiTL and ATiFL, with the ATiTL straining significantly more than in the flexible shoe simulations (Table 4-2). However, the flexible shoe constraint allowed the subtalar ligaments to deform as well, potentially increasing the amount of load the ankle could withstand before gross failure. While an applied torque to the ankle in a stiff shoe resulted in an almost pure talocrural rotation with high ATiTL and ATiFL strains, an applied torque to the ankle in a flexible shoe allowed a combination of ankle rotation and eversion. This combination of rotation and eversion

strained more ligaments, but at more moderate, sub-failure levels. This difference in talus response and corresponding ligament strain may explain the different injury mechanisms in the stiff versus flexible shoes.

To help explain some of these injuries, other studies have documented the order and mechanisms of pronation-external rotation injuries (Norkus and Floyd, 2001). The combination of medial and syndesmotic injury (specimens 1, 2, 4, and 6 in the stiff shoe and specimen 3 in the flexible shoe) closely follow the mechanism that is described in a Weber C injury (Harper, 1992). In these injuries, the medial side of the ankle is in maximum tension due to the combination of eversion and external rotation, first causing rupture of the ATiTL, or fracture of the medial malleolus. The injury may stop here, possibly explaining the medial malleolus fracture in specimen 3 with the stiff shoe and isolated ATiTL failure in specimens 4 and 6 with the flexible shoe. Once the ATiTL ruptures, the talus may continue to externally rotate and move laterally causing rupture of the ATiFL. This mechanism is supported by the computational study (Figure 4-8), as the ATiTL strain rate increases more rapidly and overtakes the ATiFL strain level near the point of failure. This supports the claim that the mechanism of injury may follow that of a Weber C classification: the ATiTL fails first, causing lateral translation of the talus and a subsequent increase in ATiFL strain to cause failure of the ATiFL.

Interestingly, 4 of the 5 combination medial/syndesmotic injuries occurred in stiff-shoe ankles, possibly suggesting that restricting motion of the talus may also lead to a more severe ankle injury. This may be supported by other studies: Haraguchi, performing eversion-external rotation tests on ankles with a rigid constraint, noted combination injuries in 19 of 22 specimens;

while Wei, performing eversion-external rotation tests on ankles with a compliant constraint, documented isolated injuries in all six specimens (Wei et al., 2012b). Isolated ATiFL tear or avulsion (specimens 1 and 2 in the flexible shoe and specimen 5 in the stiff shoe) most likely occurred as described by Wei et al. (Wei et al., 2012b): the combination of pre-eversion, pre-dorsiflexion, and axial load causing pre-tension in the ATiFL, making it the first ligament to rupture under external rotation. This mechanism of injury was also supported by the computational study, as specimens with ATiFL failure showed the highest strain in the ATiFL (Table 4-2).

One limitation of the current study was the use of older-aged cadavers. Fractures have been shown to occur more in patients with osteoporotic bone, most likely the result of advanced age (Haraguchi and Armiger, 2009). The occurrence of osseous injury instead of ligamentous injury could be related to the specimen's age and bone quality. However, these osseous injuries did not seem to bias the results. Three specimens (1, 3, and 5) suffered osseous injuries and in each case these injuries were prevalent in both the stiff and flexible shoe ankles. However, there were more fractures in the stiff shoe ankles and more avulsions in the flexible shoe ankles, potentially indicating that more rigidly constraining ankles by a stiff shoe upper may stress the bones more during external rotation of the ankle. This may be supported by a recent study analyzing injury videos posted on Youtube.com where a fracture pattern similar to that observed from the current study was noted under pronation-external rotation (Kwon et al., 2010), suggesting that bone fracture may be a common occurrence in young athletes as well. Another limitation was the limited number of shoes tested, as well as the lack of documented technical information about the shoes. A recent study has compared the rotational characteristics of the two shoes from the

current studies with other shoes (Wei et al., 2012a), but future studies may want to look at more shoes (it is important to note that a constant 1500 N axial load was applied to a surrogate ankle during this stiffness testing, and different axial loads may result in different rotational stiffnesses). Furthermore, technical characteristics of the shoes, besides rotational stiffness, were not documented, and these could have an impact on talocrural joint motion and subsequent injuries that were generated in these experiments. Future studies may want to document additional differences in shoe construction that may have an effect on talocrural joint motion.

Additionally, the effect of muscle action was not included, which, on top of the specimen age, may have been a limitation when attempting to reproduce the physiological behavior during an actual sports injury. Yet, while it has been previously suggested that human subjects generate 10-20% more ankle joint torque than cadavers during sub-injurious external rotation (Wei et al., 2011c), the magnitude of torque at failure was of little importance to the current study.

Furthermore, the proprioceptive muscle response is often too slow to have an effect on joint motion during injury (Dubin et al., 2011, Delahunt et al., 2006), so it is likely that biomechanics of the joint would differ only slightly during *in vivo* loading. Lastly, the small number of specimens has an effect on reducing the statistical power of the study. Increasing the sample size may have improved the robustness of the conclusions: more noted differences could possibly be seen in talocrural rotation/degree of tibia rotation as well as differences in complex injury frequency. However, the sample size was adequate to see differences in eversion, as well as key ligament strains at failure.

In conclusion, the current study investigated ankle injury risk and its severity under combined dorsiflexion, eversion, and external rotation while in either an American football shoe with a relatively stiff or flexible upper design. Results of the study indicated that more talus eversion occurred in flexible shoes under external rotation of the shoe, potentially allowing for a more ‘natural’ response of the ankle to rotation. As a result, the ankles in flexible shoes required slightly more torque to fail and had fewer cases of complex ankle injury. Computational models of the experiments showed that the response of the ankle to external rotation in a more flexible shoe strained more ligaments than in a stiff shoe, but at more moderate levels. However, as conclusions from this study only apply to external rotation of the ankle future studies may want to investigate the performance characteristics of stiff versus flexible shoes in a variety of circumstances in order to best recommend footwear that optimizes injury mitigation. In addition, future studies may want to investigate the effect of shoe stiffness on joint kinematics in regards to performance as well as injury, as previously studied with soccer shoes (Hennig, 2011). The current study may help drive research and design of future American football shoes in order to help limit injury risk without compromising the athlete’s comfort and performance.

CHAPTER 5:

THE EFFECT OF ROTATIONAL STIFFNESS ON ANKLE JOINT MOTION AND LIGAMENT STRAIN DURING EXTERNAL ROTATION

ABSTRACT

The rotational stiffness of footwear has been previously shown to have an effect on ankle joint kinematics and injury risk, but this relationship has not yet been quantified. The purpose of the current study was to derive equations that could be used to predict ankle joint kinematics based on the amount of ankle constraint. Three athletic tapes were tested for their ability to constrain the ankle joint during external rotation. Six subjects then performed a voluntary external foot rotation using the selected tape designs to constrain the ankle, as well as an unconstrained case. Motion capture was performed to track the motion of the hindfoot with respect to the tibia (ankle joint) up to fifteen degrees of tibia rotation and predictive equations were determined to establish ankle joint rotation, eversion, and flexion as a function of gross tibia motion and tape stiffness. These predictive equations were then used to drive a computational model in which ankle ligament strains were determined at 15 degrees of tibia rotation and for ankle constraint stiffness ranging from 0 Nm/deg to 30 Nm/deg. The three tapes provided significantly different constraint stiffness during external foot rotation. There was no statistical effect of ankle joint constraint on the dorsiflexion response of the ankle ($p=0.461$). In contrast, there was an effect of constraint stiffness on ankle joint external rotation ($p<0.001$) and ankle joint eversion ($p<0.001$). Results of the model simulation revealed the highest ligament strains in the anterior tibiotalar ligament (ATiTL) and anterior tibiofibular ligament (ATiFL). ATiTL strain increased with increasing constraint stiffness, while there was little effect of constraint stiffness on ATiFL strain. Results from this study could aid in the design of footwear, as well as the analysis of clinical injuries.

INTRODUCTION

External rotation of the foot with respect to the body is known to result in both medial and syndesmotic ankle sprains and fractures (Waterman et al., 2011, Boytim et al., 1991, Haraguchi and Armiger, 2009). Medial ankle injury involves damage to the anterior tibiotalar ligament (ATiTL) (Wolfe et al., 2001), while syndesmotic (or high) ankle injury involves damage primarily to the anterior tibiofibular ligament (ATiFL) (Dattani et al., 2008). These injuries are most prevalent in contact sports where the injury mechanism is frequently attributed to a foot being planted on the playing surface with internal rotation of the upper body (Guise, 1976). While both injuries have been shown to involve some combination of external rotation, dorsiflexion, and eversion (Waterman et al., 2010, Gerber et al., 1998, Norkus and Floyd, 2001, Wei et al., 2012b), understanding more precisely the joint kinematics at the point of failure is an important aspect for preventing injury.

Previous researchers have examined joint motion during medial and high ankle sprains using a variety of techniques. One study used a rigid-body ankle model to investigate the effect of different levels of joint eversion and dorsiflexion on ATiFL and ATiTL injury risk (Wei et al., 2011a). Conclusions from this computational study motivated a cadaver study in which pairs of ankles were rotated to failure in either an everted or neutral configuration, producing syndesmotic and medial ankle sprains, respectively (Wei et al., 2012b). Results of both studies concluded that the amount of eversion is critical in producing a syndesmotic versus a medial ankle sprain. Yet, to provide a more complete understanding of external rotation injuries occurring on the field, an in depth analysis of *in vivo* injuries may be warranted.

Krosshaug and colleagues have developed a model-based image matching (MBIM) motion analysis technique to analyze three-dimensional human motion in an un-calibrated environment using panning cameras (Krosshaug and Bahr, 2005). This technique was used to investigate two cases of inversion ankle injury from the 2008 Beijing Olympics (Mok et al., 2011) and five cases of inversion sprains in tennis (Fong et al., 2012). Results from these studies have provided new information regarding the mechanism of lateral ankle sprain and have led to recommendations for prevention of such sprains. However, accurate estimations of actual foot motion inside shoes remains challenging.

In external rotation injuries motion of the ankle joint has been considered to play an important role in generating ligament strains, particularly to the ATiTL and ATiFL (Sarsam and Hughes, 1988, Wei et al., 2011d). Therefore, in order to use MBIM to study external rotation injuries the analysis would need to accurately quantify ankle joint motion. Previous studies from this lab, however, have shown that ankle joint motion during upper body (tibial) rotation and the subsequently generated injuries are highly dependent on rotational stiffness of the shoe (Wei et al., 2012a). In order to analyze injurious scenarios or model the effect of different shoe rotational stiffness, the relationship between constraint stiffness and ankle joint motion needs to be investigated in more detail.

The purposes of the current study were (1) to have human subjects perform ankle external rotation while constraining the foot with athletic tapes of different rotational stiffness (as a means of determining the potential role of shoe stiffness on ankle motion) (2) to develop equations relating the effect of constraint stiffness on 3D ankle motion, and finally (3) to use these

equations to drive a computational model to estimate the range of ligament strains that are generated over a domain of constraint stiffness representative of various levels of shoe rotational stiffness. It was hypothesized that taped constraint of the ankle would have a significant effect on the amount of ankle joint motion during external rotation of the foot with respect to the upper body, and that the effect on ankle joint kinematics would generate differences in key ligament strains during external foot rotation. Information from this study may help investigators better estimate ankle motion within various shoe designs and improve theoretical predictions of the potential for ankle injuries during field conditions in order to optimize athletic footwear design for preventing external rotation injuries of the ankle.

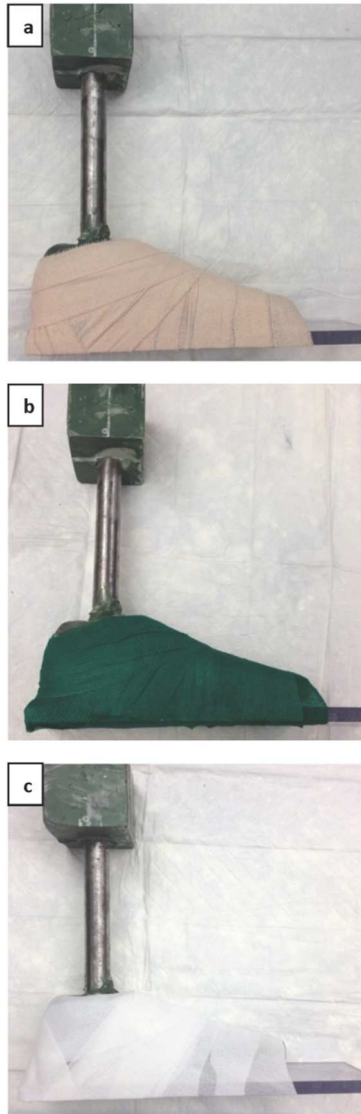


Figure 5-1 *The surrogate ankle taped to the polycarbonate plate using Elastikon (a), PowerFlex (b), and Sher-Light (c).*

METHODS

Tape stiffness tests

Three athletic tapes were evaluated to determine their rotational stiffness properties for the ankle. The experiments were conducted on a custom, hydraulic, biaxial testing machine with a 244 Nm rotary actuator (Model SS-001-1V, Micromatic, Berne, MN) and a vertically oriented linear

actuator (Model 204.53, MTS Corp., Eden Prairie, MN). The tapes evaluated in the study were Andover PowerFlex, Covidien Sher-Light, and Johnson & Johnson Elasikon. The tapes constrained a surrogate lower extremity made from room temperature curing epoxy resin (Fiber Strand, Martin Senior Corp., Cleveland, OH) to a polycarbonate plate (32 cm x 8 cm) (Figure 5-1). The taping was performed by an athletic training student (PT) with the goal of modelling the constraint provided by a football shoe upper by applying two medial and two lateral heel locks. The polycarbonate plate was clamped to a customized fixture that allowed x-y adjustments to align the surrogate shank with the linear and torsional actuators. The proximal end of the surrogate limb was inserted into an aluminum box which was attached to a rotary actuator through a biaxial load cell (Model 1216CEW-2K, Interface, Scottsdale, AZ) with a capacity of 8896 N axial force and 113 Nm torsion (Figure 5-2).

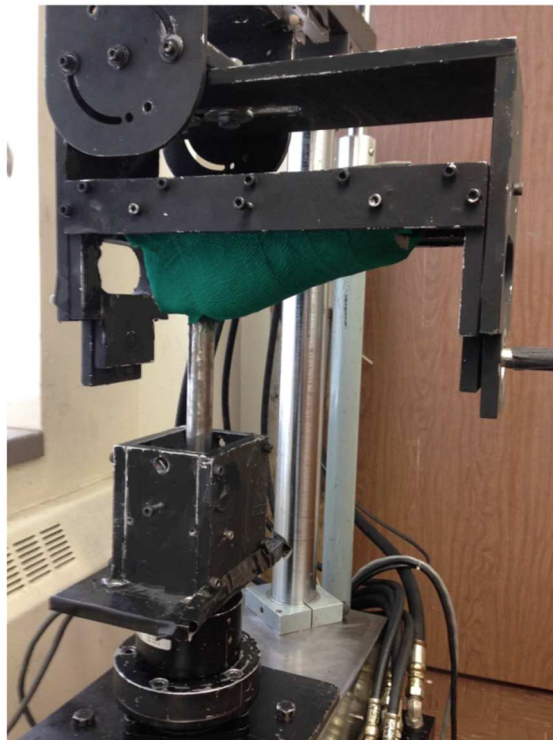


Figure 5-2 *The surrogate limb was attached to the testing machine*

The axial load was zeroed and a rotational pre-torque of 2 Nm was applied to the surrogate foot prior to internal rotation of the shank (external ankle rotation). The pre-torque was applied to ensure tape contact on the medial side of the foot. A dynamic torque of 50 Nm was input in load control at a frequency of 1 Hz (0.5 s to peak torque) and repeated six times for each tape. The loading portion of the torque-rotation curve was averaged across the final five cycles of loading. The slope of the linear portion of the curve (between 10 Nm and 50 Nm) was determined to yield a rotational stiffness for each tape in Nm/deg.

This procedure was repeated, but with the surrogate ankle constrained by shoe/cleat molds instead of tapes, as previously described by Wei et al. (Wei et al., 2012a). The shoes tested were the Nike Flyposite and Nike Air, the stiffest and most flexible shoes from a previous study, respectively (Button et al., 2015). In order to accurately mimic the tape stiffness tests, the axial load was zeroed prior to rotation, unlike the Wei study which applied a 1500N axial pre-load load to simulate body weight. The procedure from the Wei study was deemed ineffective for the tape study because of potential high levels of torsional friction between the surrogate ankle and the polycarbonate plate.

Human subject tests

Institutional Review Board approval was obtained for these experiments. Kinematic data from six young (age: 27.3 ± 4.6 years), male subjects (body weight: 77.5 ± 8.9 kg) with no history of lower body injury were collected after obtaining informed consent. A six-camera Vicon MX Motion Capture System (OMG plc. Oxford, UK) was used to capture motion data at 100 Hz. Marker arrays were placed on the anterior portion of the tibia, approximately 10 cm distal to the

patella, and on the calcaneal tuberosity (Figure 5-3). Each subject's right foot was measured prior to testing and a polycarbonate plate was cut to fit. The subject's right foot was taped to the 1/8" thick polycarbonate plate by the athletic trainer (PT) using two medial and two lateral heel locks and one of three athletic tapes for each experiment. The foot/plate was adhered to the ground using a Dycem adhesive sheet (Dycem Ltd, Warwick, RI, USA). The left foot was placed adjacent to the right foot on a raised surface so the feet were level. The subject performed an internal rotation of the body (external rotation of the foot) at a self-determined maximal effort, trying to minimize tibia flexion and eversion. Each subject repeated this motion until 10 successful trials were collected. The procedure was repeated for each tape and under a tapeless condition (note: the shoes were not used in the human subject tests).



Figure 5-3 *Marker arrays were placed on the subject's anterior tibia, about 10 cm distal to the patella, and the calcaneal tuberosity.*

Coordinate transformations were performed on the tibia and hindfoot marker arrays in order to establish orthogonal coordinate systems in line with the three axes of the ankle (Figure 5-4). A joint coordinate system (JCS) was then established between the tibia and hindfoot (henceforth referred to as the ankle joint), similar to a previously defined system (Wu et al., 2002):

$$e_1 = Ti_x \quad (1a)$$

$$e_3 = HF_z \quad (1b)$$

$$e_2 = \frac{e_3 \times e_1}{|e_3 \times e_1|} \quad (1c)$$

$$\alpha = \sin^{-1}(e_2 \cdot Ti_z) \text{ (flexion)} \quad (2a)$$

$$\gamma = \sin^{-1}(e_2 \cdot HF_x) \text{ (rotation)} \quad (2b)$$

$$\beta = \sin^{-1}(e_1 \cdot e_3) \text{ (inversion/eversion)} \quad (2c)$$

Calculations of absolute tibia rotation, eversion, and flexion with respect to the laboratory were performed by the same method, but the JCS was established between the tibia coordinate system and a fixed laboratory coordinate system aligned with the axes shown in Figure 5-4.

Calculations for ankle joint flexion, rotation, and inversion/eversion were determined over a range of 0 to 15 degrees of tibia rotation.

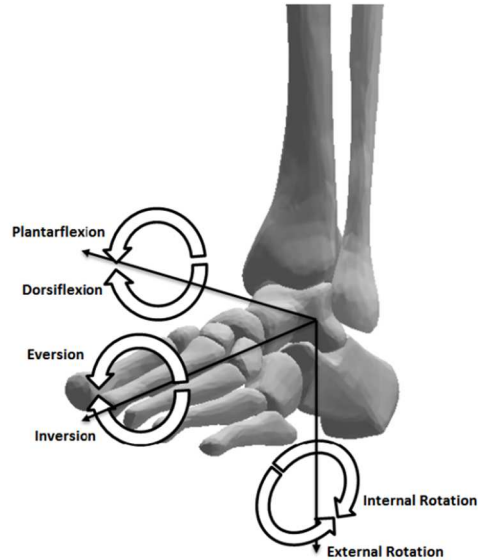


Figure 5-4 *Three orthogonal axes of the ankle. Rotations about these axes are described as plantarflexion/dorsiflexion, eversion/inversion, and internal/external rotation.*

Predictions of ankle joint dorsiflexion, eversion, and rotation were determined as a function of tibia rotation, tibia eversion, tibia dorsiflexion, and tape stiffness. Irrelevant predictors and interaction terms were eliminated by using the ‘stepwisefit’ and ‘LinearModel.fit’ functions, respectively, in MATLAB.

Computational modelling

Predicted ankle joint motion data from the curve fitting equations were used to drive a generic computational ankle model. Details of the model development and its validation have been described in previous studies (Wei et al., 2011d, Button et al., 2013), so they will only be described briefly here. The ankle model was based on a computed tomography (CT) scan of a fresh frozen, right male cadaver foot (52 years old) showing no signs of abnormal anatomy. Digital information from the scan was transferred from Digital Imaging and Communications in

Medicine (DICOM) files into Materialise's Interactive Imaging Control System (MIMICS, Leuven, Belgium) software. Three dimensional surface models of the bones, as Stereolithography (STL) files, were created and exported to SolidWorks 2011 (Trimech Solutions, LLC, Columbia, MD), where the bones were simplified and assembled. SolidWorks Motion was used to add ligaments (modelled as linear springs) and insertion locations were determined from previous dissections in this laboratory (KB and FW) and an anatomical atlas (Netter and JT, 2003). A pre-load was induced in each ligament by reducing its length by 2%, inducing *in situ* preloads (Liacouras and Waynel, 2007). The model has been previously validated based on ankle ligament strain (Colville et al., 1990a), ankle joint torque (Wei et al., 2010), talus rotation (Button et al., 2013), and injuries generated during external rotation experiments (Button et al., 2013).

The motion simulation was run in displacement control with motors driving the three-dimensional rotations of the tibia and talus. The input for the tibia motor was a ramp to 15 degrees of external rotation, with no eversion or dorsiflexion (modelling an isolated external rotation). The talus rotation, eversion, and dorsiflexion (determined from results of 'Curve Fitting' section) were dependent on the amount of tibia rotation at a given time point and the rotational stiffness parameter. The forefoot was fixed while the calcaneus, talus, tibia, and fibula were free to move. The body weight was simulated as an axial load on the proximal end of the model with one-sixth of the loading on the fibula and the rest on the tibia (Wei et al., 2011d). Ligament strains were determined during rotation.

Statistical analysis

One-way ANOVA and Tukey post-hoc tests were used to statistically determine differences in rotational stiffness between tapes/shoes. Two-way repeated measures ANOVA and Tukey post-hoc tests were used to statistically determine differences in ankle joint dorsiflexion, external rotation, and eversion for the three tape (and no tape) designs (factor one) at each rotation level (factor two). In all statistical tests, p-values less than 0.05 were considered significant.

RESULTS

The 2 Nm pre-load was zeroed out by shifting the torque-rotation curves, which showed nearly linear behavior beyond 10 Nm of input torque (Figure 5-5a and b). The rotational stiffness of the Elastikon, Sher-Light, and PowerFlex tapes were 25.7 ± 1.6 Nm/deg, 22.6 ± 0.75 Nm/deg, and 13.5 ± 0.37 Nm/deg, respectively. The rotational stiffness of the Air and Flyposite shoes were 16.5 ± 0.44 Nm/deg and 25.8 ± 1.1 Nm/deg, respectively. There were significant differences between all the tape/shoe designs, except between the Flyposite shoe and Elastikon tape ($p=0.99$).

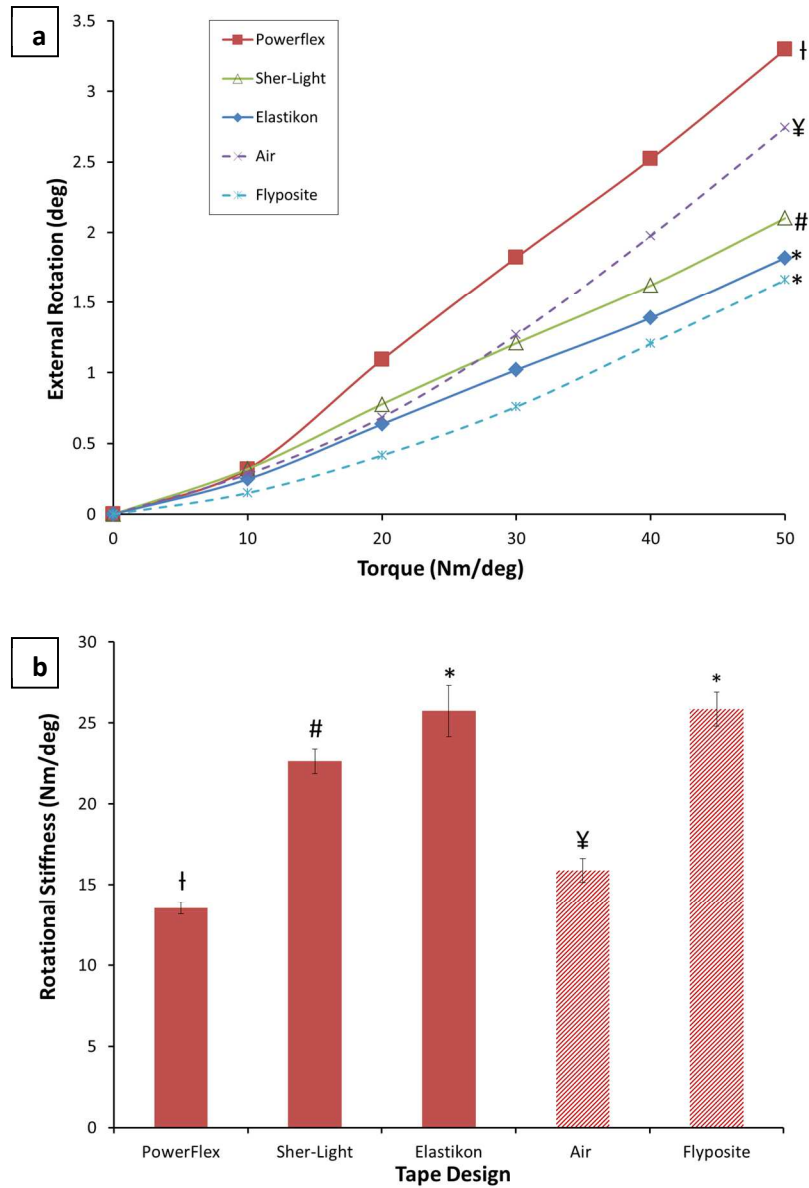


Figure 5-5 Torque-rotation curves for the three tape designs and two shoe designs from rotational stiffness tests (a), and rotational stiffness values determined from the slopes of the torque-rotation curves (b). Curves with different symbols (* # † ¥) indicate statistically different stiffness between designs.

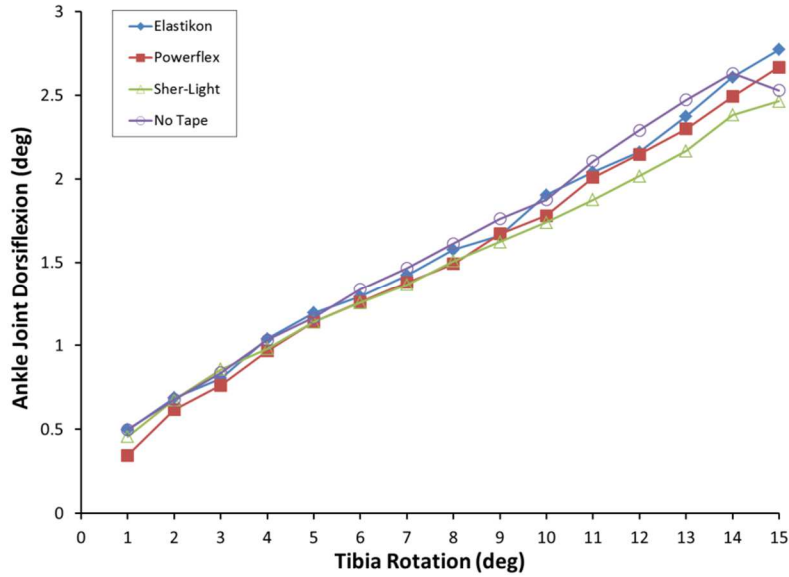


Figure 5-6 Mean ankle joint dorsiflexion-tibia rotation curves for the three tape (and no-tape) designs from an *in vivo* external foot rotation ($n=6$). There were no significant differences between tape designs.

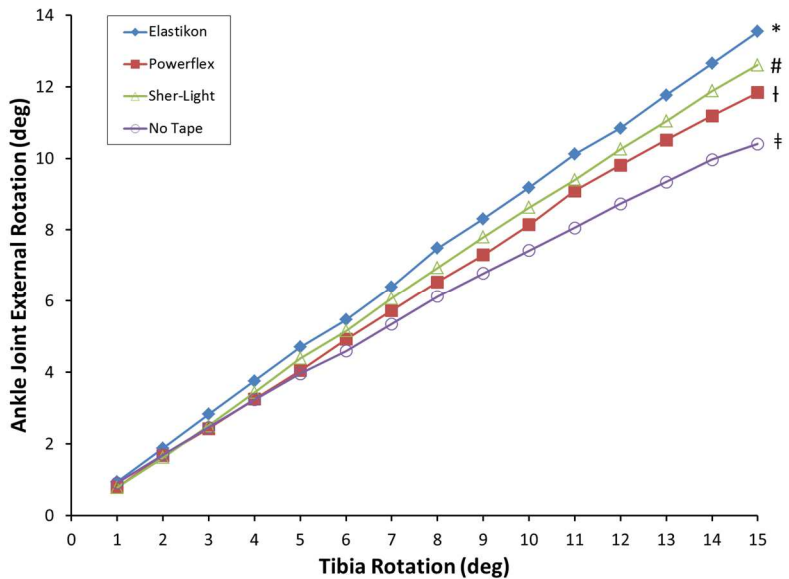


Figure 5-7 Mean ankle joint external rotation-tibia rotation curves for the three tape (and no-tape) designs from an *in vivo* external foot rotation ($n=6$). Different symbols (* # † ‡) indicate statistically different curves.

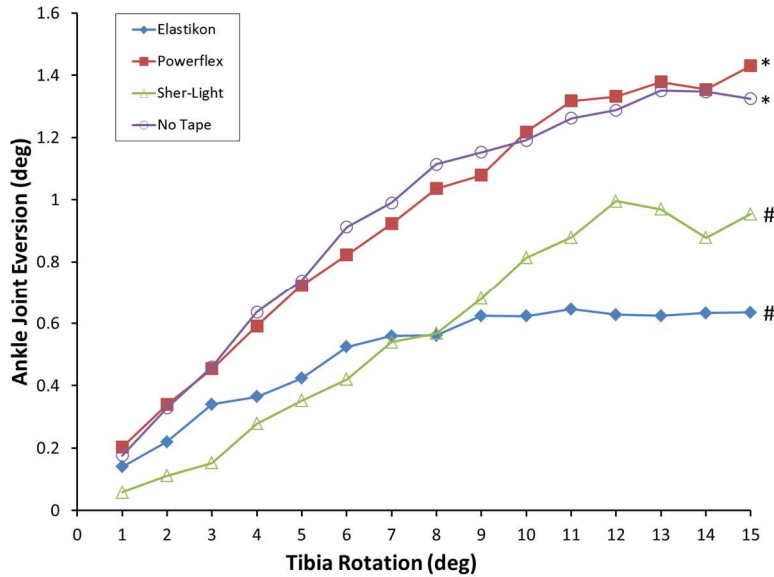


Figure 5-8 Mean ankle joint eversion-tibia rotation curves for the three tape (and no-tape) designs from an in vivo external foot rotation ($n=6$). Different symbols (* #) indicate statistically different curves.

There were no differences in ankle joint dorsiflexion response between the three tapes or the tapeless condition ($p=0.461$) (Figure 5-6). There was, however, an overall difference in ankle joint external rotation response ($p<0.001$) for the four conditions. Individually, the PowerFlex external rotation response differed from the Sher-Light response ($p=0.0001$), and all other curves differed from one other ($p<0.0001$) (Figure 5-7). There was also an overall difference in ankle joint eversion response ($p<0.001$). Individually, the Elastikon eversion response was significantly different from the PowerFlex and tapeless responses ($p<0.0001$), but not from the Sher-Light response ($p=0.659$). The PowerFlex response was significantly different than the Sher-Light response ($p<0.0001$), but not the tapeless response ($p=0.999$). The Sher-Light and tapeless curves were also significantly different ($p<0.0001$) (Figure 5-8).

Predictive equations for ankle joint dorsiflexion (AJDorsi), ankle joint rotation (AJRot), and ankle joint eversion (AJever) as a function of tibia dorsiflexion (TIdorsi), tibia rotation (TIrot), tibia eversion (TIever), and tape stiffness (Stiff) are shown in equations 3a-c with correlation coefficients 0.99, 0.99, and 0.95, respectively.

$$AJdorsi = 0.0343 + 0.6794 * TIdorsi \quad (3a)$$

$$AJrot = 0.29551 + 0.6804 * TIrot + Stiff(0.0089 * TIrot - 0.0099) \quad (3b)$$

$$AJever = 0.11525 + 0.4209 * TIever + 0.08371 * TIrot - Stiff(0.0024 * TIrot + 0.0007 * Stiff + 0.0002) \quad (3c)$$

External rotation of a neutral ankle strained the ATiFL and ATiTL the most. The effects of ankle constraint stiffness on the ATiTL strain were greater than those on the ATiFL strain (Figure 5-9a and b). Fifteen degrees of tibial rotation strained the ATiFL 15.5-16.2%, while the ATiTL strain was between 6.7% and 14.5%. At 15 deg of tibial rotation, each increment of 5 Nm/deg in stiffness theoretically increased ATiTL strain approximately 1.2%.

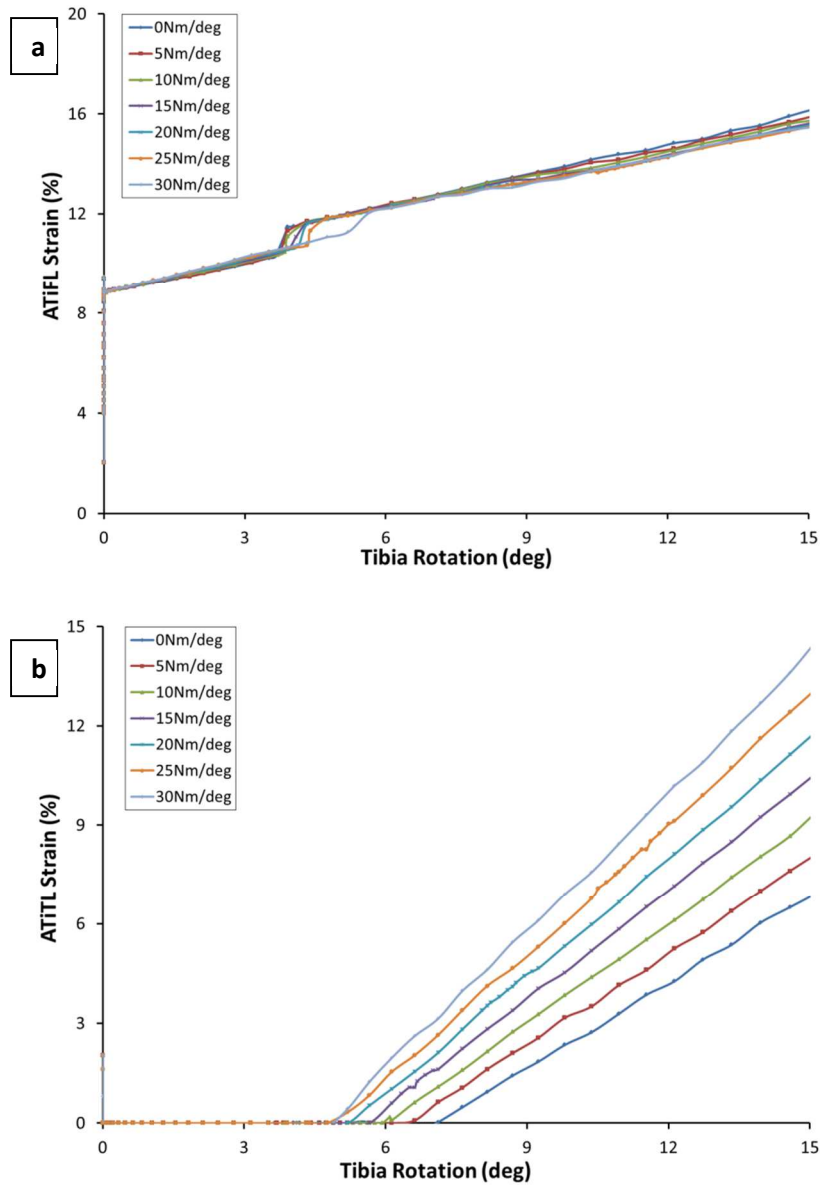


Figure 5-9 Predicted anterior tibiofibular ligament (ATiFL) (a) and anterior tibiotalar ligament (ATiTL) (b) strain versus tibia rotation for an ankle constrained with tape stiffness ranging from 0 to 30 Nm/deg. Inputs for ankle joint motion were based on predictive equations 3a-3c.

DISCUSSION

The current study investigated the effect of ankle constraint on the three-dimensional motion of the ankle using different athletic tapes. Three tapes (and a no-tape condition) were used to constrain human ankles during an *in vivo* voluntary external ankle rotation. The rotational stiffness of the tapes was comparable to those of a relatively stiff and a compliant football shoe design. Predictive equations for determining ankle joint motion as a function of tibia motion and tape stiffness were developed from human subject testing results. These predictive equations were used to drive a generic computational ankle model for the calculation of ligament strain during isolated external ankle rotation. Results of the experimental study indicated that for a given tibia rotation the amount of ankle joint eversion and external rotation was dependent on the level of ankle constraint, with a stiffer ankle constraint allowing greater ankle rotation, but less eversion. Constraint on the ankle also affected theoretical ligament strain: increasing constraint stiffness substantially increased ATiTL strain, but had little effect on ATiFL strain. These results supported the hypothesis that constraint stiffness would have a significant effect on ankle joint eversion and rotation during foot external rotation.

Previous investigations on anatomical specimens conclude that external rotation of an unconstrained ankle results in a combination of eversion and rotation (Lundberg et al., 1989b). This potentially explains the increased eversion measured in ankles constrained with a more flexible tape, likely because the applied rotation can be more easily transferred about other axes of the ankle. In particular, less constraint of the subtalar and transverse tarsal joints may allow more motion between the talus and calcaneus, generating foot eversion (Hertel et al., 1999, Wei et al., 2012a). With increased tape stiffness, however, this natural response was restricted,

resulting in nearly isolated ankle external rotation. Additionally, while eversion and external rotation are strongly coupled, they are only weakly coupled with dorsiflexion (Lundberg et al., 1989b), potentially explaining why ankle dorsiflexion was only a function of absolute tibia dorsiflexion (Equation 3a). The apparent correlation between tibia rotation and ankle joint dorsiflexion noted in Figure 5-6 was most likely due to an increased tibia flexion that occurred as a result of loading the leg.

Foot external rotation primarily strained the ATiTL and ATiFL in the computational model. Figure 5-9 shows that axial load put an ~8% pre-strain on the ATiFL, likely due to the tibiofibular syndesmosis opening slightly around the talus upon contact. External rotation put additional strain on the ligament, and constraint stiffness had little effect on strain magnitude. However, increasing constraint stiffness correlated with considerable increases in ATiTL strain. Unlike the ATiFL, the ATiTL strain did not increase with axial load, but increased linearly with tibia rotation once the ligament began to tense around 5-7° of tibia rotation. The observation of increased ATiTL strain with increasing rotational ankle constraint suggested that a stiffer constraint may predispose the ankle to medial ankle injury during external rotation. This potentially explains the results from a previous cadaver study in which pairs of cadaver ankles were rotated to failure in either a stiff (Flyposite) or flexible (Air) football shoe. A high frequency of combination medial and syndesmotoc ankle injuries were noted in the stiff shoes, while ankles in flexible shoes mostly suffered isolated syndesmotoc injuries (Button et al., 2015).

The information regarding the effect of ankle constraint on ankle joint kinematics and injury risk may benefit the future design of athletic shoes. Previous studies have examined the effects of running shoe structure (Bonacci et al., 2013, Peltz et al., 2014, Williams et al., 2012) and football shoes (Wei et al., 2012a, Button et al., 2015), as well as the effects of shoe-surface interface (Villwock et al., 2009a) on joint kinematics and injury risk, but no study has quantified and modelled these effects. Two shoe designs from a previous cadaver study (Wei et al., 2012a, Button et al., 2015) were subjected to rotational stiffness testing in order to assess whether or not the constraint offered by the athletic tapes was a realistic simulation of athletic footwear (Figure 5-5). It was noted that the stiffer shoe (Nike Flyposite) behaved almost identically to the stiffest tape (Elastikon), while the more flexible shoe (Nike Air) behaved between the moderate (Sher-Light) and most flexible tape (PowerFlex). This indicated that the tapes used in this study reasonably matched stiff and flexible shoe designs used in previously studies by this laboratory during external rotation, but future studies may want to constrain *in vivo* or cadaver ankles with different shoes instead of tapes to further investigate this effect.

Predictive equations derived in the current study may also help in the analysis of injury mechanisms during athletic competition. Using Krosshaug's MBIM technique to analyze leg and shoe kinematics in game films, Fong et al. (Fong et al., 2012) and Mok et al. (Mok et al., 2011) documented wide variations in the amount of joint motion at ligament failure, with peak inversion values ranging from 48° to 148°. However, much of this disparity could be due to different constraints on the ankle joint in different footwear. Predictive equations from the current study exhibited that 15 degrees of isolated tibia rotation could result in 10.5°-14.2° of ankle joint rotation and 6.7-14.2% ATiTL strain, depending on ankle constraint. Future studies

may want to not only use MBIM to investigate the kinematics of the leg with respect to the shoe during external rotation, but complement this information with the known rotational shoe stiffness-ankle motion relationships to more accurately assess ankle joint kinematics inside the shoe. Such information, combined with cadaver studies and computational modeling, could help provide researchers with a more complete understanding of ankle kinematics within the shoes during high and medial ankle sprains.

While the current study utilized human subjects, future studies may benefit from studying joint motion under various constraints using cadaver specimens. While *in vivo* studies rely largely on voluntary motions, using cadaver specimens would allow more precise control of input motions. Reflective markers could also be screwed into the talus, calcaneus, and tibia. Marker arrays on both the talus and calcaneus would enable the calculation of both subtalar and talocrural joint kinematics. Additionally, using screw-in marker sets instead of skin marker sets could potentially mitigate any errors associated with skin motion. Furthermore, a limitation of the current study was that the analysis was restricted to sub-failure rotations. Using cadavers could allow researchers to measure ankle kinematics and ligament behavior at failure-level foot rotations, which may differ from sub-failure behavior. Comparing results from a cadaver study with an *in vivo* study could also help quantify the effect of muscle action on ankle joint kinematics during external foot rotation.

In conclusion, the current study quantified the effect of constraint on ankle joint motion during voluntary external foot rotation. The study showed that constraint of the ankle had an effect on the amount of ankle eversion and rotation for a given degree of tibia rotation, while dorsiflexion was unaffected. A computational model of the ankle and its major ligamentous structures

showed that ATiTL strain was highly dependent on ankle constraint, while ATiFL strain was not. The current study represents an important step in understanding the effect of different footwear on ankle joint kinematics during external rotation of the foot relative to the upper body.

CHAPTER 6:

A METHOD OF DETERMINING IN VIVO DYNAMIC HUMAN ANKLE STIFFNESS DURING EXTERNAL ROTATION

ABSTRACT

This study presents a method to determine stiffness of the human ankle in internal-external rotation, inversion-eversion, and plantarflexion-dorsiflexion during an *in vivo*, single-legged, external foot rotation experiment. Five young male subjects stood on one foot and performed an internal rotation of the body (external rotation of the foot) on a force plate, while motions were captured with a motion capture system. Hindfoot rotations relative to the tibia and resistive moments in the above three directions were obtained using a commercial software package. The resistive moments were plotted against rotation during the loading portions of the curves. Linear approximations of these curves were used to determine stiffness of the ankle in directions of internal-external, inversion-eversion, and plantarflexion-dorsiflexion. Future data from the above experiment and other athletic motions may be useful for the design of surrogate devices used to evaluate the potential performance and ankle injury risk characteristics of various shoe-surface interfaces.

INTRODUCTION

Acute ankle trauma accounts for 10-30% of sports-related injuries (Hootman et al., 2007). While medial and high ankle sprains are less common than lateral ankle sprains, they represent a more disabling problem requiring longer recovery times (Wolfe et al., 2001). Preventative measures may require the assessment of current footwear and playing surfaces.

The mechanism of medial and high ankle sprains has been clinically ascribed to excessive external foot rotation (Guise, 1976, Boytim et al., 1991). Additionally, foot eversion prior to external rotation has been shown critical in generating a high ankle sprain(Wei et al., 2012b). It is also generally accepted that excessive rotational traction (Cawley et al., 2003) at the shoe-surface interface may precipitate ankle and knee injuries (Nigg and Yeadon, 1987). Livesay et al. (Livesay et al., 2006) suggest that rotational stiffness of the shoe-surface interface may be a more important parameter than torque in determining ankle injury risk. Thus, evaluations of shoe-surface interface with devices and development of preventative measures should use surrogate ankles that have appropriate 3D properties and can simulate motions of the human ankle.

Previous studies documenting human ankle stiffness (or compliance) have determined ankle stiffness using controlled input motions (Villwock et al., 2009c, Petit, 1996, Crandall et al., 1996). However, little information exists on motions of the human ankle and its stiffness during voluntary athletic maneuvers. The objective of the current study was to describe a method that integrates experimentally obtained kinematic and kinetic data to produce useful structural characteristics of the *in vivo*, human ankle during external foot rotation. This information may help in the future development of surrogate devices to assess performance and ankle injury risk characteristics of shoe-surface interfaces.



Figure 6-1 Marker set of the Oxford Foot Model (Carson et al., 2001). The subjects stood on one foot and performed an internal rotation of the body (external rotation of the foot).

METHODS

Institutional Review Board approval was obtained for this project. *In vivo* kinematic data were collected after obtaining informed consent from five young, male subjects with body mass of 77.9 ± 18 kg. A six-camera Vicon MX Motion Capture System (OMG plc. Oxford, UK) was used to capture motions at 100 Hz from a marker set defined by the Oxford Foot Model (OFM) (OMG plc., Oxford, UK) (Carson et al., 2001). An AMTI (Advanced Mechanical Technology, Inc., Watertown, MA) force plate was used to capture ground reaction data at 1000 Hz. The subjects stood with a flexed right leg on the force plate, balanced themselves, and performed an internal rotation of the body (external rotation of the foot) with a self-determined maximum effort (Figure 6-1). The subjects were instructed to internally rotate their bodies at a self-selected speed, but within 3s, while keeping their foot on the force plate. Data were acquired over four

trials and processed using commercial kinetic (Plug-in Gait, OMG plc., Oxford, UK) and kinematic (Dynamic OFM) software packages.

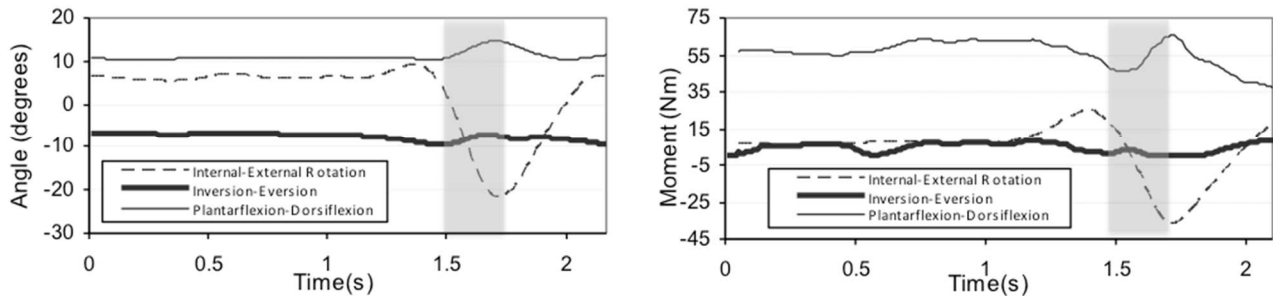


Figure 6-2 Sample of a moment versus time plot (left) and rotation versus time plot (right) for all three movements: internal-external rotation, inversion-eversion, and plantarflexion-dorsiflexion. Data from the loading phase (shaded in the figure) for moment vs. time were extracted and plotted against the extracted rotation vs. time data, as shown in Figure 6-3.

Hindfoot rotations relative to the tibia and the corresponding resistive moments of the ankle in three directions were obtained from the Plug-in Gait package. The moments were measured with respect to the center of the ankle joint, as determined by the Plug-in Gait package. Moment and rotation versus time plots were generated from the trials of each subject (Figure 6-2). The three dimensional moments were plotted against the corresponding rotations from the beginning of ankle loading (either a peak or sink in the response curve) to the end of loading (another peak or sink). A linear regression was performed on the moment-rotation plot in order to determine the slope and coefficient of determination (R^2) for each trial. The average slope of the four trials from each subject was used to represent subject ankle stiffness (Figure 6-3).

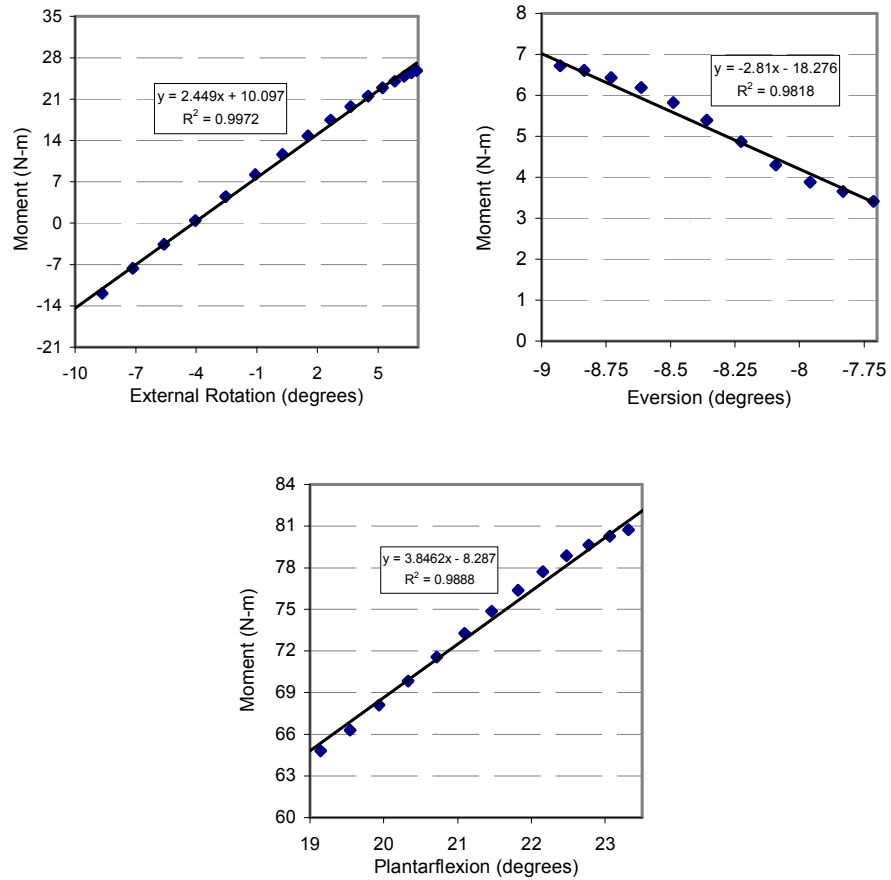


Figure 6-3 Samples of moment versus rotation plots in the loading phase for internal-external rotation (left), inversion-eversion (right), and plantarflexion-dorsiflexion (bottom).

One-way ANOVA (Minitab Inc., State College, PA) was used to compare potential differences of rotation speed between subjects. A linear regression analysis was used to determine the correlation between subject body mass and ankle stiffness.

Table 6-1 Ankle stiffnesses in three directions obtained from subjects performing a single legged external rotation of the foot with standard deviations in parenthesis. Note: the absolute value of the inversion-eversion slope was taken so that the reported number was positive.

		Subject					Mean	SD
		1	2	3	4	5		
Rotation Speed (deg/s)		52.47 (23.63)	75.20 (19.07)	61.83 (15.65)	43.00 (11.49)	86.21 (16.51)	63.75	17.3
Internal/external rotation	Stiffness (Nm/deg)	1.80 (0.86)	1.52 (0.23)	2.67 (1.03)	2.65 (0.65)	2.31 (0.04)	2.19	0.52
	Range (deg)	11.87 (6.69)	18.41 (5.78)	14.69 (4.98)	5.93 (1.00)	23.69 (4.84)	14.92	6.69
	R²	0.98 (0.00)	0.99 (0.01)	0.99 (0.00)	0.98 (0.02)	0.99 (0.00)	0.99	0.01
Inversion/eversion	Stiffness (Nm/deg)	0.71 (0.35)	1.67 (1.05)	2.13 (0.92)	2.08 [†]	2.64 (.28)	1.85	0.72
	Range (deg)	6.72 (3.78)	2.77 (1.56)	1.03 (0.50)	4.14 [†]	1.37 (0.43)	3.2	2.32
	R²	0.99 (0.00)	0.96 (0.05)	0.95 (0.05)	0.98 [†]	0.98 (0.01)	0.97	0.02
Plantarflexion/dorsiflexion	Stiffness (Nm/deg)	12.13 (0.08)	3.47 (1.13)	8.05 (1.60)	2.20 (0.53)	2.50 (1.07)	5.68	4.31
	Range (deg)	0.72 (0.35)	4.54 (1.28)	3.27 (0.23)	2.77 (2.21)	2.11 (0.95)	2.68	1.41
	R²	0.89 (0.14)	0.89 (0.08)	0.99 (0.01)	0.92 (0.04)	0.97 (0.04)	0.93	0.04

RESULTS

The average rotation speed utilized by subjects was 63.5 ± 17.3 deg/sec and showed no significant difference between subjects ($p=0.11$) (Table 6-1). The ranges of internal-external rotational motion, inversion-eversion motion, and plantarflexion-dorsiflexion motion for these experiments were 14.92 ± 6.69 , 3.20 ± 2.32 , and 2.68 ± 1.41 (deg), respectively. The level of internal-external motion was significantly different than other motions ($p<0.001$). The coefficients of determination (R^2), assuming linearity, of the moment-rotation responses for internal-external, inversion-eversion and plantarflexion-dorsiflexion rotation were 0.99 ± 0.01 , 0.97 ± 0.02 and 0.93 ± 0.04 , respectively (Table 6-1). The stiffness values of the ankle in internal-external rotation, inversion-eversion, and plantarflexion-dorsiflexion were 2.19 ± 0.52 , 1.85 ± 0.72 and 5.68 ± 4.31 (Nm/deg), respectively. A linear regression analysis revealed no correlation between subject mass and stiffness for internal-external rotational, inversion-eversion, and plantarflexion-dorsiflexion ($p=0.73$, 0.85 , and 0.38 , respectively).

DISCUSSION

The current study documented a method to extract *in vivo* ankle stiffness in internal-external, inversion-eversion and plantarflexion-dorsiflexion during a single legged, external foot rotation experiment. Results from the ATMI force plate and OFM-based motion analysis provided moments and angular rotations in the three directions. These experimentally collected data were utilized to calculate *in vivo* ankle stiffnesses in the three directions. Despite a small sample size, the method proposed in this study may provide more realistic ankle stiffness values than previous studies using either human cadavers or human subjects with passive motions (Crandall et al.,

1996, Petit, 1996, Villwock et al., 2009c) due to the fact that those muscles that were specifically needed to cause internal body rotation were being utilized.

Table 6-2 *Stiffness values obtained from previous studies*

	Stiffness (Nm/deg)	Reference
Internal/External Rotation	1.24-1.96	[9], [13]
Inversion/Eversion	0.83-1.7	[11], [10]
Dorsiflexion/ Plantar Flexion	3.7-6.4	[14, 19]

As opposed to previous studies that either applied controlled motions to human subjects or utilized cadavers, the current study, by allowing voluntary motions, showed a higher stiffness in internal-external and inversion-eversion directions, and a comparable stiffness in dorsiflexion-plantar flexion direction (Table 6-2). A study by Villwock et al. (Villwock et al., 2009c) applied an external rotation to cadaver ankles while measuring the resistive torque, showing an average internal/external rotation stiffness of 1.24 Nm/deg. Other external foot rotation experiments using cadavers document a rotational stiffness of 1.65 Nm/deg and 1.96 Nm/deg with the foot in a flexible and rigid football shoe, respectively (Wei et al., 2012a). Applying an isolated motion to human volunteers, Crandall et al. (Crandall et al., 1996) documents the inversion/eversion stiffness to be 0.83 Nm/deg while Petit et al. (Petit, 1996) measures a stiffness of 1.7 Nm/deg by applying the same motion to cadavers. Loram and Lakie (Loram and Lakie, 2002) document a stiffness in dorsiflexion/plantar flexion between 3.7 and 4.8 Nm/deg by strapping human subjects to a fixed vertical support and having them balance an inverted pendulum. Casadio et al. document a higher stiffness (6.4 Nm/deg) by mounting a motorized footplate onto a strain gauge force platform.

One limitation of the current study was that subjects generated internal rotation of their bodies with only a small amount of initial plantar-dorsiflexion or inversion-eversion rotation, resulting in fewer data points. A previous study by Smith and Wong (Smith and Wong, 2012) has noted that, when calculating ankle stiffness, more data points result in a higher reliability. Future studies may have to adjust sampling rate in order to increase data reliability. Another limitation of the current study was that ankle stiffness was determined in only the voluntary range of loading. Previous cadaver studies (Villwock et al., 2009c, Petit, 1996, Crandall et al., 1996) have noted a bilinear stiffness response of the ankle, with the stiffness increasing near failure levels. It, of course, was not possible to conduct the current *in vivo* studies at high levels of internal body rotation due to human subject safety issues. However, by comparing data from subfailure *in vivo* and cadaver studies, the role of ankle musculature may be estimated by the use of a mathematical model, similar to that utilized in a glenohumeral joint study by Elmore and Wayne (Elmore KA, 2012) and the ankle study by Wei et al. (Wei et al., 2011d) (without musculature effects). Based on such approximations, a surrogate ankle may be constructed that might yield a better tool to determine the roles of various shoe-surface-interfaces on athletic performance and their potential in producing high ankle sprains. Finally, a limitation of all studies involving human subjects is the potential for variances in subject performance, particularly evident in the ranges of motion during external rotation. This is likely a result of the complex anatomy of the talocrural joint which can result in differences in range of motion (and thus loading time) due to differences in bone shape and spacing. As a result, while we believe *in vivo* data are most appropriate for evaluations of shoe-surface interface characteristics, future studies may need to provide better control of subject motions and very likely involve a large number of human participants to generate reliable ankle stiffness information for the development of a biofidelic

surrogate device. Additionally, more trials from each subject could be taken in order to test the repeatability of the current data.

While the current study was limited to internal rotation of the body with the foot planted on a force plate, the methodology for determining ankle stiffness could be utilized in studies of other athletic maneuvers, such as external rotation of the body with a planted foot or for various cutting maneuvers. The current study utilized motion capture and a force plate to accomplish this, but future studies might also utilize pressure insoles to help determine ankle stiffness during more complex motions outside the laboratory (Weaver et al., 2013). Such data could more completely characterize human ankle stiffness under a variety of situations on the athletic field. These data may then be useful for the development of future surrogate test devices to evaluate potential athletic performance and ankle injury risk characteristics of shoe-surface interfaces.

CHAPTER 7:

CONCLUSIONS

Overview

The first hypothesis of the current research was that the movement of the talocrural joint and the location of injury during external rotation is a function of both the position of the ankle prior to rotation and the amount of constraint on the ankle. This was investigated through both *in vivo* and cadaveric testing. *In vivo* testing allowed for the measurement of ankle joint motion with various constraints on the foot while accounting for muscle force and dynamic weight bearing. These conditions closely replicated injurious conditions in real-life, but at sub-failure levels. Cadaveric studies, despite not accounting for muscle-force, were advantageous because they allowed for precision in experimental design and measurement, an accurate calculation of joint motion by using screw-in marker sets, and an in-depth diagnosis of injury via post-test dissection.

The second hypothesis of the current research was that specimen-specific, rigid-body modelling can be utilized to simulate injury-level ankle rotation in addition to modelling the effect of various shoe rotational stiffnesses on talocrural and subtalar joint kinematics. Computational modelling was an efficient, cost-effective, and non-invasive way to supplement information measured from cadaveric and *in vivo* tests. Computational modelling enabled the calculation of failure properties of ligaments given different boundary conditions. This was useful in explaining experimental results and subsequently drawing conclusions regarding external rotation ankle injury risk factors. Together, computational modelling, *in vivo* testing, and cadaveric testing helped explain the functional roles of various structures of the ankle and how those roles contribute to injury.

Chapter 2

Chapter 2 was a computational study which utilized CT scans to build specimen-specific models and replicate injurious motions. Per previous laboratory testing, pairs of cadaver ankle models were pre-everted 20 degrees or neutral in the coronal plane prior to external rotation up to the angle of failure in the experiments, at which point peak strains in the ligaments were calculated. The neutral ankle models showed highest strain in the ATiTL ($29.1 \pm 5.3\%$), correlating with the medial ankle sprains in the neutral cadaver experiments. Everted ankle models showed highest strain in the ATiFL ($31.2 \pm 4.3\%$) correlating with the high ankle sprains documented in everted experiments. Combining both neutral and everted simulations, strains of $31.8 \pm 3.8\%$ computed from the models of experiments that showed grossly ruptured ligaments were statistically greater than $25.5 \pm 4.2\%$ for the partial tear simulations. The correlation between strain and ligament damage demonstrated the potential for modelling to provide important information for the study of injury mechanisms along with aiding in prevention of future injury.

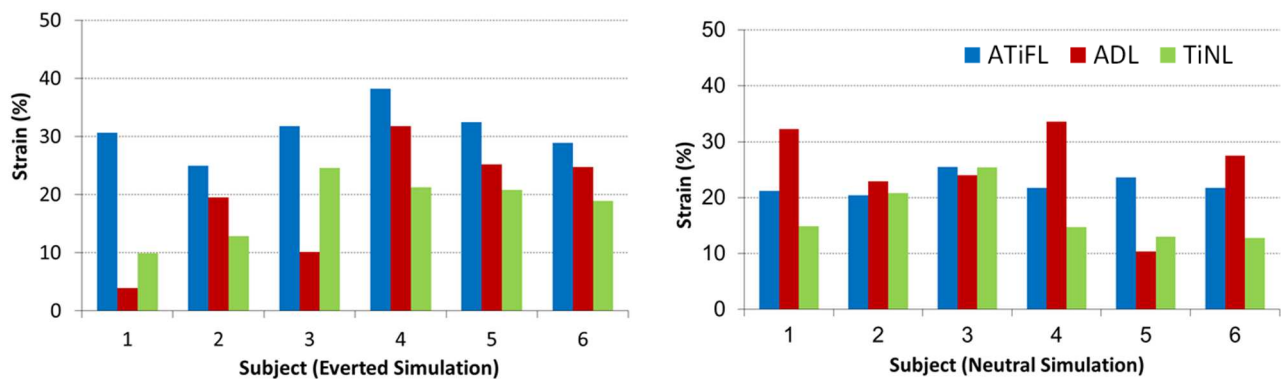


Figure 7-1 Strains in the ATiFL and two deltoid ligaments (ATiTL and TiNL) for neutral and everted simulations.

Chapter 3

Chapter 3 was an experimental study that investigated the effect of pre-eversion on talocrural and subtalar joint motion during external rotation. Fourteen (seven pairs) cadaver lower extremities were externally rotated 20 degrees in either a pre-everted or neutral configuration. Vicon motion capture was used to track the motion of marker arrays on the tibia, talus, and calcaneus. Joint coordinate systems between the tibia and talus (talocrural) and talus and calcaneus (subtalar) were established to measure rotation, flexion, and in-eversion. While talocrural joint rotation was greater in the neutral ankle (13.33 ± 2.09 deg versus 10.51 ± 2.75 deg, $p=0.006$), subtalar joint rotation was greater in the pre-everted ankle (2.38 ± 1.89 deg versus 1.12 ± 1.04 deg, $p=0.014$). Overall, the talocrural joint rotated more than the subtalar joint (11.92 ± 2.77 deg versus 1.75 ± 1.61 degrees, $p<0.001$).

It was proposed that the calcaneus and talus ‘lock’ when axial load is applied to a neutral joint, limiting subtalar motion, but maximizing talocrural rotation. When the foot is everted prior to axial load, the subtalar joint may ‘unlock’ enabling the tibiotalar ligaments to pull the talus with the rotation of the tibia, resulting in lower relative motion. This ‘unlocking’ of the subtalar joint puts less strain on the medial ligaments potentially explaining why the combination of eversion and external rotation does not always damage the anterior deltoid. This study may improve our understanding of various mechanisms of ankle injury during external rotation of the foot.

Table 7-1 *Motions of the subtalar and talocrural joint for 20 degrees of external rotation*

Specimen	Subtalar Eversion (deg)		Talocrural Eversion (deg)		Subtalar Dorsiflexion (deg)		Talocrural Dorsiflexion (deg)		Subtalar Rotation (deg)		Talocrural Rotation (deg)	
	Neutral	Everted	Neutral	Everted	Neutral	Everted	Neutral	Everted	Neutral	Everted	Neutral	Everted
1	0.59	0.29	0.39	0.19	1.46	0.16	0.03	0.34	0.04	0.69	15.81	11.08
2	1.66	2.43	2.68	3.80	2.24	1.43	0.98	4.09	1.11	1.70	12.30	10.97
3	0.50	0.21	1.53	1.03	1.29	0.75	3.11	3.50	2.53	5.78	11.84	6.41
4	0.25	0.32	1.35	0.30	0.97	0.53	0.55	0.52	0.23	0.88	15.67	12.87
5	0.97	0.41	1.30	1.34	0.84	0.16	0.79	0.02	0.02	0.94	14.93	14.20
6	1.04	1.99	1.50	1.31	1.23	1.02	2.91	0.78	1.98	2.88	12.09	10.53
7	1.71	0.84	0.58	0.85	0.04	0.52	0.72	0.48	1.90	3.81	10.65	7.52
AVG	0.96	0.93	1.33	1.26	1.15	0.65	1.30	1.39	1.12	2.38	13.33	10.51
STDEV	0.56	0.91	0.74	1.21	0.67	0.46	1.21	1.67	1.04	1.89	2.09	2.75
p-value	0.39		0.79		0.054		0.882		0.014		0.006	
	0.787				0.197				<0.001			

Chapter 4

Chapter 4 was a two-part study with the goal of investigating the effect of shoe rotational stiffness on talocrural joint motion and injury during external rotation. The first part of the study involved externally rotating pairs of cadaver ankles to failure in either a stiff or flexible shoe while tracking the motion of the talus and tibia using motion capture. The second part of the study involved modelling the experiments using specimen specific computational models. Ankles in flexible shoes allowed 6.7 ± 2.4 degrees of talus eversion during rotation, significantly greater than the 1.7 ± 1.0 degrees for ankles in stiff shoes. All ankles failed by either medial ankle injury or syndesmotic injury, or a combination of both. Complex (more than one ligament or bone) injuries were noted in 4 of 6 ankles in stiff shoes and 1 of 6 ankles in flexible shoes (Table 7-2). The computational study provided information regarding the mechanisms of complex injury (Figure 7-2). Despite a $\sim 10\%$ ATiFL pre-strain, the ATiTL strain rate increased more rapidly and overtook the ATiFL strain level near the point of failure. This supported the Weber C classification of failure: the ATiTL failed first, causing lateral translation of the talus and a subsequent increase in ATiFL strain to cause failure of the ATiFL. In the flexible shoes, limited

talocrural rotation often resulted in lower ATiTL strain, potentially explaining the lower incidence of complex injuries. Information from this study may help drive research and design of athletic footwear in order to limit injury severity during external foot rotation in sport.

Table 7-2 Summary of injury mechanisms and failure metrics from cadaver experiment

Specimen	Failure Torque (Nm)		Tibia Failure Rotation (deg)		Talocrural Failure Rotation (deg)		Talocrural Failure Eversion (deg)		Injury Mechanism	
	Stiff	Flexible	Stiff	Flexible	Stiff	Flexible	Stiff	Flexible	Stiff	Flexible
1	85.6	83.4	44.7	46.5	19.3	17.5	3.5	3.9	1) Medial malleolus fracture 2) Spiral fracture of the fibula	ATiFL avulsion
2	75.8	93.4	37.0	39.4	27.9	21.5	0.9	7.4	1) ATiFL rupture 2) ATiTL rupture	ATiFL rupture
3	44.9	51.0	44.6	31.1	28.4	18.5	0.8	5.2	Medial malleolus fracture	1) ATiFL avulsion 2) ATiTL avulsion
4	55.8	59.0	29.4	33.2	19.3	13.9	1.7	5.1	1) ATiFL rupture 2) ATiTL rupture	ATiTL rupture
5	102.4	117.9	37.4	43.0	13.9	15.1	2.0	8.2	ATiFL avulsion	Fibular head fracture
6	170.7	179.7	48.1	63.2	20.3	27.2	1.1	10.4	1) ATiFL rupture 2) ATiTL rupture	ATiTL rupture
Average	89.2	97.4	40.2	42.7	21.5	19.0	1.7	6.7*		
<i>Standard Deviation</i>	44.9	47.0	6.9	11.6	5.6	4.9	1.0	2.4		

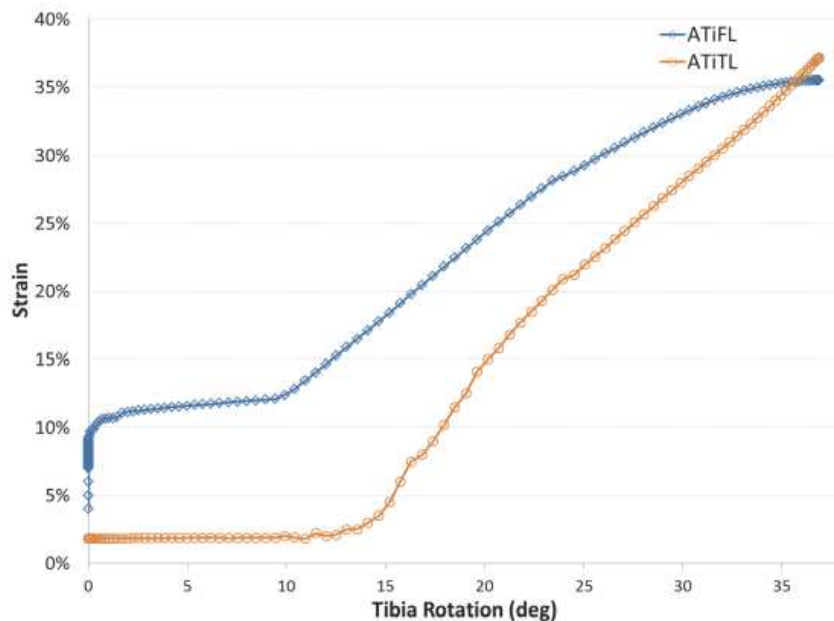


Figure 7-2 Representative plot of the ATiFL and ATiTL strains versus tibia rotation

Chapter 5

Chapter 5 was a two-part study that involved quantifying the amount of ankle joint motion as a function of tibia rotation and constraint rotational stiffness. The first part was an *in vivo* experiment where subjects performed external ankle rotation with one of four foot constraints of varying rotational stiffnesses while tracking the tibia and hindfoot using motion capture. Ankle joint rotations in three directions (flexion, in-eversion, and rotation) were determined for each subject up to 15 degrees of tibia rotation and the values were averaged to give a general curve (Figure 7-3). Using the `LinearModel.fit` function in MATLAB, an equation was determined for ankle joint dorsiflexion versus tape stiffness and tibia motion, ankle joint eversion versus tape stiffness and tibia motion, and ankle joint external rotation versus tape stiffness and tibia motion

The second part of the study involved inputting predicted ankle joint motion for tibia rotations 0-15 degrees and tape rotational stiffnesses from 0 to 30 Nm/deg. Ligament strain was determined during rotation to provide a range of strains for key ligaments over a domain of stiffnesses. It was determined that constraint has a substantial effect on ATiTL strain during rotation, and a small effect on ATiFL strain (Figure 7-4). Information from this study may help the design of footwear in the future, as well as the analysis of game-time injuries given leg rotation and footwear properties.

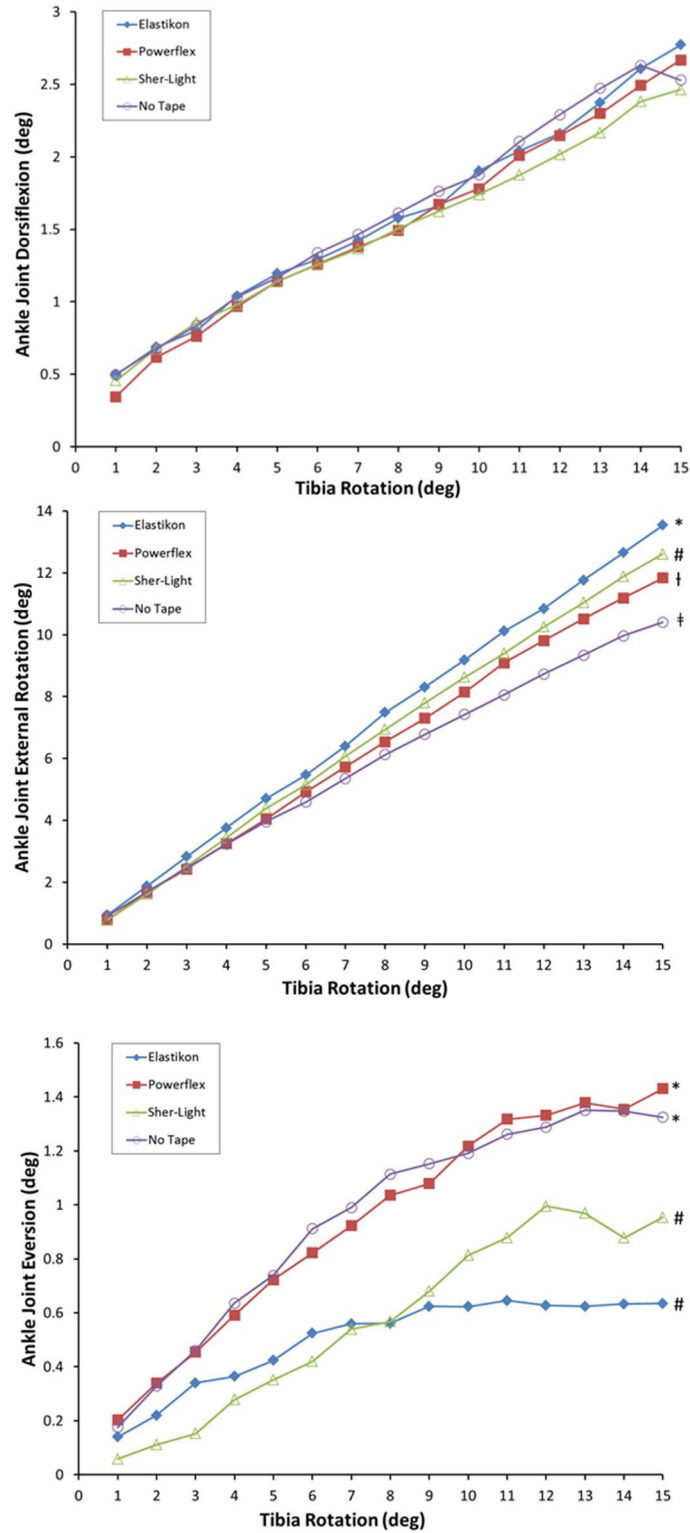


Figure 7-3 Mean ankle joint dorsiflexion, external rotation, and eversion vs. tibia rotation for three tapes and a tapeless condition.

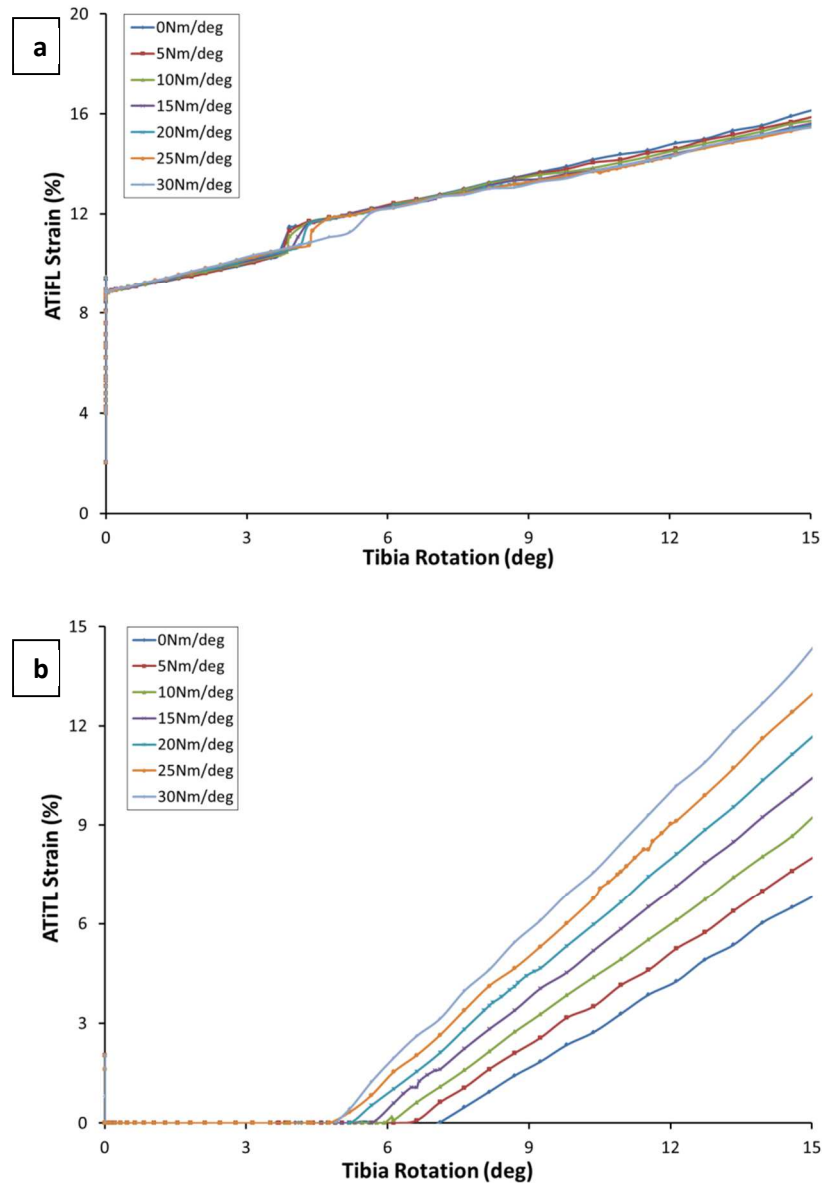


Figure 7-4 Predicted anterior tibiofibular ligament (ATiFL) (a) and anterior tibiotalar ligament (ATiTL) (b) strain versus tibia rotation for an ankle constrained with tape stiffness ranging from 0 to 30 Nm/deg. Inputs for ankle joint motion were based on predictive equations 3a-3c.

Chapter 6

Chapter 6 was an *in vivo* study which involved providing a method to determine stiffness of the human ankle in internal-external rotation, inversion-eversion, and plantarflexion-dorsiflexion

during a single-legged external foot rotation experiment. Five male subjects stood on one foot and performed an internal rotation of the body (external rotation of the foot) on a force plate, while motions were captured with a motion capture system. Hindfoot rotations relative to the tibia and resistive moments in the above three directions were obtained using a commercial software package. The resistive moments were plotted against rotation during the loading portions of the curves. Linear approximations of these curves were used to determine stiffness of the ankle in directions of internal-external, inversion-eversion, and plantarflexion-dorsiflexion. This method can be used in the future for a variety of athletic motions in order to more fully characterize human ankle stiffness under different loading situations on the athletic field. The data can then be useful for the development of surrogate test devices to evaluate athletic performance and ankle injury risk characteristics of shoe-surface interfaces.

Table 7-3 *Ankle stiffness in three directions obtained from subjects performing a single legged external rotation of the foot.*

		Subject					Mean	SD
		1	2	3	4	5		
Rotation Speed (deg/s)		52.47 (23.63)	75.20 (19.07)	61.83 (15.65)	43.00 (11.49)	86.21 (16.51)	63.75	17.3
Internal/external rotation	Stiffness (Nm/deg)	1.80 (0.86)	1.52 (0.23)	2.67 (1.03)	2.65 (0.65)	2.31 (0.04)	2.19	0.52
	Range (deg)	11.87 (6.69)	18.41 (5.78)	14.69 (4.98)	5.93 (1.00)	23.69 (4.84)	14.92	6.69
	R²	0.98 (0.00)	0.99 (0.01)	0.99 (0.00)	0.98 (0.02)	0.99 (0.00)	0.99	0.01
Inversion/eversion	Stiffness (Nm/deg)	0.71 (0.35)	1.67 (1.05)	2.13 (0.92)	2.08 [†]	2.64 (.28)	1.85	0.72
	Range (deg)	6.72 (3.78)	2.77 (1.56)	1.03 (0.50)	4.14 [†]	1.37 (0.43)	3.2	2.32
	R²	0.99 (0.00)	0.96 (0.05)	0.95 (0.05)	0.98 [†]	0.98 (0.01)	0.97	0.02
Plantarflexion/dorsiflexion	Stiffness (Nm/deg)	12.13 (0.08)	3.47 (1.13)	8.05 (1.60)	2.20 (0.53)	2.50 (1.07)	5.68	4.31
	Range (deg)	0.72 (0.35)	4.54 (1.28)	3.27 (0.23)	2.77 (2.21)	2.11 (0.95)	2.68	1.41
	R²	0.89 (0.14)	0.89 (0.08)	0.99 (0.01)	0.92 (0.04)	0.97 (0.04)	0.93	0.04

Contributions to the Literature

This dissertation has made three major contributions to the current literature:

Influence of shoe design on ankle movement and injury

Previous studies have investigated shoe-surface interaction as an indicator of rotational injury risk, but few studies have studied the effect of a shoe's rotational stiffness on injury. A primary contribution of this dissertation was the investigation of the effect shoe rotational stiffness has on ankle joint motion, ligament strain, and injury generated. This was first looked at in Chapter 4, which showed that shoe rotational stiffness not only affected the amount of talocrural joint eversion and rotation during external foot rotation, but also the severity of injury generated and distribution of ligament strains. It was concluded that stiff shoes limit talocrural joint eversion during ankle external rotation, but maximize talocrural joint rotation. This resulted in high anterior deltoid strains and complex injuries. The interaction between rotational stiffness and talocrural joint motion was quantified in Chapter 5. The equations presented in this chapter will enable future researchers to more accurately assess ankle joint motion given gross foot rotation and shoe rotational stiffness. Additionally, this may aid in the design of footwear with the goal of limiting time-loss due to severe ankle injury.

Determination of failure-level ligament strains

While previous studies have performed mechanical testing on *ex vivo* ligaments in order to determine failure properties, little information exists regarding the amount of strain ligaments undergo at failure *in situ*. A second major contribution of this dissertation was the correlation of ligament strain level with severity of damage. This was accomplished first in Chapter 2, which

involved using specimen-specific computational models to simulate failure-level cadaver studies. The strain magnitudes in grade II vs. grade III sprains were compared and were determined to be significantly different ($25.5 \pm 4.2\%$ vs. $31.8 \pm 3.8\%$, respectively). This was verified in Chapter 4, in which simulations modelling complete ruptures showed ligament failure at $29.1 \pm 6.7\%$. These magnitudes could be used to assess potential injury risk (such as in Chapter 6), in order to design shoes, or determine the effect of different loading conditions on injury likelihood.

Use of specimen-specific computational models

While a generic model provides useful information regarding relationships between motion and injury mechanisms, it is believed that specimen-specific modeling provides more exact strain information. A third contribution of this dissertation to the literature was the use of specimen-specific computational modelling to analyze ankle kinematics and injury. The curvature of the talar dome (top surface of the talus) determines the stability of the ankle in the anterior posterior direction and the talar facets (contacting surfaces) have a significant impact on the position of the axis of movements between the talus and calcaneus. The differences in ankle mechanics can significantly affect injury risk as talar motion plays a significant role in both medial and high ankle sprains. The use of specimen-specific ankle modeling can be expanded to investigate *in vivo* injuries by looking at scenarios where the geometry and motion of a subject are known. By looking at these scenarios, the specifics of the injury can be analyzed, thus aiding in the design of intervention strategies and equipment to limit the severity and frequency of athletic ankle injuries.

APPENDICES

APPENDIX 1: RESEARCH PUBLICATIONS

Peer Reviewed Manuscripts

1. Dutchshen N, Maerz T, Rabban P, Haut RC, Button KD, Baker KC, Guettler J. (2012) The acute effect of bipolar radiofrequency energy thermal chondroplasty on intrinsic biomechanical properties and thickness of chondromalacic human articular cartilage. *Journal of Biomechanical Engineering*. 134(8):081007.
2. Meyer EG, Wei F, Button KD, Haut RC. (2012) Determination of ankle ligament strain using a rigid body computational model for sports injury scenarios. *Proceedings-International Research Council on the Biomechanics of Injury*. 277-288.
3. Button KD, Wei F, Meyer EG, Haut RC. (2012) Specimen-specific computational models of ankle sprains produced in a laboratory setting. *Journal of Biomechanical Engineering*. 135(4), 041001.
4. Button KD, Braman JE, Wei F, Haut RC. (2013) A method of determining in vivo dynamic human ankle stiffness under external foot rotation. *Journal of Sports Engineering and Technology*. 228(2), 120-124.
5. Fischenich KM, Button KD, Decamp CD, Haut RC, Donahue TL. (2014) Evaluation of meniscal mechanics and proteoglycan content in a modified ACL transection model for osteoarthritis. *Journal of Biomechanical Engineering*. 136(7), 071001. ***Editors' Choice Paper for 2014***
6. Fischenich KM, Button KD, Coatney GA, Fajardo RS, Leikert KM, Haut RC, Donahue TL. (2014) Chronic changes in the articular cartilage and meniscus following traumatic impact to the lapine knee. *Journal of Biomechanics*. doi:10.1016/j.jbiomech.2014.11.038
7. Wheatley BB, Fischenich KM, Button KD, Haut RC, Haut Donahue TL. (2015) An optimized transversely isotropic, hyper-poro-viscoelastic finite element model of the meniscus to evaluate mechanical degradation. *Journal of Biomechanics*. (In Press).
8. Button KD, Braman JE, Davison MA, Wei F, Schaeffer MC, Haut RC. (2014) Rotational stiffness of American football shoes affects ankle biomechanics and injury severity. *Journal of Biomechanical Engineering*. doi: 10.1115/1.4029979
9. Coatney GA, Abraham AC, Fischenich KM, Button KD, Haut RC, Haut Donahue TL. (2014) Efficacy of P188 on lapine meniscus preservation following blunt trauma. *Journal of the Mechanical Behavior of Biomedical Materials*. (In Publication).
10. Button KD, Braman JE, Davison MA, Wei F, Haut RC. (2014) Effect of pre-eversion on talocrural and subtalar joint motion during ankle external rotation. *Journal of Biomechanics*. (In Revision).

11. Pauly HM, Larson BE, Coatney GA, Button KD, DeCamp CE, Fajardo RS, Haut RC, Haut Donahue TL. (2015) Assessment of cortical and trabecular bone changes in two models of post-traumatic osteoarthritis. *Journal of Orthopaedic Research* (In Revision).
12. Fischenich KM, Button KD, Fajardo RS, DeCamp CE, Haut RC, Haut Donahue TL. (2015) Tissue changes in surgical and traumatically-induced experimental models of knee joint injury using magnetic resonance imaging. *Magnetic Resonance Imaging* (In Review).
13. Button KD, Thornton PA, Braman JE, Wei F, Haut RC. (2015) Determining ankle joint motion and ligament strain during ankle rotation for a given rotational stiffness constraint. *Journal of Sports Engineering and Technology* (In Review)

Peer Reviewed Abstracts

1. Button KD, Braman JE, Wei F, Haut RC. (2012) Determination of in vivo dynamic human ankle stiffness under external foot rotation. ASME Summer Bioengineering Conf. Fajardo, Puerto Rico. SBC2012-80373.
2. Button KD, Wei F, Meyer EG, Fitzsimons K, Haut RC. (2012) Determination of in situ ankle ligament strains in cases of high and medial ankle sprains. ASME Summer Bioengineering Conf. Fajardo, Puerto Rico. SBC2012-80378.
3. Pauly HM, Larson BE, Button KD, Haut RC, Donahue TL. (2013) Micro-Computed tomography analysis of bone volume following traumatic closed joint injury. Rocky Mountain American Society of Biomechanics Meeting, April, 2013, Estes Park, CO.
4. Coatney GA, Abraham AC, Button KD, Haut RC, Donahue TL. (2013) P188 efficacy on lapine meniscus preservation following blunt trauma. Rocky Mountain American Society of Biomechanics Meeting, April, 2013, Estes Park, CO.
5. Fischenich KM, Button KD, Fajardo RS, Decamp CD, Haut RC, Donahue TL. (2013) Mechanical evaluation of menisci following surgical transection of both menisci and anterior cruciate ligament. Rocky Mountain American Society of Biomechanics Meeting, April, 2013, Estes Park, CO.
6. Fischenich KM, Button KD, Fajardo RS, Haut RC, Donahue TL. (2013) Evaluation of menisci following a traumatic compressive tibiofemoral load. ASME Summer Bioengineering Conf. Sunriver, Oregon. SBC2013-14193.
7. Button KD, Leikert K, Donahue TL, Haut RC. (2013) Development of a traumatic anterior cruciate ligament and meniscal rupture model to study osteoarthritis. ASME Summer Bioengineering Conf. Sunriver, Oregon. SBC2013-14287.

8. Button KD, Davison M, Braman JE, Schaefer MC, Haut RC. (2013) Effect of shoe stiffness on injury produced under external rotation of the foot in human cadavers. ASME Summer Bioengineering Conf. Sunriver, Oregon, 2013. SBC2013-14719.
9. Fischenich KM, Coatney GA, Haverkamp J, Button KD, DeCamp C, Haut RC, Haut Donahue TL. (2013) Meniscal glycosaminoglycan coverage twelve weeks post injury in two models of knee joint injury. 11th World Congress of the International Cartilage Repair Society, Sept. 15-18, 2013, Izmir, Turkey.
10. Button KD, Steibel JP, Karcher DM, Haut RC. (2014) A non-invasive method to predict laying hen bone mechanical properties. Poultry Science Association Annual Meeting. Christi, Texas. PSA-161.
11. Button KD, Davison M, Braman JE, Schaefer MC, Haut RC. (2014) Investigating the effects of shoe stiffness on ankle injury risk using computational models. 7th World Congress in Biomechanics. Boston, MA. 14-IS-2161-WCB.
12. Button KD, Leikert KM, DeCamp CD, Donahue TL, Haut RC. (2014) Comparison of a traumatic ACL rupture and modified transection model to study osteoarthritis. 7th World Congress in Biomechanics. Boston, MA. 14-A-1633-WCB.
13. Donahue TL, Fischenich KM, Coatney G, Pauly H, Button KD, Haut RC. (2014) Two new experimental models of post-traumatic knee joint injury. 7th World Congress in Biomechanics. Boston, MA. 14-IS-2706-WCB.
14. Fischenich KM, Button KD, Fajardo RS, Decamp CD, Haut RC, Donahue TL. (2014) A longitudinal comparison of mechanical changes of the menisci in two models of posttraumatic osteoarthritis of the knee. 7th World Congress in Biomechanics. Boston, MA. 14-A-1696-WCB.
15. Pauly HM, Larson BE, Button KD, DeCamp CD, Haut RC, Donahue TL. (2014) Micro-computed tomography comparison of trabecular bone changes in rabbits following surgical transection of anterior cruciate ligament and menisci or traumatic impact to the tibiofemoral joint. 60th Annual Meeting of the Orthopaedic Research Society. March 15-18, 2014. New Orleans, LA.

APPENDIX 2: SOP (Standard Operating Procedure) for Building Specimen-Specific Computational Ankle Models

Each individual ankle is scanned following test preparation. The ankle is potted and placed in a neutral position prior to CT scan.

The software used are MIMICS 12.1c (Materialise, Ann Arbor, MI) and SolidWorks 2011 x64 Edition (TriMech Solutions, LLC, Columbia, MD).

Mimics Procedures

Open new project wizard with CT disc inserted. Choose CT as image type → Convert.

If more than one CT is available for you to choose from the disc select the one with the most frames/slides.

*Note: Distance between images is usually 0.6 mm

Create new mask. (this will highlight entire CT)

*can change contrast by using thresholding feature. For bone it is easiest to use default

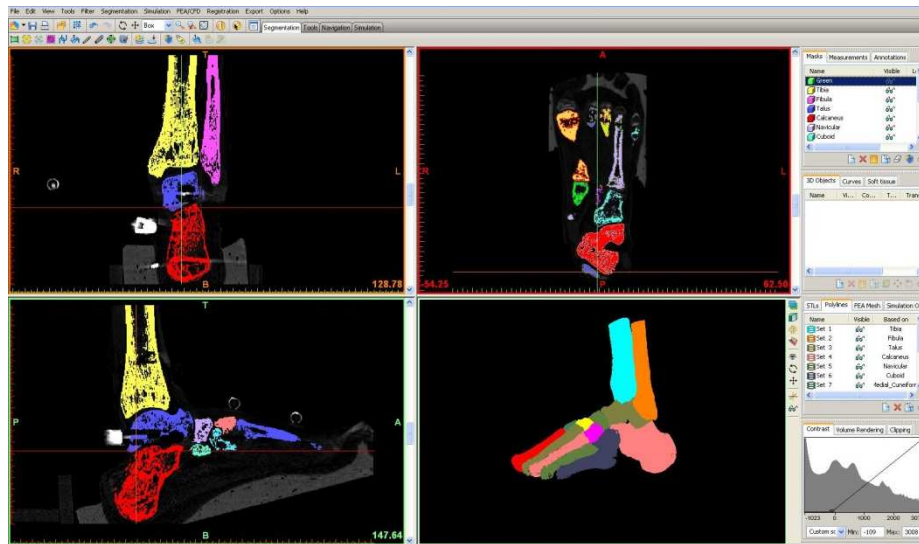


Figure A-1 Typical MIMICS interface

Select Region Growing. Use cursor to select highlighted area of bone of interest in one of the 3 CT scan viewing windows. This will create a new mask; rename it for the current bone. Deselect the original mask.

Use the edit mask in 3D feature to check that only the bone of interest is selected under the new mask.

If there is more than one bone selected go through the CT scan frame by frame and outline the bone of interest with eraser using edit masks feature. This will give you a large enough gap between bone of interest and excess area to use the edit mask in 3D feature to erase remaining excess bone.

- *use Edit in 3D cautiously, it will erase anything in the plane behind the cursor

- *also you can change size and shape of the erasing cursor using the options at the bottom of the screen or in its toolbar

When excess mask is removed choose Calculate 3D and select the mask that was just cleaned up. For quality choose high. A 3D model will appear in the lower right screen.

Right click the 3D model just created in the side bar and choose surface wrap. (For larger bones use 4 mm for both settings, for smaller use 3 mm to 2.5 mm for both settings.)

Right click the surface wrapped model and choose calculate Mask from 3D. This will generate a new mask which you must check for overlap with other bones in the CT scan and for hollow spaces in the center. When this mask is sufficient, repeat step 7. You may delete all masks and 3D models except for the final mask and final model created.

Again right click the 3-D model and choose smoothing. Use a smoothing factor of 0.9 for all bones. The Number of iterations varies, and is somewhat at your discretion for how much important detail should be kept. Make sure that keep originals is unchecked and compensate

shrinkage is checked. (# of iterations used for tibia and fibula was 4, calcaneus and talus was 2, navicular, cuneiforms and metatarsals was 1, no smoothing was done on the phalanges)

Repeat steps 4 thru 10 for all bones of interest. (Hint: it may be helpful to use the Boolean operator after finishing each bone to delete the mask created from the general mask that you start your region growing from)

After all bones are completed, Go to FEA/CFD>>remesh>>select all

For smoothing (1st) and remeshing (2nd) use the following settings

Fixing>>Smooth

Method: Laplacian (1st order)

Smooth Factor: 0.9

Number of Iterations: 5

Remeshing>>Auto Remesh

Shape Quality Threshold: 0.3

Max Geometrical Error: 0.5

Number of Iterations: 3

Goto File>>Export>>Binary STL file and select appropriate folder for solidworks files. (File size should be 100KB or less, If files are too large consider reprocessing with less detail)

Solid Works Processing

To open files in Solid works, you must go to open, and choose file type of mesh files. Select the STL that was exported from MIMICS

Goto Tool>>ScanTo3D>>Mesh Prep Wizard>>select bone file

Continue to hit the next arrow in the dialog box that appears until you get to global simplification. Here choose reduction amount of 50% unless the number of surfaces is already less than 200.

Choose no smoothing in the next dialog box and when the option is available check the box to launch the surface wizard.

Use surface wizard to create 3D object select Automatic creation from the radial buttons in the first window.

Under surface detail select Update Preview. Check the number of surfaces and surface errors.

If more than one surface error occurs, choose the red x in the upper left corner of the surface wizard. Go back to mesh prep wizard and change global smoothing by moving the slider bar one tick mark to the right. Repeat steps with surface wizard.

If there is still more than one error go back to mesh prep wizard and reduce by 10%. Repeat until there are only one or two surface errors.

With only one or two surface errors move slider bar to increase surface detail and update the preview again. Continue to move slider to the right and update until error is gone.

Check the number of surfaces. If over 300 continue same reduction and smoothing process as was used for multiple errors in the preview.

If there are no errors and there are less than 300 surfaces choose the green checkmark to finish the bone and save in a new folder of revised files.

Repeat process with all bones exported from MIMICS.

*Hint: for best luck with spring placement in assembly be sure that calcaneus and talus have at least 150 surfaces, closer to 300 would be better because of the number of springs that are placed on these bones.

SolidWorks Assembly and Motion Analysis

Choose new SolidWorks document type assembly.

Insert Components>>Choose tibia first as fixed part of the assembly.

Order of insertion for remaining components doesn't matter. Mate components origin and align axes to adjacent bones in order to place them in correct 3D space

Go to motion study tab; in drop down menu choose study type: Motion Analysis.

For new spring, choose the spring icon. Make it a linear spring and choose two insertion nodes based on insertions of previous models and references. (Atlas of Human Anatomy works well)

Choose stiffness based on literature and previous models. To pre-strain the springs, take the original free length shown in the spring tool box and divide by 1.02 to get 2% strain. Copy this value back into the spring toolbox and check the box to update to model changes.

Add 3D surface contacts by selecting two adjacent bones and clicking on the '3D surface contacts'.

Uncheck the 'material' and 'friction' box. This will allow your model to run much quicker.

Under 'Elastic Properties', set:

Stiffness: 10000 N/mm

Exponent: 1.75

Max. Damping: 50 N/(mm/s)

Penetration: 0.001 mm

If there is still overlap after running a model, decrease the penetration or increase stiffness and run again.

Before running either motor or motion data for calculation, check that the fibula, calcaneus, and talus are not mated and are free to move.

To create more than one simulation with same model, right click motion study tab and 'Duplicate', this will save time in placing a springs in a new motion study.

Under study properties, lower the accuracy and the number of frames persecond. (Frames per second can be lowered to as little as 5 per second). Check the box to show all motion analysis messages—this will be helpful in troubleshooting the simulation.

Under the advanced options, the integrator can be either gstiff or wstiff and the initial integrator step size can be lowered to if an error occurs during calculation.

Close all other programs on the computer and select the calculate icon. Running background programs will slow the calculation and sometimes cause the program to get hung up for hours.

Torques, displacements, velocities and other motion data can be retrieved after the simulation is finished by opening the plots toolbox.

In order to calculate strain values, click on the 'Results' icon and select a spring. Select 'Displacement/Velocity/Acceleration>>Linear Displacement>>Magnitude'. Right click on the plot and select 'Export to Spreadsheet'. This will give you the length of the spring over time.

To calculate strain, copy the length values into 'Ligament_Strain_Template.xls' in the SOP folder. Enter the original ligament length. Repeat this step for all ligaments of interest.

APPENDIX 3: SOP (Standard Operating Procedure) For Calculating Ankle Joint Motion Given Vicon Data

This document will outline how to calculate the amount of talocrural joint inversion/eversion, plantarflexion/dorsiflexion, and internal/external rotation given a three dimensional, orthogonal axis on each bone (Figure A-2). The same procedure can be followed for the subtalar joint. The raw motions can come from either cadaver data (where the marker arrays are screwed into the bone) (Figure A-3a) or *in vivo* data (where the markers are taped to the skin) (Figure A-3b)

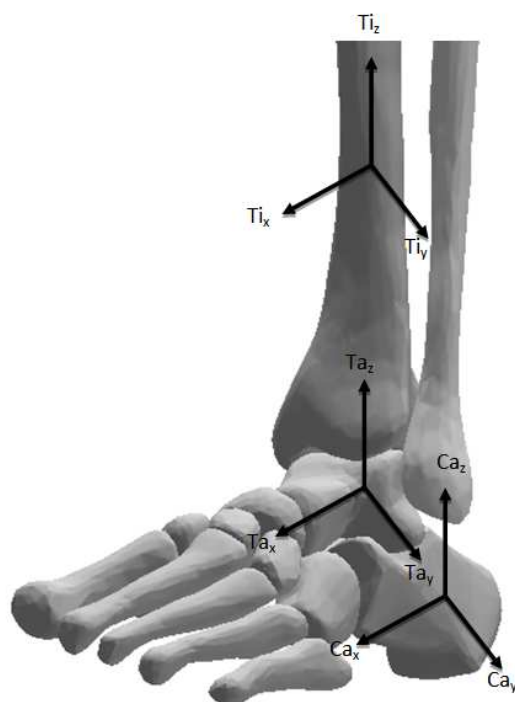


Figure A-2 Orthogonal coordinate axes on the tibia, talus, and calcaneus.

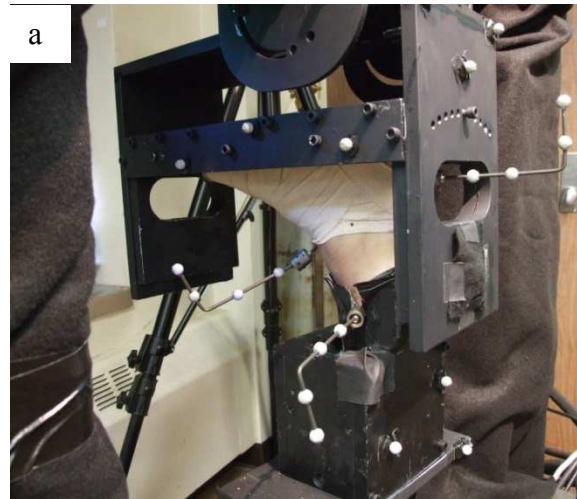


Figure A-3 *Marker arrays in a cadaver ankle (a) and human subject (b)*

Mathematical Background

Since the arrays are randomly oriented, transformations need to be performed to align the local x, y, and z axes with the global Cartesian coordinate system. For the talus:

$$A = \begin{bmatrix} 1 & 0 & 0 \\ 0 & 1 & 0 \\ 0 & 0 & 1 \end{bmatrix}$$

B=Initial orientation of talus in local coordinates

C=Final position of talus in local coordinates

$$R_1 = \begin{bmatrix} Bx \cdot Ax & Bx \cdot Ay & Bx \cdot Az \\ By \cdot Ax & By \cdot Ay & By \cdot Az \\ Bz \cdot Ax & Bz \cdot Ay & Bz \cdot Az \end{bmatrix}$$

$$R_2 = \begin{bmatrix} Cx \cdot Ax & Cx \cdot Ay & Cx \cdot Az \\ Cy \cdot Ax & Cy \cdot Ay & Cy \cdot Az \\ Cz \cdot Ax & Cz \cdot Ay & Cz \cdot Az \end{bmatrix}$$

$$R_3 = R_1^T R_2$$

$$R_4 = R_3^T$$

C' = R₄A (Final orientation of talus in global coordinates)

Establish Joint Coordinate System based on final positions of arrays. For talocrural (C'=final talus, D'=final tibia):

$$e_1 = D'_x$$

$$e_3 = C'_z$$

$$e_2 = \frac{e_3 \times e_1}{|e_3 \times e_1|}$$

$$\alpha = \sin^{-1}(e_2 \cdot D'_z) \text{ (flexion)}$$

$$\gamma = \sin^{-1}(e_2 \cdot C'_x) \text{ (rotation)}$$

$$\beta = \sin^{-1}(e_1 \cdot e_3) \text{ (inversion/eversion)}$$

Procedure

Open up 'JCS.m' in 'Z:\bimgrad\SOP\JCS ANALYSIS'

The program is written for a right ankle oriented with the foot on the ground. If the foot is upside down, or the analysis is run for a left ankle, adjustments will need to be made to the signs of alpha, gamma, and beta in lines 80-82 and 91-93.

Line 9: type the location of your Vicon data

Line 10: specify where you want the output data to go (note: this file must be closed when running the program)

Line 105: specify what sheet you want to write the data to (term 3) and what range within the sheet (term 4).

Run the program by hitting the green arrow in the task bar.

The program will give 6 columns of data. The columns should be labelled accordingly:

Tibia External Rotation Relative to Global	Talus Dorsiflexion Relative to Tibia	Talus External Rotation Relative to Tibia	Talus Eversion Relative to Tibia	Tibia Dorsiflexion Relative to Global	Tibia Eversion Relative to Global

The program is shown below.

```

%*****
%written by Keith D. Button
%*****
%file to calculate talocrural dorsiflexion, external rotation, and eversion
%for a right ankle. For a left ankle, multiply lines 76 and 77 by -1.
%*****
clear, clc
%*****
file='(Vicon data file name and location)';%Input Vicon data file location
out='(Output file location)';%specify output file location
M=xlsread(file,1,'AG1:BD10000'); %data range in file for both tibia and talus positions (should
be 24 columns)
sizem=size(M);
r=size(m,1); %number of data points in file
Result=zeros(r,6);
tibial=M(1,1:12); %initial talus position
talus1=M(1,13:24); %initial tibia position
%*****
origin=[0 0 0 1 0 0 0 1 0 0 0 1];
Axraw= [origin(4)-origin(1),origin(5)-origin(2),origin(6)-origin(3)];
Ax=Axraw/norm(Axraw);
Ayraw= [origin(7)-origin(1),origin(8)-origin(2),origin(9)-origin(3)];
Ay=Ayraw/norm(Ayraw);
Azraw= [origin(10)-origin(1),origin(11)-origin(2),origin(12)-origin(3)];
Az=Azraw/norm(Azraw);
A=[Ax; Ay; Az]; %matrix for orthogonal neutral axis
%*****
i=1;
for i=1:r
    tibia2=M(i,1:12); %talus position
    talus2=M(i,13:24); %tibia position
    Bxraw= [talus1(4)-talus1(1),talus1(5)-talus1(2),talus1(6)-talus1(3)];
    Bx=Bxraw/norm(Bxraw);
    Byraw= [talus1(7)-talus1(1),talus1(8)-talus1(2),talus1(9)-talus1(3)];
    By=Byraw/norm(Byraw);
    Bzraw= [talus1(10)-talus1(1),talus1(11)-talus1(2),talus1(12)-talus1(3)];
    Bz=Bzraw/norm(Bzraw);
    B=[Bx; By; Bz]; %talus initial position in local coordinates
    Cxraw= [talus2(4)-talus2(1),talus2(5)-talus2(2),talus2(6)-talus2(3)];
    Cx=Cxraw/norm(Cxraw);
    Cyraw= [talus2(7)-talus2(1),talus2(8)-talus2(2),talus2(9)-talus2(3)];
    Cy=Cyraw/norm(Cyraw);
    Czraw= [talus2(10)-talus2(1),talus2(11)-talus2(2),talus2(12)-talus2(3)];
    Cz=Czraw/norm(Czraw);
    C=[Cx ; Cy; Cz]; %talus position after external rotation in local coordinates
    %*****
    Dxraw= [tibial(4)-tibial(1),tibial(5)-tibial(2),tibial(6)-tibial(3)];
    Dx=Dxraw/norm(Dxraw);
    Dyraw= [tibial(7)-tibial(1),tibial(8)-tibial(2),tibial(9)-tibial(3)];
    Dy=Dyraw/norm(Dyraw);
    Dzraw= [tibial(10)-tibial(1),tibial(11)-tibial(2),tibial(12)-tibial(3)];
    Dz=Dzraw/norm(Dzraw);
    D=[Dx; Dy; Dz]; %tibia initial position in local coordinates
    Exraw= [tibia2(4)-tibia2(1),tibia2(5)-tibia2(2),tibia2(6)-tibia2(3)];
    Ex=Exraw/norm(Exraw);
    Eyraw= [tibia2(7)-tibia2(1),tibia2(8)-tibia2(2),tibia2(9)-tibia2(3)];
    Ey=Eyraw/norm(Eyraw);
    Ezraw= [tibia2(10)-tibia2(1),tibia2(11)-tibia2(2),tibia2(12)-tibia2(3)];
    Ez=Ezraw/norm(Ezraw);
    E=[Ex ; Ey; Ez]; %tibia position after external rotation in local coordinates
    %*****

ROT21=[dot(Bx,Ax),dot(Bx,Ay),dot(Bx,Az);dot(By,Ax),dot(By,Ay),dot(By,Az);dot(Bz,Ax),dot(Bz,Ay),do
t(Bz,Az)];

ROT22=[dot(Cx,Ax),dot(Cx,Ay),dot(Cx,Az);dot(Cy,Ax),dot(Cy,Ay),dot(Cy,Az);dot(Cz,Ax),dot(Cz,Ay),do
t(Cz,Az)];
    ROT23=ROT22*transpose(ROT21);
    ROT24=transpose(ROT21)*ROT22;
    ROT25=transpose(ROT24);
    C2=ROT25*A; %talus final position along anatomical axis

```

```

%*****
ROT26=[dot(Dx,Ax),dot(Dx,Ay),dot(Dx,Az);dot(Dy,Ax),dot(Dy,Ay),dot(Dy,Az);dot(Dz,Ax),dot(Dz,Ay),do
t(Dz,Az)];

ROT27=[dot(Ex,Ax),dot(Ex,Ay),dot(Ex,Az);dot(Ey,Ax),dot(Ey,Ay),dot(Ey,Az);dot(Ez,Ax),dot(Ez,Ay),do
t(Ez,Az)];
ROT28=ROT27*transpose(ROT26);
ROT29=transpose(ROT26)*ROT27;
ROT30=transpose(ROT29);
E2=ROT30*A; %tibia final position along anatomical axis
%*****
%talocrural rotations
e1=E2(1,:);
e3=C2(3,:);
e2raw=cross(e3,e1);
e2=e2raw/norm(e2raw);
alpha=asind(dot(e2,E2(3,:))); %dorsiflexion
gamma=asind(dot(e2,C2(1,:))); %external rotation
beta=asind(-dot(e1,e3)); %eversion
Result(i,2)=alpha;
Result(i,3)=gamma;
Result(i,4)=beta;
%tibia rotations
e4=Ax;
e6=E2(3,:);
e5raw=cross(e6,e4);
e5=e5raw/norm(e5raw);
alpha2=-asind(dot(e5,Az)); %tib dorsiflexion
gamma2=-asind(dot(e5,E2(1,:)));%tib external rotation
beta2=-asind(-dot(e4,e6)); %tib eversion
Result(i,1)=gamma2;
Result(i,5)=alpha2;
Result(i,6)=beta2;
i=i+1;
end
Tibrot=real(Result(:,1));
TCdors=Result(:,2);
TCrot=Result(:,3);
TCev=Result(:,4);
Tibdorsi=Result(:,5);
Tibev=Result(:,6);
xlswrite(out,Result,1,'A2:F500');

```

Table A-1: Raw Data from Cadaver Failure Tests (Chapter 4)

1477 Left		1477 Right	
<i>Failure Point</i>		<i>Failure Point</i>	
Torque (Nm)	Rotation (deg)	Torque (Nm)	Rotation (deg)
85.55	44.69	83.39	46.48
<i>Incremental</i>		<i>Incremental</i>	
4.04	5.03	5.47	5.05
11.46	10.03	13.85	10.12
18.66	15.13	22.75	15.15
26.56	20.02	32.63	20.14
36.06	25.06	43.07	25.12
46.19	30.10	54.88	30.16
57.04	35.02	66.50	35.14
68.63	40.11	76.56	40.03
77.68	45.06	79.56	45.02

1466 Left		1466 Right	
<i>Failure Point</i>		<i>Failure Point</i>	
Torque (Nm)	Rotation (deg)	Torque (Nm)	Rotation (deg)
75.80	37.02	93.35	39.42
<i>Incremental</i>		<i>Incremental</i>	
6.36	5.06	8.33	5.07
15.62	10.06	17.82	10.05
26.47	15.06	29.44	15.08
38.99	20.04	43.13	20.10
52.47	25.13	57.66	25.10
65.89	30.05	72.82	30.03
73.81	35.08	85.30	35.05

Table A-1 (cont'd)

1066 Left		1066 Right	
<i>Failure Point</i>		<i>Failure Point</i>	
Torque (Nm)	Rotation (deg)	Torque (Nm)	Rotation (deg)
44.94	44.60	50.96	31.12
<i>Incremental</i>		<i>Incremental</i>	
2.26	5.08	4.28	5.09
5.90	10.13	11.06	10.06
10.19	15.14	19.32	15.06
15.71	20.02	28.51	20.04
22.28	25.10	38.78	25.07
29.94	30.08	49.05	30.10
38.68	35.10		
40.63	40.09		

1026 Left		1026 Right	
<i>Failure Point</i>		<i>Failure Point</i>	
Torque (Nm)	Rotation (deg)	Torque (Nm)	Rotation (deg)
55.76	29.40	58.97	33.20
<i>Incremental</i>		<i>Incremental</i>	
6.13	5.01	2.79	5.01
13.45	10.00	9.62	10.06
21.68	15.10	17.78	15.06
30.39	20.13	27.77	20.00
40.16	25.05	39.85	25.11
		40.17	25.25
		51.88	30.05

Table A-1 (cont'd)

1180 Left		1180 Right	
<i>Failure Point</i>		<i>Failure Point</i>	
Torque (Nm)	Rotation (deg)	Torque (Nm)	Rotation (deg)
102.44	37.40	117.92	43.02
<i>Incremental</i>		<i>Incremental</i>	
4.41	5.06	7.75	5.01
15.40	10.09	17.80	10.02
27.74	15.11	29.40	15.01
43.02	20.07	42.33	20.05
59.25	25.11	57.42	25.10
76.99	30.09	74.01	30.02
92.41	35.03	91.99	35.08
		108.64	40.05

141 Left		141 Right	
<i>Failure Point</i>		<i>Failure Point</i>	
Torque (Nm)	Rotation (deg)	Torque (Nm)	Rotation (deg)
170.65	48.06	179.68	63.19
<i>Incremental</i>		<i>Incremental</i>	
8.00	5.05	6.14	5.01
19.20	10.01	14.10	10.01
34.21	15.01	26.02	15.15
52.36	20.04	40.44	20.19
74.43	25.13	57.66	25.07
99.07	30.01	76.87	30.05
125.53	35.03	120.25	40.18
145.52	40.01	137.73	45.04
161.49	45.04	161.67	50.09
		177.05	55.02
		172.32	60.12

Table A-2: Raw Data from Tape Stiffness Tests (Chapter 5)

Elastikon		PowerFlex		Sher-Light	
Torque (Nm)	Rotation (deg)	Torque (Nm)	Rotation (deg)	Torque (Nm)	Rotation (deg)
10	0.35	10	0.30	10	0.30
20	0.80	20	1.12	20	0.79
30	1.23	30	1.91	30	1.21
40	1.62	40	2.64	40	1.68
50	2.10	50	3.37	50	2.19
10	0.24	10	0.31	10	0.32
20	0.62	20	1.09	20	0.79
30	1.03	30	1.92	30	1.23
40	1.41	40	2.53	40	1.68
50	1.83	50	3.36	50	2.10
10	0.22	10	0.35	10	0.35
20	0.58	20	1.12	20	0.78
30	0.97	30	1.80	30	1.21
40	1.32	40	2.50	40	1.68
50	1.73	50	3.28	50	2.10
10	0.20	10	0.32	10	0.31
20	0.60	20	1.11	20	0.78
30	0.97	30	1.75	30	1.22
40	1.33	40	2.49	40	1.56
50	1.74	50	3.27	50	2.07
10	0.22	10	0.31	10	0.31
20	0.58	20	1.03	20	0.74
30	0.91	30	1.73	30	1.18
40	1.27	40	2.45	40	1.58
50	1.69	50	3.20	50	2.05

Table A-3: Input Motions for Computational Model (Chapter 5)

Tibia Rotation (deg)	Tape Stiffness (Nm/deg)	Talocrural Dorsiflexion (deg)	Talocrural Rotation (deg)	Talocrural Eversion (deg)
0	0	0.03	0.30	0.12
1	0	0.03	0.98	0.20
2	0	0.03	1.66	0.28
3	0	0.03	2.34	0.37
4	0	0.03	3.02	0.45
5	0	0.03	3.70	0.53
6	0	0.03	4.38	0.62
7	0	0.03	5.06	0.70
8	0	0.03	5.74	0.78
9	0	0.03	6.42	0.87
10	0	0.03	7.10	0.95
11	0	0.03	7.78	1.04
12	0	0.03	8.46	1.12
13	0	0.03	9.14	1.20
14	0	0.03	9.82	1.29
15	0	0.03	10.50	1.37
0	5	0.03	0.35	0.11
1	5	0.03	1.07	0.19
2	5	0.03	1.80	0.26
3	5	0.03	2.52	0.33
4	5	0.03	3.25	0.40
5	5	0.03	3.97	0.47
6	5	0.03	4.70	0.54
7	5	0.03	5.42	0.62
8	5	0.03	6.15	0.69
9	5	0.03	6.87	0.76
10	5	0.03	7.60	0.83
11	5	0.03	8.32	0.90
12	5	0.03	9.05	0.97
13	5	0.03	9.78	1.04
14	5	0.03	10.50	1.12
15	5	0.03	11.23	1.19

Table A-3: (cont'd)

Tibia Rotation (deg)	Tape Stiffness (Nm/deg)	Talocrural Dorsiflexion (deg)	Talocrural Rotation (deg)	Talocrural Eversion (deg)
0	10	0.03	0.39	0.11
1	10	0.03	1.17	0.17
2	10	0.03	1.94	0.23
3	10	0.03	2.71	0.29
4	10	0.03	3.48	0.35
5	10	0.03	4.25	0.41
6	10	0.03	5.02	0.47
7	10	0.03	5.79	0.53
8	10	0.03	6.56	0.59
9	10	0.03	7.33	0.65
10	10	0.03	8.10	0.71
11	10	0.03	8.87	0.77
12	10	0.03	9.64	0.83
13	10	0.03	10.41	0.89
14	10	0.03	11.18	0.94
15	10	0.03	11.95	1.00
0	15	0.03	0.44	0.11
1	15	0.03	1.26	0.16
2	15	0.03	2.08	0.21
3	15	0.03	2.89	0.25
4	15	0.03	3.71	0.30
5	15	0.03	4.52	0.35
6	15	0.03	5.34	0.40
7	15	0.03	6.15	0.44
8	15	0.03	6.97	0.49
9	15	0.03	7.78	0.54
10	15	0.03	8.60	0.58
11	15	0.03	9.41	0.63
12	15	0.03	10.23	0.68
13	15	0.03	11.04	0.73
14	15	0.03	11.86	0.77
15	15	0.03	12.67	0.82

Table A-3: (cont'd)

Tibia Rotation (deg)	Tape Stiffness (Nm/deg)	Talocrural Dorsiflexion (deg)	Talocrural Rotation (deg)	Talocrural Eversion (deg)
0	20	0.03	0.49	0.11
1	20	0.03	1.35	0.15
2	20	0.03	2.21	0.18
3	20	0.03	3.07	0.22
4	20	0.03	3.94	0.25
5	20	0.03	4.80	0.29
6	20	0.03	5.66	0.32
7	20	0.03	6.52	0.36
8	20	0.03	7.38	0.39
9	20	0.03	8.24	0.43
10	20	0.03	9.10	0.46
11	20	0.03	9.96	0.50
12	20	0.03	10.82	0.53
13	20	0.03	11.68	0.57
14	20	0.03	12.54	0.60
15	20	0.03	13.40	0.64
0	25	0.03	0.54	0.11
1	25	0.03	1.45	0.13
2	25	0.03	2.35	0.16
3	25	0.03	3.26	0.18
4	25	0.03	4.16	0.20
5	25	0.03	5.07	0.23
6	25	0.03	5.97	0.25
7	25	0.03	6.88	0.27
8	25	0.03	7.78	0.29
9	25	0.03	8.69	0.32
10	25	0.03	9.60	0.34
11	25	0.03	10.50	0.36
12	25	0.03	11.41	0.38
13	25	0.03	12.31	0.41
14	25	0.03	13.22	0.43
15	25	0.03	14.12	0.45

Table A-3: (cont'd)

Tibia Rotation (deg)	Tape Stiffness (Nm/deg)	Talocrural Dorsiflexion (deg)	Talocrural Rotation (deg)	Talocrural Eversion (deg)
0	30	0.03	0.59	0.11
1	30	0.03	1.54	0.12
2	30	0.03	2.49	0.13
3	30	0.03	3.44	0.14
4	30	0.03	4.39	0.15
5	30	0.03	5.34	0.16
6	30	0.03	6.29	0.17
7	30	0.03	7.24	0.18
8	30	0.03	8.19	0.20
9	30	0.03	9.14	0.21
10	30	0.03	10.09	0.22
11	30	0.03	11.04	0.23
12	30	0.03	11.99	0.24
13	30	0.03	12.94	0.25
14	30	0.03	13.89	0.26
15	30	0.03	14.84	0.27

REFERENCES

REFERENCES

- Attarian, D. E., McCrackin, H. J., Devito, D. P., McElhaney, J. H. & Garrett, W. E. 1985. A biomechanical study of human lateral ankle ligaments and autogenous reconstructive grafts. *American Journal of Sports Medicine*, **13**.
- Barbaix, E., Van Roy, P. & Clarys, J. P. 2000. Variations of anatomical elements contributing to subtalar joint stability: intrinsic risk factors for post-traumatic lateral instability of the ankle. *Ergonomics*, **43**, 1718-1725.
- Beumer, A., van Hemert, W. L. W., Swierstra, B. A., Jasper, L. E. & Belkoff, S. M. 2003. A biomechanical evaluation of the tibiofibular and tibiotalar ligaments of the ankle. *Foot & Ankle International*, **24**.
- Beynon, B. D., Murphy, D. F. & Alosa, D. M. 2002. Predictive factors for lateral ankle sprains: A literature review. *Journal of Athletic Training*, **37**, 376-380.
- Bonacci, J., Saunders, P. U., Hicks, A., Rantalainen, T., Vicenzino, B. T. & Spratford, W. 2013. Running in a minimalist and lightweight shoe is not the same as running barefoot: a biomechanical study. *British Journal of Sports Medicine*, **47**, 387-392.
- Boruta, P. M., Bishop, J. O., Braly, W. G. & Tullos, H. S. 1990. Acute ankle ligament injuries; a literature review. *Foot & Ankle*, **11**, 107-113.
- Boytim, M. J., Fischer, D. A. & Neumann, L. 1991. Syndesmotic ankle sprains. *American Journal of Sports Medicine*, **19**.
- Button, K., Braman, J., Davison, M., Wei, F., Schaeffer, M. & Haut, R. 2015. Rotational stiffness of American football shoes affects ankle biomechanics and injury severity. *Journal of Biomechanical Engineering*, **137**(6), 061004.
- Button, K. D., Wei, F., Meyer, E. G. & Haut, R. C. 2013. Specimen-Specific Computational Models of Ankle Sprains Produced in a Laboratory Setting. *Journal of Biomechanical Engineering-Transactions of the ASME*, **135**.
- Carson, M. C., Harrington, M. E., Thompson, N., O'Connor, J. J. & Theologis, T. N. 2001. Kinematic analysis of a multi-segment foot model for research and clinical applications: a repeatability analysis. *Journal of Biomechanics*, **34**.
- Cawley, P. W., Heidt, R. S., Scranton, P. E., Losse, G. M. & Howard, M. E. 2003. Physiologic axial load, frictional resistance, and the football shoe-surface interface. *Foot & Ankle International*, **24**.

- Chao, E. Y. S. 2003. Graphic-based musculoskeletal model for biomechanical analyses and animation. *Medical Engineering & Physics*, **25**, 201-212.
- Cheung, J. T. M., An, K. N. & Zhang, M. 2006. Consequences of partial and total plantar fascia release: A finite element study. *Foot & Ankle International*, **27**, 125-132.
- Colville, M. R., Marder, R. A., Boyle, J. J. & Zarins, B. 1990a. Strain measurement in lateral ankle ligaments. *American Journal of Sports Medicine*, **18**.
- Colville, M. R., Marder, R. A., Boyle, J. J. & Zarins, B. 1990b. Strain-measurement in lateral ankle ligaments. *American Journal of Sports Medicine*, **18**.
- Crandall, J., Portier, L., Petit, P. & Hall, G. 1996. Biomechanical response and physical properties of the leg, foot, and ankle.) *40th Stapp Car Crash Conference*.
- Dattani, R., Patnaik, S., Kantak, A., Srikanth, B. & Selvan, T. P. 2008. Injuries to the tibiofibular syndesmosis. *Journal of Bone and Joint Surgery-British Volume*, **90B**.
- Delahunt, E., Monaghan, K. & Caulfield, B. 2006. Altered neuromuscular control and ankle joint kinematics during walking in subjects with functional instability of the ankle joint. *American Journal of Sports Medicine*, **34**, 1970-1976.
- Dias, L. S. 1979. Lateral ankle sprain: An experimental study. *Journal of Trauma-Injury Infection and Critical Care*, **19**, 266-269.
- Dubin, J. C., Comeau, D., McClelland, R. I., Dubin, R. A. & Ferrel, E. 2011. Lateral and syndesmotomic ankle sprain injuries: a narrative literature review. *Journal of Chiropractic Medicine*, **10**, 204-19.
- Edwards, G. S. & Delee, J. C. 1984. Ankle diastasis without fracture. *Foot & Ankle*, **4**.
- Elmore KA 2012. Soft tissue structures resisting anterior instability in a computational glenohumeral joint model.
- Fallat, L., Grimm, D. J. & Saracco, J. A. 1998. Sprained ankle syndrome: prevalence and analysis of 639 acute injuries. *The Journal of foot and ankle surgery : Official Publication of the American College of Foot and Ankle Surgeons*, **37**, 280-5.
- Fassbind, M. J., Rohr, E. S., Hu, Y., Haynor, D. R., Siegler, S., Sangeorzan, B. J. & Ledoux, W. R. 2011. Evaluating Foot Kinematics Using Magnetic Resonance Imaging: From Maximum Plantar Flexion, Inversion, and Internal Rotation to Maximum Dorsiflexion, Eversion, and External Rotation. *Journal of Biomechanical Engineering-Transactions of the ASME*, **133**.
- Fong, D. T.-P., Ha, S. C.-W., Mok, K.-M., Chan, C. W.-L. & Chan, K.-M. 2012. Kinematics Analysis of Ankle Inversion Ligamentous Sprain Injuries in Sports Five Cases From Televised Tennis Competitions. *American Journal of Sports Medicine*, **40**, 2627-2632.

- Fong, D. T.-P., Hong, Y., Chan, L.-K., Yung, P. S.-H. & Chan, K.-M. 2007. A systematic review on ankle injury and ankle sprain in sports. *Sports Medicine*, **37**, 73-94.
- Fong, D. T.-P., Wei, F., Hong, Y., Krosshaug, T., Haut, R. C. & Chan, K.-M. 2011. Ankle ligament strain during supination sprain injury—a computational biomechanics study.) *ISBS-Conference*.
- France, E. P., Paulos, L. E., Abbott, P. J., Roberts, P. F., Muhic, L. A., Lemaster, J. H. & Kazarian, L. E. 1987. Failure characteristics of the medial collateral ligament of the knee - effects of high-strain rate. *Aviation Space and Environmental Medicine*, **58**.
- Funk, J. R., Hall, G. W., Crandall, J. R. & Pilkey, W. D. 2000. Linear and quasi-linear viscoelastic characterization of ankle ligaments. *Journal of Biomechanical Engineering-Transactions of the ASME*, **122**.
- Funk, J. R., Srinivasan, S. C. M., Crandall, J. R., Khaewpong, N., Eppinger, R. H., Jaffredo, A. S., Potier, P. & Petit, P. Y. 2002. The effects of axial preload and dorsiflexion on the tolerance of the ankle/subtalar joint to dynamic inversion and eversion. *Stapp Car Crash Journal*, **46**, 245-65.
- Garrick, J. G. & Requa, R. K. 1989. The epidemiology of foot and ankle injuries in sports. *Clinics in Podiatric Medicine and Surgery*, **6**, 629-37.
- Gerber, J. P., Williams, G. N., Scoville, C. R., Arciero, R. A. & Taylor, D. C. 1998. Persistent disability associated with ankle sprains: A prospective examination of an athletic population. *Foot & Ankle International*, **19**.
- Golano, P., Vega, J., de Leeuw, P. A. J., Malagelada, F., Cristina Manzanares, M., Gotzens, V. & van Dijk, C. N. 2010. Anatomy of the ankle ligaments: a pictorial essay. *Knee Surgery Sports Traumatology Arthroscopy*, **18**, 557-569.
- Guise, E. R. 1976. Rotational ligamentous injuries to the ankle in football. *The American Journal of Sports Medicine*, **4**.
- Haraguchi, N. & Armiger, R. S. 2009. A New Interpretation of the Mechanism of Ankle Fracture. *Journal of Bone and Joint Surgery-American Volume*, **91A**.
- Harper, M. C. 1992. Ankle fracture classification systems: a case for integration of the Lauge-Hansen and AO-Danis-Weber schemes. *Foot & ankle*, **13**, 404-7.
- Heilman, A. E., Braly, W. G., Bishop, J. O., Noble, P. C. & Tullos, H. S. 1990. An anatomic study of subtalar instability. *Foot & Ankle*, **10**, 224-228.
- Hennig, E. M. 2011. The Influence of Soccer Shoe Design on Player Performance and Injuries. *Research in Sports Medicine*, **19**, 186-201.

- Hertel, J., Denegar, C. R., Monroe, M. M. & Stokes, W. L. 1999. Talocrural and subtalar joint instability after lateral ankle sprain. *Medicine and Science in Sports and Exercise*, **31**, 1501-1508.
- Hicks, J. H. 1953. The mechanics of the foot: 1. the joints. *Journal of Anatomy*, **87**, 345-357.
- Hirsch, C. & Lewis, J. 1965. Experimental ankle-joint fractures. *Acta Orthopaedica Scandinavica*, **36**, 408-&.
- Holzbour, K. R. S., Murray, W. M. & Delp, S. L. 2005. A model of the upper extremity for simulating musculoskeletal surgery and analyzing neuromuscular control. *Annals of Biomedical Engineering*, **33**, 829-840.
- Hootman, J. M., Dick, R. & Agel, J. 2007. Epidemiology of collegiate injuries for 15 sports: Summary and recommendations for injury prevention initiatives. *Journal of Athletic Training*, **42**.
- Hopkinson, W. J., StPierre, P., Ryan, J. B. & Wheeler, J. H. 1990. Syndesmosis sprains of the ankle. *Foot & Ankle*, **10**.
- Hughes, J. L., Weber, H., Willenegger, H. & Kuner, E. H. 1979. Evaluation of ankle fractures: non-operative and operative treatment. *Clinical Orthopaedics and Related Research*, 111-119.
- Iaquinto, J. M. & Wayne, J. S. 2010. Computational model of the lower leg and foot/ankle complex: application to arch stability. *Journal of Biomechanical Engineering*, **132**.
- Kato, T. 1995. The diagnosis and treatment of instability of the subtalar joint. *Journal of Bone and Joint Surgery-British Volume*, **77B**, 400-406.
- Kent, R., Crandall, J., Forman, J., Lessley, D., Lau, A. & Garson, C. 2012. Development and assessment of a device and method for studying the mechanical interactions between shoes and playing surfaces in situ at loads and rates generated by elite athletes. *Sports Biomechanics*, **11**, 414-429.
- Kitaoka, H. B., Luo, Z. P. & An, K. N. 1997. Three-dimensional analysis of normal ankle and foot mobility. *American Journal of Sports Medicine*, **25**, 238-242.
- Kleipool, R. P. & Blankevoort, L. 2010. The relation between geometry and function of the ankle joint complex: a biomechanical review. *Knee Surgery Sports Traumatology Arthroscopy*, **18**, 618-627.
- Konradsen, L. & Voigt, N. 2002. Inversion injury biomechanics in functional ankle instability: a cadaver study of simulated gait. *Scandinavian Journal of Medicine & Science in Sports*, **12**.

- Krosshaug, T. & Bahr, R. 2005. A model-based image-matching technique for three-dimensional reconstruction of human motion from uncalibrated video sequences. *Journal of Biomechanics*, **38**, 919-929.
- Kuhlman, S., Sabick, M., Pfeiffer, R., Cooper, B. & Forhan, J. 2010. Effect of loading condition on the traction coefficient between shoes and artificial turf surfaces. *Proceedings of the Institution of Mechanical Engineers Part P-Journal of Sports Engineering and Technology*, **224**, 155-165.
- Kwak, S., Blakevoort, L. & Ateshian, G. 2000. A mathematical formulation for 3D quasi-static multibody models of diarthrodial joints. *Computer Methods in Biomechanics and Biomedical Engineering*, **3**, 41-64.
- Kwon, J. Y., Chacko, A. T., Kadzielski, J. J., Appleton, P. T. & Rodriguez, E. K. 2010. A Novel Methodology for the Study of Injury Mechanism: Ankle Fracture Analysis Using Injury Videos Posted on YouTube.com. *Journal of Orthopaedic Trauma*, **24**, 477-482.
- Lambson, R. B., Barhmill, B. S. & Higgins, R. W. 1996. Football cleat design and its effect on anterior cruciate ligament injuries - A three-year prospective study. *American Journal of Sports Medicine*, **24**, 155-159.
- Laugehansen, N. 1950. Fractures of the Ankle. *Archives of Surgery*, **60**.
- Leardini, A., Stagni, R. & O'Connor, J. J. 2001. Mobility of the subtalar joint in the intact ankle complex. *Journal of Biomechanics*, **34**, 805-809.
- Liacouras, P. C. & Waynel, J. S. 2007. Computational modeling to predict mechanical function of joints: Application to the lower leg with simulation of two cadaver studies. *Journal of Biomechanical Engineering-Transactions of the ASME*, **129**, 811-817.
- Lin, C. F., Gross, M. T. & Weinhold, P. 2006. Ankle syndesmosis injuries: Anatomy, biomechanics, mechanism of injury, and clinical guidelines for diagnosis and intervention. *Journal of Orthopaedic & Sports Physical Therapy*, **36**.
- Livesay, G. A., Reda, D. R. & Nauman, E. A. 2006. Peak torque and rotational stiffness developed at the shoe-surface interface - The effect of shoe type and playing surface. *American Journal of Sports Medicine*, **34**.
- Loram, I. D. & Lakie, M. 2002. Direct measurement of human ankle stiffness during quiet standing: the intrinsic mechanical stiffness is insufficient for stability. *Journal of Physiology-London*, **545**, 1041-1053.
- Lundberg, A., Svensson, O. K., Bylund, C., Goldie, I. & Selvik, G. 1989a. Kinematics of the ankle/foot complex--part 2: pronation and supination. *Foot & Ankle*, **9**, 248-253.

- Lundberg, A., Svensson, O. K., Bylund, C. & Selvik, G. 1989b. Kinematics of the foot/ankle complex--part 3: influence of leg rotation. *Foot & Ankle*, **9**, 304-309.
- Meyers, M. C. 2010. Incidence, Mechanisms, and Severity of Game-Related College Football Injuries on FieldTurf Versus Natural Grass A 3-Year Prospective Study. *American Journal of Sports Medicine*, **38**, 687-697.
- Miller, C. D., Shelton, W. R., Barrett, G. R., Savoie, F. H. & Dukes, A. D. 1995. Deltoid and syndesmotric ligament injury of the ankle without fracture. *American Journal of Sports Medicine*, **23**.
- Mok, K.-M., Fong, D. T.-P., Krosshaug, T., Engebretsen, L., Hung, A. S.-L., Yung, P. S.-H. & Chan, K.-M. 2011. Kinematics Analysis of Ankle Inversion Ligamentous Sprain Injuries in Sports 2 Cases During the 2008 Beijing Olympics. *American Journal of Sports Medicine*, **39**.
- Netter, F. H. & JT, H. 2003. *Atlas of Human Anatomy*, Teterboro, NJ, Icon Learning Systems.
- Ng, B. H., Chou, S. M., Lim, B. H. & Chong, A. 2004. Strain rate effect on the failure properties of tendons. *Proceedings of the Institution of Mechanical Engineers Part H-Journal of Engineering in Medicine*, **218**.
- Nigg, B. M. & Yeadon, M. R. 1987. Biomechanical aspects of playing surfaces. *Journal of Sports Sciences*, **5**.
- Norkus, S. A. & Floyd, R. T. 2001. The anatomy and mechanisms of syndesmotric ankle sprains. *Journal of Athletic Training*, **36**.
- Parenteau, C. S., Viano, D. C. & Petit, P. Y. 1998. Biomechanical properties of human cadaveric ankle-subtalar joints in quasi-static loading. *Journal of Biomechanical Engineering-Transactions of the ASME*, **120**, 105-111.
- Peltz, C. D., Haladik, J. A., Hoffman, S. E., McDonald, M., Ramo, N. L., Divine, G., Nurse, M. & Bey, M. J. 2014. Effects of footwear on three-dimensional tibiotalar and subtalar joint motion during running. *Journal of Biomechanics*, **47**, 2647-53.
- Petit, P. 1996. *Quasi-static Characterization of the human foot-ankle joints in a simulated tensed state and updated accidentological data.* IRCOBI.
- Rasmussen, O. & Kromannandersen, C. 1983. Experimental ankle injuries--Analysis of the traumatology of the ankle ligaments. *Acta Orthopaedica Scandinavica*, **54**, 356-362.
- Renstrom, P. & Konradsen, L. 1997. Ankle ligament injuries. *British Journal of Sports Medicine*, **31**.
- Safran, M. R., Benedetti, R. S., Bartolozzi, A. R. & Mandelbaum, B. R. 1999. Lateral ankle sprains: a comprehensive review - Part 1: etiology, pathoanatomy, histopathogenesis, and diagnosis. *Medicine and Science in Sports and Exercise*, **31**.

- Sarsam, I. M. & Hughes, S. P. F. 1988. The role of the anterior tibiofibular ligament in talar rotation: an anatomical study. *Injury*, **19**, 62-64.
- Siegler, S., Chen, J. & Schneck, C. D. 1988. The 3-dimensional kinematics and flexibility characteristics of the human ankle and subtalar joints--part 1: kinematics. *Journal of Biomechanical Engineering-Transactions of the ASME*, **110**, 364-373.
- Smith, A. W. & Wong, D. P. 2012. Effects of window size on ankle joint stiffness calculation during quiet standing: How the rule changes the result. *Journal of Biomechanics*, **45**, 2301-2305.
- Soutas-Little, R. W., Beavis, G. C., Verstraete, M. C. & Markus, T. L. 1987. Analysis of Foot Motion During Running Using a Joint-Coordinate System. *Medicine and Science in Sports and Exercise*, **19**.
- Torg, J. S. & Quedenfeldt, T. 1973. Effect of shoe type and cleat length on incidence and severity of knee injuries among high school football players. *Journal of Bone and Joint Surgery-American Volume*, **A 55**, 1319-1319.
- Vanlangelaan, E. J. 1983. A kinematical analysis of the tarsal joints. *Acta Orthopaedica Scandinavica*, **54**, 11-269.
- Viladot, A., Lorenzo, J. C., Salazar, J. & Rodriguez, A. 1984. The subtalar joint-embryology and morphology. *Foot & Ankle*, **5**, 54-66.
- Villwock, M. R., Meyer, E. G., Powell, J. W., Fouty, A. J. & Haut, R. C. 2009a. Football Playing Surface and Shoe Design Affect Rotational Traction.
- Villwock, M. R., Meyer, E. G., Powell, J. W., Fouty, A. J. & Haut, R. C. 2009b. Football Playing Surface and Shoe Design Affect Rotational Traction. *American Journal of Sports Medicine*, **37**.
- Villwock, M. R., Meyer, E. G., Powell, J. W. & Haut, R. C. 2009c. Development and evaluation of a surrogate ankle for use with a rotational traction measurement apparatus. *Proceedings of the Institution of Mechanical Engineers Part P-Journal of Sports Engineering and Technology*, **223**.
- Vitale, T. D. & Fallat, L. M. 1988. Lateral ankle sprains: evaluation and treatment. *The Journal of Foot Surgery*, **27**.
- Waterman, B. R., Belmont, P. J., Jr., Cameron, K. L., DeBerardino, T. M. & Owens, B. D. 2010. Epidemiology of Ankle Sprain at the United States Military Academy. *American Journal of Sports Medicine*, **38**.
- Waterman, B. R., Belmont, P. J., Jr., Cameron, K. L., Svoboda, S. J., Alitz, C. J. & Owens, B. D. 2011. Risk Factors for Syndesmotic and Medial Ankle Sprain Role of Sex, Sport, and Level of Competition. *American Journal of Sports Medicine*, **39**.

Weaver, B., Fitzsimons, K., Braman, J. & Haut, R. 2013. Torque prediction at the shoe-surface interface using insole pressure technology. *Journal of Sports Engineering and Technology*, **In Print**.

Wei, F., Braman, J., Meyer, E., Powell, J. & Haut, R. 2011a. Mechanism of injury in a high ankle sprain: A simulation study.) *Summer Bioengineering Conference*. Farmington, PA.

Wei, F., Braman, J. E., Weaver, B. T. & Haut, R. C. 2011c. Determination of dynamic ankle ligament strains from a computational model driven by motion analysis based kinematic data. *Journal of Biomechanics*, **44**, 2636-2641.

Wei, F., Hunley, S. C., Powell, J. W. & Haut, R. C. 2011d. Development and Validation of a Computational Model to Study the Effect of Foot Constraint on Ankle Injury due to External Rotation. *Annals of Biomedical Engineering*, **39**.

Wei, F., Meyer, E. G., Braman, J. E., Powell, J. W. & Haut, R. C. 2012a. Rotational Stiffness of Football Shoes Influences Talus Motion during External Rotation of the Foot. *Journal of Biomechanical Engineering-Transactions of the ASME*, **134**.

Wei, F., Post, J. M., Braman, J. E., Meyer, E. G., Powell, J. W. & Haut, R. C. 2012b. Eversion during external rotation of the human cadaver foot produces high ankle sprains. *Journal of Orthopaedic Research*, **30**.

Wei, F., Villwock, M. R., Meyer, E. G., Powell, J. W. & Haut, R. C. 2010. A Biomechanical Investigation of Ankle Injury Under Excessive External Foot Rotation in the Human Cadaver. *Journal of Biomechanical Engineering-Transactions of the ASME*, **132**.

Williams, D. S. B., 3rd, Green, D. H. & Wurzinger, B. 2012. Changes in lower extremity movement and power absorption during forefoot striking and barefoot running. *International Journal of Sports Physical Therapy*, **7**, 525-32.

Williams, G. N., Jones, M. H. & Amendola, A. 2007. Syndesmotic ankle sprains in athletes. *American Journal of Sports Medicine*, **35**.

Wolfe, M. W., Uhl, T. L., Mattacola, C. G. & McCluskey, L. C. 2001. Management of ankle sprains (vol 63, pg 93, 2001). *American Family Physician*, **64**.

Wong, Y. S., Kim, W. & Ying, N. 2005. Passive motion characteristics of the talocrural and the subtalar joint by dual Euler angles. *Journal of Biomechanics*, **38**, 2480-2485.

Wu, G., Siegler, S., Allard, P., Kirtley, C., Leardini, A., Rosenbaum, D., Whittle, M., D'Lima, D. D., Cristofolini, L., Witte, H., Schmid, O. & Stokes, H. 2002. ISB recommendation on definitions of joint coordinate system of various joints for the reporting of human joint motion - part 1: ankle, hip, and spine. *Journal of Biomechanics*, **35**, 543-548.

Yahia, L., Brunet, J., Labelle, S. & Rivard, C. H. 1990. A scanning electron-microscopic study of rabbit ligaments under strain. *Matrix*, **10**.

Yeung, M. S., Chan, K. M., So, C. H. & Yuan, W. Y. 1994. An epidemiological survey on ankle sprain. *British Journal of Sports Medicine*, **28**, 112-116.